

PHOSPHORUS DYNAMICS IN RESTORED RIPARIAN WETLANDS ON FORMER  
AGRICULTURAL LAND IN VERMONT

A Dissertation Presented

by

Adrian R. H. Wiegman

to

The Faculty of the Graduate College

of

The University of Vermont

In Partial Fulfillment of the Requirements  
for the Degree of Doctor of Philosophy  
specializing in Natural Resources

January, 2022

Defense Date: November 10, 2021  
Dissertation Examination Committee:

Eric D. Roy, Ph.D., Advisor

Donna M. Rizzo, Ph.D., Chairperson

William B. Bowden, Ph.D.

Beverley C. Wemple, Ph.D.

Taylor H. Ricketts, Ph.D.

Cynthia J. Forehand, Ph.D., Dean of the Graduate College

## ABSTRACT

Wetland restoration has numerous potential ecological and societal benefits, one of which is the retention of phosphorus (P) and consequent protection of downstream water bodies from eutrophication. Past studies focused on influents to and effluents from a variety of wetland types have documented net P retention. However, some wetland systems are less effective at P capture and wetland P retention capacity can change over time. Certain wetland types - especially riparian wetlands restored on former agricultural land - remain understudied. In Vermont, most of the over 4000 potential wetland restoration sites in the Lake Champlain Basin are located on current or former agricultural fields, and little information is available to inform estimates of net P retention (i.e., P balances) for such sites.

In this dissertation, I examined various factors affecting P balances in riparian wetlands restored on historically farmed soils of Vermont. P balance in a riparian wetland is largely a function of particulate P capture (e.g., deposition of particle-attached P during floods) and soluble reactive P (SRP) loss (e.g., release of SRP from soils). In Chapter 1, I determined the threshold in

P saturation ratio (PSR) for riparian soils in Vermont, enabling calculation of a soil P storage capacity (SPSC) metric. I then quantified soil SRP release using intact soil core incubations with simulated floods for sites ranging from active farms to mature wetlands and confirmed that PSR, SPSC, and other soil parameters were strong predictors of SRP loss during inundation.

In Chapter 2, I monitored P dynamics in soil, water, and vegetation at three restored riparian wetlands on former agricultural land in the Lake Champlain Basin, focusing on factors that affect P deposition and SRP release. At wetland sampling plots, observed inorganic sediment gain and decreased water column total suspended solids concentrations relative to the river/inflow indicated that wetlands were effectively trapping particles. Accretion of inorganic P (i.e., best estimate for mineral P deposited during floods) ranged from 0.1 to 1 g P m<sup>-2</sup> yr<sup>-1</sup> depending on site and elevation. Elevated SRP concentrations in wetland water columns relative to the river sources indicated internal SRP release from soils, and high frequency data indicated that factors such as temperature, dissolved oxygen, and primary production likely influence SRP dynamics.

In Chapter 3, I developed a wetland P dynamics model that can generate estimates of net P retention from a simple set of soil and hydrologic inputs, considering both P deposition and SRP release. For proof of concept, I simulated the wetlands monitored in Chapter 2 using two years of monitoring data and a set of model scenarios. I found that net total P balance was typically positive (-0.04 to 0.24 g P m<sup>-2</sup> yr<sup>-1</sup>), with average P retention efficiency of ~40%, though there was substantial variability depending on site and scenario. P retention efficiency was especially sensitive to changes in influent P and total suspended solids concentrations, with the greatest net

P retention predicted for systems receiving influent floodwater with high P concentrations.

Reduction of influent SRP concentrations promoted SRP release from soils, suggesting that legacy soil P in the wetlands might cause a time lag between the adoption of upstream best management practices and reduction in downstream SRP concentrations. In the future, the model developed in Chapter 3 can be applied more broadly to investigate the potential P retention benefits of wetland restoration at candidate sites across Vermont. Together, the information put forth by this dissertation provides a suite of data and tools that researchers and managers can use to enhance the P retention benefits of riparian wetland restoration.

## **ACKNOWLEDGEMENTS**

This work would not have been possible without the support of many wonderful people. Thanks to my wife, family, and friends for providing motivation and reprieve when I needed it. I had the pleasure to work with many UVM student employees and volunteers, who not only worked very hard but made my research more fun, especially: Isabelle Augustin, Harrison Myers, Marcos Kubow, Maya Fein-Cole, and Elijah Schreiber. Thanks to my fellow Nutrient Cycling and Ecological Lab members for taking time out of their research schedule to help with mine, especially: Kate Porterfield, Finn Bondeson, and Brendan O'Brien. I would also like to thank my fellow collaborators at UVM for their support, this includes: my advising committee (named on title page), Dr. Rebecca Diehl, Dr. Kristen Underwood, the UVM horticultural farm, UVM extension, and Dan Needham of the UVM agricultural and environmental testing lab. Matt Trueheart was very generous with his time running a HEC-RAS model of Otter Creek that I relied on for selecting sampling locations in Chapter 2 and guiding wetland modeling in Chapter 3. Thanks to the many landowners who participated in my field studies, especially the Burleigh and Des Marais families who were always gracious and good for a nice chat after a long day in the mud.

Thanks to the following institutions who provided financial support: the UVM Rubenstein School of Environment and Natural Resources, the UVM Gund Institute for Environment, Vermont Natural Resources Conservation Service (NRCS), the Lake Champlain Basin Program, and the Vermont Department of Environmental Conservation (DEC). Several agencies and non-profit organizations were key in setting up the field studies. Thanks to The Nature Conservancy for providing site access. Thanks to the Vermont DEC wetlands division for helping with soil sampling efforts. I am especially appreciative of Jim Eikenberry of Vermont NRCS for teaching me about the history of wetland restoration in Vermont, organizing site access, providing opportunities to engage with landowners, and more.

## TABLE OF CONTENTS

LIST OF TABLES .....	vi
LIST OF FIGURES .....	vii
COMPREHENSIVE LITERATURE REVIEW .....	1
CHAPTER 1. POTENTIAL FOR SOIL LEGACY PHOSPHORUS RELEASE FROM RESTORED FLOODPLAIN WETLANDS WITHIN AN AGRICULTURAL LANDSCAPE .....	6
Abstract.....	6
1.1    Introduction .....	6
1.2    Methods .....	9
1.2.1    Site Selection .....	9
1.2.2    Field Sampling .....	10
1.2.3    Soil Characterization.....	11
1.2.4    Intact Core Monitoring.....	13
1.2.5    Land Use Classification .....	14
1.2.6    Calculations & Statistics .....	14
1.3    Results .....	16
1.3.1    Land Use Classification .....	16
1.3.2    Soil Properties and Farming History.....	16
1.3.3    Intact Core SRP Flux .....	21
1.4    Discussion.....	23
1.4.1    SRP Release, Soils and Farming Frequency .....	23
1.4.2    Intact Core Gas Treatments.....	25
1.4.3    Restoration and SRP Release.....	26

1.5	Conclusions .....	27
1.6	Appendix .....	28
1.6.1	Supplemental Figures and Tables .....	28
1.6.1	Farming History of Wetland Restoration Candidates .....	31
CHAPTER 2. PHOSPHORUS CYCLING IN RIPARIAN WETLANDS RESTORED ON FORMERLY DRAINED AND FARMED LAND IN THE VERMONT PORTION OF THE LAKE CHAMPLAIN BASIN .....		32
Abstract.....		32
2.1	Introduction .....	32
2.2	Methods .....	34
2.2.1	Study Area .....	34
2.2.2	Field Sampling and Laboratory Analysis.....	37
2.2.3	Calculations and Statistics .....	43
2.3	Results .....	44
2.3.1	Soil Analyses .....	44
2.3.2	Diffusion of SRP from soils.....	47
2.3.3	Vegetation Biomass .....	47
2.3.4	Litterfall and Litter Decomposition .....	48
2.3.5	Accretion.....	49
2.3.6	Floodwater Monitoring .....	51
2.4	Discussion.....	56
2.4.1	Particle Trapping.....	56
2.4.2	SRP Dynamics .....	57
2.4.3	Hydrogeomorphic Controls on P Cycling.....	59
2.4.4	Landscape Position .....	60
2.5	Conclusions .....	61
2.6	Appendix .....	63
2.6.1	Supplemental Figures and Tables .....	63
CHAPTER 3. NUMERICAL MODELING OF PHOSPHORUS RETENTION IN RESTORED RIPARIAN WETLANDS HAVING AGRICULTURAL LEGACIES .....		68
Abstract.....		68
3.1	Introduction .....	68
3.2	Methods .....	71

3.2.1	Model Documentation.....	71
3.2.2	Simplifying Assumptions.....	73
3.2.3	Parameterization (Calibration and Verification).....	75
3.2.4	Baseline Simulations.....	76
3.2.5	Scenarios .....	78
3.3	Results .....	79
3.4	Discussion.....	83
3.4.1	Legacy P Impacts on Dissolved P Loads .....	84
3.4.2	TP Loads Compared to Agriculture .....	85
3.4.3	Assumptions.....	86
3.4.4	Next Steps .....	87
3.5	Conclusions .....	88
3.6	Appendix .....	89
3.6.1	Supplemental Figures and Tables .....	89
3.6.2	Calibration.....	92
3.6.3	Inflow Concentrations.....	97
3.6.4	Hydroclimate Inputs.....	98
3.6.5	Hydraulic Residence Time.....	99
3.6.6	Sensitivity Analysis .....	101
3.6.7	Modeling Langmuir Parameters.....	105
	SUMMARY AND CONCLUSION .....	107
	COMPREHENSIVE BIBLIOGRAPHY .....	111

## LIST OF TABLES

Table 1-1 Spearman rank correlation ( $r$ ) matrix comparing bulk density weighted mean soil properties (0-10cm) for each sampling plot ( $n=42$ , unless specified otherwise). Variable names are listed on the top, left and diagonal of the matrix, variable definitions are given below the matrix. The upper right triangle shows the correlations significance code (* $0.05 > p \geq 0.01$ , ** $0.01 > p \geq 0.001$ , *** $0.001 > p$ ), the lower left triangle shows $r$ values. Negative $r$ values are in red, positive are in black. Nonsignificant ( $p>0.05$ ) correlations are left blank.	20
Table 1-2 Average soil properties in the top 0-10cm soil layer for grouped by farming frequency. † sand and clay have respective $n$ values of 6, 6, and 3; ‡ MM-Al and MM-Fe have respective $n$ values of 12, 8, 6.....	29
Table 1-3 Linear regression summary from the top 15 best fitting predictor ( $x$ ) variables on the natural log of Final SRP (mean of both treatments at each sampling plot, $n = 20$ ). To translate the values in this table to final SRP ( $\text{mg P L}^{-1}$ ) use $y = e^{\text{intercept}} + \text{slope} * x$ . All models meet the assumptions of normality and homoskedasticity. Variables with the prefix “ln_” were transformed using natural log. Homoskedasticity was verified with Breusch-Pagan test, and normality of residuals was verified with the Shapiro-Wilks test. Ox-P2Fe = Ox-[P:Fe], FF = farming frequency, YSF = years since farming.....	31
Table 2-1 Averages ( $\pm 1$ standard deviation) for soil properties at each site by depth. Letters in common across rows (site and depth) indicate no significant difference in median value (Dunn-Bonferroni).....	63
Table 2-2 Soil to water SRP flux rates observed in simulated floods inside intact cores (average flux rate over the first 7 days after flooding) and related soil properties (reported as averages for the top 0-5cm).....	65
Table 2-3 Total mass and P stocks by site (mean $\pm$ standard deviation, units given in table). Significant differences across rows are denoted by lowercase letters, differences are determined based on the Kruskal-Wallace test with Dunn-Bonferonni post-hoc adjustment. Abbreviations: TM = total mass, IM = mass of inorganic material, OM = mass of organic material, C = P content of material, dw = dry weight.....	66
Table 3-1 Date, time, location of peak discharge of Otter Creek HEC-RAS simulated flood peaks.....	100

## LIST OF FIGURES

Figure 1-1 Panel of box and whisker plots for soil properties of the top 0-10cm grouped by farming frequency. Letters denote significant differences with alpha>0.05 for the Dunn Kruskal-Wallace test with Bonferroni post-hoc adjustment. Plots with no letter show no significant differences among groups .....	18
Figure 1-2 Scatter plot of segmented regression fit of WEP and Ox-PSR (left) and WEP and Ox-SPSC (right), with color and shape corresponding to farming frequency between 1993 and the date of sample collection: less than 40% (yellow circles), between 40% and 80% (cyan squares), greater than 80% (magenta diamonds). Vertical dashed lines and shaded areas correspond to mean and standard error of breakpoints for segmented regression fit using the `segmented` package. ....	19
Figure 1-3 Scatter plot of modified Morgan P (MM-P) verses Ox-PSR (A) and Ox-SPSC (B) with color and shape denoting different farming frequency groups. ....	19
Figure 1-4 Panel scatter plots showing of Final SRP (mean and sd of day 10 – 14) on the y axis against (a.) Ox-PSR, (b.) Ox-SPSC, (c.) Ox-[P:Fe] and (d.) Farming Frequency on the x axis. Grey circles = N <sub>2</sub> treatment, red squares = O <sub>2</sub> treatment. Vertical (y) and horizontal (x) bars are the standard deviation of mean estimates for a given variable at each sampling plot. The best fitting model and summary statistics are given in each plot. ....	22
Figure 1-5 Disagreement rate amongst student classified points by dominant class (the most frequently identified cover type). ....	28
Figure 1-6 Agreement rate for farmed vs unfarmed classification for all student evaluated points.....	29
Figure 1-7 Intact core incubation soluble reactive phosphorus (SRP) concentration over time for each site and plot, showing mean ± 1 standard deviation gas treatment, aerobic (O <sub>2</sub> ) in red and anaerobic (N <sub>2</sub> ) gas treatments in grey (n = 3 per plot per treatment). ....	30
Figure 2-1 Map of the Lake Champlain and Richelieu River basin (A, grey area) showing sampling plot locations at each of the three study sites at Prindle Rd (B), Swamp Rd (C), Union St (D). Yellow arrows indicate observed water flow directions. USDA national areal imagery color imagery from 2016; Plot label key: 0-4 = soil and vegetation sampling plots, C = culvert, D = drainage ditch, BR = bridge, + = ISCO 6712 automatic water samplers and miniDOT dissolved oxygen and temperature logger, * = HOBO MX2100 water level logger.....	35
Figure 2-2 Flow diagram of sequential P fractionation showing inorganic and organic pools. ....	38
Figure 2-3 Soil P fractions of soil at each sampling plot faceted by depth (columns) and site (rows). Fraction 1, readily available P (1 M KCl [SRP]), is smaller than the minimum plotting resolution. ....	46
Figure 2-4 Site level averages for litter stocks over time estimated from the litterbag decomposition experiment, with (A) stock of dry mass, (B) total P content of litter, and (C) stock of total P. Error bars denote standard deviation. ....	48
Figure 2-5 Accretion (including litter, sediment and detritus) over ceramic tiles plotted against fraction the 90% percentile flooding depth for each site, showing mass stocks	

(top row), P stocks (bottom row) for total accretion (a & d), macrophyte litter (b & e) and sediment and detritus (c & f). Sediment + detritus is calculated as the difference between total accretion and macrophyte litter. Black bars around points indicate standard deviation. Black lines and shaded areas show best fit lines for regressions, fit statistics are given on the top right of each sub-plot.....	50
Figure 2-6 Accretion (including litter, sediment and detritus) over ceramic tiles plotted against 90 <sup>th</sup> percentile flooding depth for each site, showing mass stocks (top row), P stocks (bottom row) for total accretion (a & d), inorganic accretion (b & e) and organic accretion (c & f). Organic accretion is calculated as the difference between total and inorganic accretion. Black bars around points indicate standard deviation. Black lines and shaded areas show best fit lines for regressions, fit statistics are given on the top right of each sub-plot. ....	51
Figure 2-7 Panel showing box-and-whisker plots of concentrations of total suspended solids (TSS), dissolved oxygen (DO), SRP, and TP, in grab samples at each site. Shading of boxes denotes the condition of the system when samples were collected, dark grey for filling (water level rising) and white for draining (water level falling). The number of observations is given in parentheses above each group. Letters denote significant differences among groups (origin and condition) within sites (Dunn-Bonferroni, alpha = 0.05). ....	53
Figure 2-8 Scatterplot of TSS and TP in grab samples taken at each sample site: Prindle Rd (a, left), Union St (b, center), Swamp Rd (c, right); shapes correspond to sample origin: river/inflow (white triangles), outflow (grey diamonds), wetland (black circles); the black line shows the best fit regression line and the shaded grey area shows the 95% confidence interval for the best fit line, model fits are shown for river samples at Union St and Swamp Rd fit statistics are given on the upper right.....	54
Figure 2-9 Scatterplot of TP and SRP water samples (including grabs, siphons and ISCOs) taken at each sample site: Prindle Rd (a, left), Union St (b, center), Swamp Rd (c, right); shapes correspond to sample origin: river/inflow (white triangles), outflow (grey diamonds), wetland (black circles); the black line shows the 1:1 line. ....	54
Figure 2-10 Scatterplot of DO and SRP in grab samples taken at each sample site: Prindle Rd (a, left), Union St (b, center), Swamp Rd (c, right); shapes correspond to sample origin: river/inflow (white triangles, dot-dash ellipse), outflow (grey diamonds, solid ellipse), wetland (black circles, dotted ellipse); red ellipses are plotted to show differences in clusters between sample origins, log-linear regression fit statistics of SRP vs DO are given on the upper right for each site.....	55
Figure 2-11 Comparison of soil P fractions estimated from different methods. The top row compares total P methods: P-3051a vs frac-TP (a), frac-TP vs HCl-TP (b), and P-3051a vs HCl-TP (c). The bottom row compares organic (d) and inorganic (e) P measures from the sequential and parallel schemes used. All regressions include leverage and outlier points except for inorganic P (e). In each scatter plot the red line is the regression fit and black line is the 1:1 line. ....	64
Figure 2-12 High frequency sensor data including water level, dissolved oxygen, and temperature (R1), and concentrations of SRP (R2), TP (R3), TSS (R4) at Prindle Rd (C1-C3), Union St (C4-C6), and Swamp Rd (C7-C9). Points show values measured in	

each wetland, while dashed lines and shaded area show the mean and standard deviation, respectively, of the river concentrations for each pulse. All data for Union St and Swamp Rd correspond with the median elevation plot at each site (plot 2). The data first column at Prindle Rd was collected at plot 2, while the second and third columns were collected at plot.....	67
Figure 3-1 Diagram of the mass stocks and flows represented by the wetland P model. Model compartments include belowground (_b) surface soil and porewater, and aboveground (_a) surface water. Inflows and outflows are determined by externally generated forcing hydroclimate data. BP/BM = biomass P/mass, OP/OM = organic P/mass, IP/IM = inorganic P/mass, LOP = Labile Organic P (fast decomposing), ROP = Refractory Organic P (lignin/humic substances), DIP = dissolved inorganic P (aka orthophosphate, aka SRP), PIP = particulate organic P.....	72
Figure 3-2 Power model of Hydraulic Residence Time (HRT), as a function of Water Elevation relative to the lowest elevation plot in the wetland. The parameters for each site were generated from data points extracted for system wide volume and discharge at various flood stages.....	77
Figure 3-3 Box and whisker plots showing concentrations measured in the stream or inflow locations of each site. Median concentrations are marked by horizontal lines in the middle of each box, the mean concentration is marked by x. Pr = Prindle Rd, Sw = Swamp Rd, Un = Union St.....	78
Figure 3-4 Simulated net total phosphorus (TP) balance (bars) with inflow TP and TSS concentrations set to 0.5x stream (i.e., river) median, stream median (baseline conc. 1 x), or 2x stream median for sampling plots (0, 2, 4) in Prindle Rd (Pr), Swamp Rd (Sw), and Union St (Un) sites. The baseline concentration for TP and TSS is given at the above each site. The result in the top row assumes 100% trapping, while the bottom row uses Stokes' Law to simulate settling. Gross P imports (blue) and P exports (red) on the basis of TP (circles) and SRP = DIP (X's) are also shown for various scenarios. Dynamic HRT simulated with power model.....	81
Figure 3-5 Box and whisker plot of TP retention efficiency (%) for all simulations of stream concentrations entering wetland plots, grey boxes indicate simulations where sedimentation is via Stokes' Law, white boxes indicate simulations where 100% particle trapping is assumed.....	82
Figure 3-6 Box and whisker plots of DIP retention efficiency, grouped by site and stream concentration factor, for all simulations forced by stream concentrations.....	82
Figure 3-7 Simulated net total phosphorus (TP) balance (bars) with inflow P and TSS concentrations set to 0.5x stream (i.e., river) median or 2x stream median at observed (x1) and larger (x1.2) flood magnitudes for median elevation plots in Prindle Rd (left), Swamp Rd (center), and Union St (right). Particle trapping is estimated based on settling velocity. Gross P imports (blue) and exports (red) on the basis of TP (circles) and SRP (X's) are also shown for various scenarios. HRT is dynamic based on site-specific power models.....	83
Figure 3-8 Comparison of total P retention efficiency between estimates from studies in (Land et al. 2016) and this chapter.....	84

Figure 3-9 Relationship between depth of flooding and floodplain hydraulic residence time predicted for the two Otter Creek riparian wetland sites using a 2D HEC-RAS model for Otter Creek (Trueheart, 2019).....	89
Figure 3-10 Relationship between depth of flooding (Hw_meters) in meters and hydraulic residence time (log10(HRT), days) based on system volume and outflow as estimated by field measurements for the Prindle Rd site. Different colors represent three distinct sections of apparent beaver dam influence during the monitoring period. ....	90
Figure 3-11 Comparison of concentration verses HRT driven changes on net TP balance assuming 100% particle trapping for the median elevation sampling plot. Concentrations include median concentrations from passive siphons data collected at sampling plots (see Chapter 2), and stream medians multiplied by a factor of 0.5, 1 and 2, while HRT is varied between 10 and 100 days.....	91
Figure 3-12 Biomass tissue P concentrations verses oxalate P saturation ratio for various above and belowground biomass. ....	91
Figure 3-13 Biomass calibration results showing parameter table (top), plots of temperature (middle), and biomass (bottom) over time in days starting on January 1. ....	94
Figure 3-14 Simulated vs observed biomass for plots 0, 2, and 4 at all sites. Red points are biomass stocks observed on 9/02/19, green points are biomass + fresh litter collected on 10/15/19, and black points are biomass and fresh litter observed on 10/15/20. The black line is the 1:1 line. ....	95
Figure 3-15 Observed verses modeled stock of litter P 7/15/20 for plots 0, 2, and 4 at all sites. The black line is the 1:1 line. ....	96
Figure 3-16 Observed versus simulated change in inorganic matter for plots 0, 2, and 4 for a range of concentration, HRT assumptions, and particle trapping assumptions. Siphon = median siphon concentrations at each plot, stream = median stream concentrations, 0p5xC = 0.5 x stream median concentration, 2xC = 2 x stream concentration, power = power model of HRT, 10d = 10 day HRT, 100d = 100 day HRT. Red/pink points = 100% particle trapping, blue points = modeled particle trapping. ....	96
Figure 3-17 Observed vs predicted non-SRP concentrations using local (a, k=9), partial (b, k=6), and global (c, k=3) parameter estimates (n=131). ....	98
Figure 3-18 Observed vs predicted non-SRP (TP – SRP, mg P/L) and estimates of scaling coefficients convert SRP to LOP (k_SRP2LOP), ISS to PIP (k_ISS2PIP), at Prindle Rd (a), Swamp Rd (b) and Union St (c). The 1:1 line is the thick black line. Dotted line shows the regression on observed (x) vs predicted (y). ....	98
Figure 3-19 Relationships observed between elevation/stage (continuously logged by HOBO MX2100), storage volume estimated from LiDAR (A) and outflow (B). The black vertical line on A shows the elevation of the water level logger in the wetland. Water levels were continuously logged, while discharge calculated from velocity and cross-sectional measurements at outflows. ....	99
Figure 3-20 Depth of inundation in otter creek showing location of sampling plots and the reach polygons (blue shaded areas) used to calculated system storage volume, and cross sections (red) were velocity and cross-sectional area were used to estimate discharge through the floodplain.....	101

Figure 3-21 Global sensitivity analysis showing Spearman (top) and Pearson (bottom) correlation for the varying local concentrations only. The box on the right shows the R code used to draw random values for each parameter.....	103
Figure 3-22 Global sensitivity analysis showing Spearman (top) and Pearson (bottom) correlation for the varying all local parameters. The box on the right shows the R code used to draw random values for each parameter .....	103
Figure 3-23 Global sensitivity analysis showing Spearman (top) and Pearson (bottom) correlation for the varying all stochastic parameters. The box on the right shows the R code used to draw random values for each parameter.....	104
Figure 3-24 Observed versus predicted final water column SRP (mg/L) in intact cores after ~14 day simulation.....	105

## COMPREHENSIVE LITERATURE REVIEW

Phosphorus (P) is an irreplaceable element of life's essential molecules (e.g., phosphodiester in DNA and RNA, ATP, and phospholipids). In the last two centuries, human civilizations have become the primary force influencing the flows of P on Earth through development of mined fertilizers, globalization of the food system, alteration of river hydrology, and changes in land use patterns (Smil, 2000). The use of mined P for fertilizer and industrial processes has been crucial to expansion of the global human population. The spatial distribution of P in ecologically available forms will have major impacts on future food and drinking water security and perhaps even geopolitical stability (Chowdhury et al., 2017; Cordell & White, 2014; Scholz et al., 2013).

Phosphorus exists in the environment primarily as the highly stable orthophosphate ion ( $\text{PO}_4^{3-}$ ), which occupies only aqueous and solid phases (Schlesinger & Bernhardt, 2020). Weathering converts particulate mineral forms of P into orthophosphate ( $\text{PO}_4^{3-}$ ) – also known as soluble reactive P (SRP), dissolved inorganic P (DIP), dissolved reactive P (DRP), or molybdate reactive P (MRP) depending on the context. In this dissertation, I will use SRP and (in Chapter 3) DIP to refer to orthophosphate. SRP has the tendency to adsorb to positively charged surfaces like hydrated clays and form compounds with metal hydroxides, rendering it difficult for biology to access. The biological demand for P and the tendency of P to cling or bind to particles often makes it a limiting nutrient for primary production in ecosystems (Vitousek et al., 2010). Changes in the amount, mobility, and bioavailability of terrestrial P have cascading environmental impacts that can lead to long term state changes in aquatic ecosystems (Carpenter, 2005, 2008; Jarvie et al., 2013). Increased P loading to aquatic environments can raise phytoplankton productivity where P is limiting, most commonly in freshwater and oligohaline ecosystems. Excess phytoplankton growth causes negative impacts in coastal zones, such as loss of benthic plants, benthic oxygen depletion, and harmful algal blooms (Nixon, 2009).

P fertilizer and manure application often results in accumulation of elevated levels of P in watershed soils and sediments, which is commonly referred to as “legacy P” (Jarvie et al., 2013). As described above, accumulation of legacy P at the landscape scale often leads to eutrophication especially in freshwater systems (Motew et al., 2017). There is growing recognition among scientists and policy makers that legacy P will constrain efforts to maintain or improve water quality in regions that are already experiencing negative impacts of eutrophication (Jarvie et al., 2013; Rowe et al., 2016; Sharpley et al., 2013). Legacy P, may impact water quality for centuries

even after P inputs are stopped due to watershed P buffering capacity (Goyette et al., 2018). In the United States, P-influenced eutrophication has resulted in a growing number of waterbodies that have total maximum daily load limits imposed by the U.S. Environmental Protection Agency (Motew et al., 2017).

In addition to widespread water quality impacts of excess P loading, the activities of many industrial nations during the 20<sup>st</sup> century also resulted in ubiquitous hydrologic modifications to wetlands and river corridors that resulted in displacement of sediments and nutrients, wetland loss, disconnection of rivers and floodplain, and a general degradation of watershed functioning (F. Cheng & Basu, 2017; Syvitski et al., 2020). Now, there is growing evidence that restoring hydrology in wetlands and river corridors has ecological, human health, and economic benefits in the form of mitigated flood damages (Kiedrzynska, et al. 2015; Thorslund et al., 2017). Furthermore, high intensity events that are becoming more frequent with climate change threaten infrastructure in developed floodplains (Kiedrzynska et al., 2015). In response, scientists and managers are rethinking how humans live in and use floodplains across the developed world (Kiedrzynska et al., 2015; VTDEC, 2021).

Wetlands are generally thought to be nutrient sinks and hydrologic restoration can enhance P retention on degraded floodplains and wetlands by increasing water and sediment retention (Thorslund et al., 2017). The P balance of wetlands containing legacy P is generally determined by the difference in amount of P gained through sediment deposition and the amount P lost due to SRP release. Restoration of sites with farming history is potentially problematic because hydrologic changes on formerly drained croplands can potentially facilitate the release of soil legacy P, offsetting some of the particulate P captured or possibly even resulting in net export of total P or soluble reactive P (SRP) after restoration (Kristensen et al., 2020; Land et al., 2016a; Walton et al., 2020; Hoffmann et al., 2012a). SRP release can occur due to increased flow of water through the soils and associated P desorption, mineralization of organic P, and/or the dissolution of Fe-P due to iron reduction in anaerobic soils (Aldous et al. , 2005; Maranguit et al., 2017; Penrák et al. 2013). If a wetland restoration project promotes longer periods of flooding with slower water flow, the tendency for soils and surface waters to become anaerobic may increase. Increased water flow through a system can occur when a restoration reconnects a river to a previously disconnected floodplain. While the mechanisms of SRP release have been identified, quantitative estimates of P fluxes and P balances in restored floodplain wetlands on former agricultural land are scarce and very little is known about the magnitude and time horizon of legacy P release in these restored ecosystems. Without such estimates, managers have little

information to guide restoration design to achieve the goals of increased watershed functioning and reduced P loading to downstream ecosystems.

In this dissertation, I focus on the net P retention of wetland restoration on former agricultural soils in the Vermont portion of the Lake Champlain Basin, which is subject to a US EPA TMDL requiring substantial reductions in non-point source P loading to Lake Champlain (US EPA, 2015). There is growing support among Vermont policy makers to fund projects that achieve P load reductions, improvements to soil health, and ecosystem services provisioning across the agricultural landscape (Hammond-Wagner et al., 2019). At the same time, efforts are underway in the basin to enhance the functioning of floodplains, including riparian wetlands, providing benefits including flood mitigation and water quality improvement (Vermont DEC, 2021).

Over 4000 candidate wetland restoration sites have been identified in Vermont (Vermont DEC, 2018). Singh et al. (2019) estimated that targeted restoration of the above restoration candidates may reduce P loading to Lake Champlain by 2% for a budget of \$5M (Singh et al., 2019). The results from Singh et al. (2019) are valuable in that they have identified key “irreplaceable” zones where wetland restoration sites would intercept high nutrient loads. However, the InVEST model used by Singh et al. (2019) explicitly does not simulate stream processes and assumes that sediment transport processes alone drive P fluxes (Redhead et al., 2018). Under the InVEST land cover framework, all wetlands are lumped together as one class with a single P retention efficiency value. For example, Singh et al. (2019) used a P retention efficiency of 40% for all wetlands.

However, as recent literature has shown and as this will dissertation show in Chapter 3, nutrient retention efficiency varies based on a variety of factors, soil properties, water chemistry, and hydrology. In some cases, restored wetlands on land with a history of farming can even release more P than they retain due to mobilization of SRP from soil legacy P (Land et al., 2016b; Walton et al., 2020). This is problematic because I have determined that over 90% of the area (~35,000 ha) within the thousands of potentially restorable wetlands in the Vermont drainages to Lake Champlain overlaps with soils that were farmed as recently as 2016 (see section 1.6.1 for methods). Considering all this, accounting for spatial variation in legacy P and the impacts of legacy P on internal loading of SRP will be critical in efforts to improve the effectiveness of wetland restoration and agricultural conservation practices implemented for P load reductions (Dodd & Sharpley, 2016).

In this dissertation, I examined the various factors affecting P balances in riparian wetlands restored on historically farmed soils of Vermont. I provide information that researchers and managers can use to quantify the potential P load reduction benefits of riparian wetland restoration. Furthermore, the tools I developed here can guide site selection and design in efforts to improve P retention benefits and minimize mobilization of legacy P in watersheds. My dissertation consists of three research chapters. The objectives and research questions of each chapter are summarized below.

### **Chapter 1 Objectives:**

- Sample a wide range of floodplain and riparian wetlands soils with a history of agriculture across Vermont
- Lay an empirical foundation for using soil properties to predict soil SRP release risk during flooding in restored riparian wetlands and floodplains

### Research Questions:

- How do soil properties and SRP release rates vary in floodplain and riparian wetland soils with a history of farming?
- Which soil properties best predict SRP release rates?
- Does farming history help explain variation in soil properties and SRP release rates?

### **Chapter 2 Objectives:**

- Examine evidence for two fluxes - (1) particulate P deposition and (2) SRP release - in three restored riparian wetlands by measuring an array of attributes in soil, water, and vegetation during a 2-year field monitoring campaign.

### Research questions:

- Is there in-field evidence of particulate P deposition?
- Is there in-field evidence of internal SRP release?
- What factors explain variation in these fluxes?
- What methods are most useful for estimating these fluxes?

**Chapter 3** Objectives:

- Develop a model that can estimate the net P balances of a wide range of wetland sites from simple soil and hydrologic metrics.
- Apply the model by simulating P dynamics in three wetlands studied in Chapter 2.

Research Questions:

- What is the net balance and retention efficiency of TP and SRP in the study wetlands?
- What influence do changes in influent stream concentrations (e.g., due to improvements and/or reductions in upstream water quality) and discharge (e.g., due to a wetter climate) have on retention rates when they are varied within a plausible range of future change?

## **CHAPTER 1. POTENTIAL FOR SOIL LEGACY PHOSPHORUS RELEASE FROM RESTORED FLOODPLAIN WETLANDS WITHIN AN AGRICULTURAL LANDSCAPE**

### **Abstract**

Most of the ~4000 potential wetland restoration sites in Vermont tributary watersheds to Lake Champlain are on current or former farm fields that may contain soil legacy phosphorus (P). This legacy P could potentially be liberated from soils to surface waters as soluble reactive P (SRP) upon re-wetting. Little information is available to predict the magnitude of potential SRP release at a given site. Soil P metrics have been used to assess SRP runoff risk for active farm fields in Vermont and elsewhere, but this approach has yet to be tested in riparian wetlands with a history of farming. In this study, I sampled an array of riparian soils in Vermont ranging from active farms to mature wetlands. I determined the threshold in P saturation ratio (PSR) for Vermont riparian soils, enabling calculation of the soil P storage capacity (SPSC) metric. I then quantified potential SRP release to overlying water by simulating floods using intact soil cores. SRP release spanned two orders of magnitude and was predicted well by SPSC ( $r^2 = \sim 0.66$ ,  $n=20$ ,  $p=1E-5$ ). Modified Morgan P – the most widely used soil P test in Vermont – was a fair predictor of SRP release ( $r^2 = \sim 0.46$ ,  $n=20$ ,  $p=9E-4$ ). Several soil properties, including PSR and SPSC, were correlated to the recency and frequency of farming at the sampling sites. SRP release generally was lower at sites with longer time since farming. However, SRP release still occurred for soils that had not been farmed for over a decade, indicating that legacy soil P in riparian areas may have lasting impacts on SRP loads to Lake Champlain.

### **1.1 Introduction**

Wetlands are generally thought to be nutrient sinks and hydrologic restoration can enhance phosphorus (P) retention on degraded floodplains and wetlands by increasing water and sediment retention (Thorslund et al., 2017). Wetland restoration is being investigated as a potential P retention strategy in the Vermont portion of the Lake Champlain Basin, which is subject to a US EPA TMDL requiring substantial reductions in non-point source P loading to Lake Champlain (US EPA, 2015). However, over 90% of the many thousands of potential wetland restoration of sites in the Lake Champlain Basin were farmed as recently as 2016. This is potentially problematic because hydrologic changes on formerly drained croplands can potentially facilitate the release of soil legacy P from accumulated fertilizer and manure, possibly resulting in net export of total P or soluble reactive P (SRP) after restoration (Kristensen et al., 2020; Land et al., 2016a; Walton et al., 2020; Hoffmann et al., 2012a).

The P balance of wetlands overlying soils impacted by agriculture is determined largely by the difference between particulate P deposition and soil SRP release (Hoffmann et al., 2012a). Quantitative estimates of such fluxes in restored floodplain wetlands on former agricultural land are scarce and very little is known about the magnitude and time horizon of SRP release from soils containing legacy P (Ardón, et al., 2010b; Land et al., 2016a). Without such estimates, managers have little information to guide restoration design to achieve the goals of increased watershed functioning and reduced P loading to downstream ecosystems. In this Chapter, I focus on soil legacy P in historically drained and farmed wetlands in Vermont and produce data and models to predict potential SRP release from soils in this region.

SRP dynamics in floodplain wetlands are affected by numerous biogeochemical processes, including desorption of adsorbed P ( Nair & Reddy, 2013), dissolution of iron-associated P under anaerobic conditions (Aldous et al. , 2005; Maranguit et al., 2017; Penrák et al. 2013), and mineralization of organic P during drying and rewetting cycles ( Dupas et al., 2015; Gu et al., 2018; Kinsman-Costello et al., 2016). Few existing numerical models simulate all of the processes above (Hantush et al., 2013; Sharifi et al., 2017), and the ones that do require time- and resource-intensive data collection, model verification and implementation. Therefore, simpler tools may be more appropriate for vetting the large number of potential restoration sites across the Lake Champlain Basin and other watersheds in terms of SRP release.

Soil metrics are often used as a proxy for soluble P runoff risk at the site, field, or plot scale (Welikhe et al., 2020). Soil P saturation ratio (PSR) and soil P storage capacity (SPSC) are two related metrics that have been increasingly used in the past decade due to their relative ease of interpretation and their ability to predict sorption and desorption of P across a wide range of soils (Nair & Harris, 2004; Mukherjee et al. 2009; Nair & Reddy, 2013; Dari et al., 2018). PSR is the molar ratio of P to Al plus Fe in oxalate, Mehlich-1, or Mehlich-3 extracts (Nair & Harris, 2004). The significance of this ratio is that in many soils – and particularly acidic soils – amorphous forms of Al and Fe account for most potential P storage sites (Dari et al., 2018). Several recent studies indicate that Fe plays a more important role in explaining SRP release than Al in flooded riparian wetlands soils, especially when anaerobic conditions develop (Gu et al., 2019, 2017; Kjaergaard et al., 2012; Mendes et al., 2018). SPSC is an estimate of the capacity of a soil to act as either P sink or source based on the threshold soil PSR above which deionized water-extractable P (WEP) abruptly increases (Nair et al., 2015; VanZomeren et al., 2019; Welikhe et al., 2020). Dari et al. (2018) demonstrated that the PSR threshold for the Mehlich-3 soil test was consistent across acidic soil that varied in texture and organic matter. However, in

Vermont, Modified Morgan P (MM-P) – which has poor ability to extract Al and Fe compared to Mehlich-3 (Ketterings, 2001) – is the most commonly applied soil P test in agriculture and the Mehlich-3 test is not typically conducted on soils, instead the acid ammonium oxalate extraction has been used to calculate PSR (Perillo et al., 2019; Young et al., 2017; Young & Ross, 2016). The consistency of the PSR threshold for the ammonium oxalate extraction in Vermont floodplain soils has not yet been verified. Doing so will enable the leveraging of existing data to calculate SPSC.

Multiple field and laboratory studies have demonstrated that historically farmed soils in Vermont have potential to release SRP upon flooding (Young & Ross, 2001, 2018). However, these studies were not designed to test the ability of oxalate PSR and/or SPSC to predict P solubilization and release from soils to overlying floodwater. In fact, I am not aware of a study that quantifies the relationship between soil SPSC and soil SRP flux rates under flooded conditions and over timescales relevant for intermittently flooded riparian wetland soils – where important biogeochemical drivers of P transformation like oxygen depletion, iron reduction, pH change, and organic matter mineralization can affect rates (Audet et al., 2019; Dupas et al., 2015; Gu et al., 2019, 2018; Herndon et al., 2020).

To move beyond individual sites or a relatively small number of sites, geospatial methods are needed to predict soil metrics that proxy soluble P loss risk. Such methods should account for inherent soil properties that influence P sorption capacity and soil P present in forms vulnerable to loss. Where agricultural land is being converted back to wetlands within floodplains, land use history is likely an important factor for the latter (Sharpley et al., 2013). Hydrologic setting is also an important consideration, since soluble P release from wetland soils depends on hydrology-influenced redox conditions, floodwater movement, and water column SRP concentrations, in addition to several other biotic and abiotic factors (Reddy et al., 1998). Farming patterns can vary depending on floodplain hydrogeomorphology (Hudson et al., 2006). Existing studies in Vermont indicate that there is covariance between soil types and land use within floodplains (e.g., crops, wetlands, forests) (Perillo et al., 2019; Young & Ross, 2016). However, little work has been done in Vermont to examine how soil types relate to retirement of farm fields or how soils change after farming stops.

Soil development theory suggests that soil P solubility will decrease over time after farming ceases as hydric soil conditions develop and inorganic P transitions gradually to more recalcitrant organic P forms or adsorb to freshly deposited mineral sediments (Craft, 2000; Inglett

& Inglett, 2013; Walker & Syers, 1976). However, few studies have tested this theory in restored wetlands on former agricultural land (Craft et al., 2002). As a result, the time horizon for legacy P impacts in such ecosystems remains poorly characterized, sparse literature estimates for net SRP losses range from months to decades (Aldous et al., 2007; Ardón et al. 2010a; Ardón et al. 2010b; Surridge et al., 2012).

There are three key outcomes of this chapter. (1) First, I determined the PSR threshold (used to calculate SPSC) for the ammonium oxalate extraction in Vermont floodplains. (2) Second, I developed farming history metrics that can be estimated by anyone using free Google software. (3) Third, I fit models to predict SRP flux from soils to overlying floodwater from floodwater oxygen concentration, soil (e.g., PSR, SPSC, and MM-P), and farming history metrics. This information provides tools, data and relationships that can be used to estimate SRP release risk on a site-by-site basis, and to eventually model SRP loss rates from floodplain wetlands and assess the impacts of management on SRP release (see Chapter 3). While this study was focused on Vermont, the findings herein have implications for agricultural watersheds across the Global North, where legacy P could have a persistent impact on water quality (Goyette et al., 2018; Kusmer et al., 2018).

Based on prior literature, I hypothesized that there would be correlations between soil organic matter, clay content, and extractable P, Al and Fe (Kang et al., 2009; Zhang et al., 2005) and that there would be differences in soil properties across sites that fall under different prior land use groupings (Perillo et al., 2019). Specifically, PSR would be greater, and texture would be courser in more frequently and recently farmed soils. I also hypothesized that SRP flux in intact cores would significantly correlate with MM-P (positively), PSR (positively) and SPSC (negatively) and would be greater under anaerobic conditions.

## 1.2 Methods

### 1.2.1 Site Selection

I sampled and characterized soils in the Vermont portion of the Lake Champlain Basin USA at a total of 76 sampling plots at 42 sites that varied in time since farming and hydrogeomorphic characteristics. For the purposes of this chapter, I define “sites” as zones that flood at least every 2 years on average with unique land use history and I define “plots” as a discrete area where sampling occurs within a site. Sites were selected based on knowledge of flooding frequency, land use history, and the ability to obtain landowner permission.

I sampled sites in several hydrogeomorphic regions to represent the variability in potentially restorable wetlands in Vermont. I attempted to represent at least one site in active agricultural use and one formerly agricultural site in each hydrogeomorphic setting, but this was not always possible, given site access and resource constraints. I biased my sampling efforts by placing more than half of my sites along a well-connected segment of Otter Creek between the USGS gauges at Rutland and Middlebury Vermont that contains the largest wetland complex in the northeastern United States. This stretch of Otter Creek has the highest density of restored wetlands in Vermont and allowed us to examine post agricultural succession in sites with similar hydrogeomorphology. I sampled soils from additional sites along different Lake Champlain tributaries: Malletts Creek in Colchester, VT, the Winooski River in Burlington, VT, Prindle Brook (a low order tributary of Lewis Creek) in Charlotte, VT, and Lewis Creek in Starksboro, VT. I also collected soils from the watershed of Lake Carmi, which is a small lake in Franklin, VT that is also under a TMDL for P. In general I established one sampling plot within each site, but at a subset of sites, two in Otter Creek, one at Prindle Brook, and one at Malletts Creek, I quantified within site variability by establishing triplicate plots placed randomly within low, average, and high elevation zones of the wetland (see Chapter 2).

### **1.2.2 Field Sampling**

Sampling occurred during the warm seasons (June through early October, before plant senescence) in 2018, 2019, 2020 and 2021. At sampling plots, soils were collected in one of two ways depending upon whether the site was undergoing a rapid assessment or if intact cores were being collected. The rapid assessment method was designed to require minimal field equipment and be quickly carried out by Vermont DEC technicians during wetland rapid assessment monitoring. The intact core sampling protocol was designed to capture inherent variability within a spatial unit with fixed ecohydrological conditions.

At each rapid assessment plot, ten cores of 2.7 cm diameter were collected to a depth of 10cm every 3 m along a 30 m transect using 60ml BD syringes that were cut and sharpened with a serrated tip. The transect sampling protocol was designed to capture average conditions for a particular elevation within a site. The location of the ~30m of the transect would be determined in the field by a technician who would orient perpendicular to the elevation gradient of the site (or parallel to an imaginary contour line) then walk forward, collecting a sample every 3 paces (~1 m in length) until 10 syringes were collected. The syringes were initially twisted to cut roots and, if conditions were wet and the soil was easily compressed, the stopper was pulled out as the syringe

was pushed into the soil to create suction and minimize compaction. A GPS point was collected at the start, middle, and end of the transect. The cores were kept inside their syringes upon collection and placed in a sealed polyethylene bag and placed inside a cooler on ice.

At plots selected for intact core incubations, I collected nine soil cores from predetermined random polar coordinates within a 5m radius from the center of each plot. Soil cores were collected with clear polycarbonate cylinders of 7.6cm diameter and 60cm in length. Prior to sampling each core tube was beveled sharp at the bottom edge to reduce compaction and labeled with the site, plot, treatment (control, O<sub>2</sub> or N<sub>2</sub>), and polar coordinates. Soil cores were sampled in between plant shoots and visible plant litter was removed from the surface before sampling. Each soil core was carefully inserted to a depth of ~20cm; In wetter, peaty soils, cores were inserted deeper than 15cm to reduce sample disturbance upon extrusion, while in dry clay pan soils some cores could not be inserted further than 15cm. Cores that compressed more than 1cm upon insertion were discarded and resampled. To obtain a suitable sample, it was necessary in some cases to cut surface roots around the core with a serrated knife. Cores were extruded from the soil carefully to avoid expansion: tube tops were plugged using a size 12.5 rubber stopper then tubes were carefully pulled from the soil. Cores that expanded significantly upon extrusion were discarded.

I characterized three cores per plot (see Soil Characterization), and left six cores per plot intact for laboratory incubations (see Intact Core Monitoring). Characterization cores were sectioned in 5cm increments up to 20cm depth and immediately sealed free of excess air in labeled polyethylene bags and stored in a cooler over ice during transport to the lab. Intact cores were sealed at the bottom with a size 12.5 rubber stopper and duct tape, placed upright in buckets and kept at ambient temperatures during transport to the lab. Site water, to be used in intact core incubations, was collected from the adjacent stream of each sampling site in polypropylene carboys and stored at ambient temperature during transport. In all cases, time from sample collection to arrival at the lab took less than 4hrs.

### **1.2.3    Soil Characterization**

At the lab, soils were maintained at 4°C inside plastic bags sealed free of excess air for no more than 24hrs until a technician prepared samples for analysis. Soil core sections from intact core plots were weighed (for bulk density), then homogenized, while cores from rapid assessment plots were composited, weighed, then homogenized. From each soil sample, one 20-30g subsample was dried at 60°C until constant weight inside a forced-air drying oven; another

subsample was air dried at (25°C) for one week for use in certain methods; in both cases, sample masses were recorded before and after drying. I calculated gravimetric moisture content (MC, g/g) from soils dried at 60°C (Reddy et al., 2013). Bulk density (BD, g/cm<sup>3</sup>) was calculated by dividing soil oven dry mass [initial wet weight \* (1-MC)], by the volume of each core section.

Within one week of collection, I measured water extractable P (WEP, mg P kg<sup>-1</sup>) on field moist soils by adding 20ml of Type 1 deionized water to the wet equivalent of 2g dry oven dry soil [wet weight = 2/(1-MC)] then equilibrated samples on a reciprocating shaker for 1 hour (Nair et al., 2015). Inorganic P (HCl-P<sub>i</sub>, mg P kg<sup>-1</sup>) was estimated by extracting 0.3g ground soils with 15ml of 1 M HCl (1:50 weight/volume ratio) and equilibrated on shaker for 16 hours (Richardson & Reddy, 2013). Organic matter (OM, g/g) was estimated as loss-on-ignition (LOI) by ashing ground soil at 550°C for 4hrs (Reddy et al., 2013). Total P (TP, mg P kg<sup>-1</sup>) was measured by extracting 0.3g dry weight equivalent ashed-ground soil with 15ml 1 M HCl on a shaker for 16hrs (Levy & Schlesinger, 1999). Organic P (HCl-P<sub>o</sub>, mg P kg<sup>-1</sup>) was calculated as the difference between HCl-TP and HCl-P<sub>i</sub>. The ratio of inorganic to total P was calculated by dividing HCl-P<sub>i</sub> by HCl-TP and is abbreviated as HCl-[P<sub>i</sub>:TP]. Extracted samples for WEP, HCl-P<sub>i</sub>, and TP centrifuged at 4066 x g and were filtered through a 0.45 µm nitrocellulose membrane into 20ml scintillation vials for frozen storage. For WEP, HCl-TP, and HCl-P<sub>i</sub>, SRP was analyzed by measuring absorbance at a wavelength of 660 nm on a microplate reader (Synergy HT, BioTek) using the malachite green method (D'Angelo et al., 2001a; Rahutomo et al., 2019). Air-dried sieved (<2mm) and ground soils (0.2g) were extracted in the dark 1:50 (weight/volume) with a pH 3.0 acid ammonium oxalate solution following Courchesne and Turmel (2008) and analyzed for Al (Ox-Al), Fe (Ox-Fe), P (Ox-P) and Mn (Ox-Mn) by ICP-OES (Avio 200, Perkin-Elmer).

I sent air-dried sieved (<2mm) soil samples to the University of Maine Analytical Lab (Orono, Maine USA) for particle size analysis and Modified Morgan (MM) extraction. Concentrations of P in MM extracts were quantified colorimetrically (MM-P) using Flow Injection analysis (Murphy & Riley 1962) and by ICP-OES (MM-P-ICP). Particle size analysis was run on air-dried sieved (<2mm) soils after overnight dispersion in Calgon solution. Clay was determined by the hydrometer method (Bouyoucos, 1962; Day, 1965). Sand was determined gravimetrically by wet sieving to <53µm (sieve # 270). Silt was calculated as the remainder. Particle size groups and texture classifications are from the USDA Soil Survey Manual (Soil Science Division Staff, 2017).

#### **1.2.4 Intact Core Monitoring**

At the lab, technicians immediately prepared intact cores for incubation. Site water was filtered using Whatman # 2 paper, and stored in amber 1L high-density polyethylene bottles and refrigerated at 4°C. The intact soil core tubes were drained of any remnant surface water with a siphon, cleaned and dried and resealed at the bottom with a 12.5 rubber stopper and duct tape, marked with black permanent marker or colored tape at 20cm above the soil surface. Intact cores were then carefully topped with site water – using an upside-down funnel to disperse flow to the walls and minimize soil surface disturbance. Site water was added in this fashion until surface water stabilized at the 20cm mark, for a surface water volume of 0.9L.

Technicians separated cores into two black plastic tanks filled with tap water based on their predetermined gas treatment, three cores per plot per treatment. Cores in the O<sub>2</sub> treatment were bubbled with room air (20% O<sub>2</sub>), while cores in the anaerobic (N<sub>2</sub>) treatment were bubbled with O<sub>2</sub> free nitrogen gas (NI UHP from Airgas, Williston, VT). To avoid pressure gradients that would promote advective exchange of water between the tub and intact cores, the height of each core was adjusted so that the surface water in the core was flush with the water in the tub. Once filled with site water, each core was sealed with a two-hole rubber stopper fitted with borosilicate glass tubes and clear vinyl tubing then purged with gas for 24hrs. For subsequent days in the >14d incubation period, cores were purged with their respective gas treatment for 90 minutes every 24hrs.

A technician monitored each core daily during the first week and at least every other day thereafter during the incubation period. Monitoring consisted of collecting water samples and measuring dissolved oxygen (DO), pH, and temperature. To ensure saturation/depletion of DO in the water column in the respective O<sub>2</sub>/N<sub>2</sub> gas treatments, once per incubation period the intact cores were monitored for DO concentrations after the 90min purge, then subject to another 90min purge to maintain the experiment conditions. Technicians collected water samples at roughly 5cm below the water surface using a 5ml syringe and tube and immediately filtered samples through a 0.45 m membrane into a pre-labeled 20ml polypropylene vial for frozen storage until analysis for SRP (D'Angelo et al., 2001a; Rahutomo et al., 2019). After sampling, filtered site water was added using a graduated syringe so that the surface was flush with the 20cm mark, and the volume added was recorded. After the experiment ceased, the top 0-5 and 5-10cm of each intact core was sectioned, and weighed, processed for bulk density and moisture content then stored for future analysis.

### **1.2.5 Land Use Classification**

I classified the prior land use at each site into groups of farmed and not farmed, using areal imagery available in Google Earth Pro. I also used the classified images to estimate the years since farming (YSF) and farming frequency (FF). I defined years since farming as the amount of time in years since each site was farmed, calculated as the difference in the sample date and date of the last year farmed. I defined farming frequency as the number of years with images that were classified as farmed divided by the total number years where images were classified. If there were multiple images available in a year, I used the image that most clearly distinguished the land use for that year. The earliest available imagery was in 1993, and the number of years with images available per sampling plot ranged from 9 to 13.

To assess the accuracy and reproducibility of classifying images using Google Earth Pro, I conducted an exercise with students of the Ecological Restoration (ENSC 201) class taught by Dr. Eric Roy at the University of Vermont in spring of 2021. Students were randomly assigned points within potential wetland restoration sites to classify images using a Google Form that contained a decision tree, which had the following land cover classes: farmed row crop, farmed hay/pasture, unfarmed herbaceous, unfarmed shrub, unfarmed woody, unfarmed other. Ten percent of points were classified by at least two students. I verified the accuracy of the classifications by comparing student classifications for randomly generated sites against the Croplands Data Layer (NASS, 2021) and the Vermont 2016 (0.5m resolution) land cover layer (VTADS, 2021). I assessed the reproducibility of the classifications by comparing the rate of disagreement amongst students who classified the same points.

### **1.2.6 Calculations & Statistics**

All data manipulation, calculations, statistics and plotting were performed with R statistics and modeling software R version 4.0.3 (R Core Team, 2020) using the `tidyverse` suite packages (Wickham et al., 2019). I calculated several soil metrics from raw physicochemical soil properties. PSR was calculated using the molar ratio of Ox-P to the sum of Ox-Fe and Ox-Al (Equation 1-1).

#### **Equation 1-1**

$$\text{PSR (molar ratio, mol/mol)} = (\text{Ox-P}/1)/(\text{Ox-Al}/27 + \text{Ox-Fe}/56)$$

Where 31, 27, and 56, are the respective molar masses ( $\text{mg mmol}^{-1}$ ) of P, Al, and Fe. Ox-P, Ox-Fe and Ox-Al are in units of  $\text{mg kg}^{-1}$ . In a similar fashion to PSR, I calculated the molar ratio of

Ox-P to Ox-Al (Ox-[P:Al]), and Ox-P to Ox-Fe (Ox-[P:Fe]). Following Dari et al. (2018), I calculated SPSC by multiplying P Storage Maximum (PSM), by the difference between the PSR threshold and the PSR of a given soil (Equation 1-2).

### Equation 1-2

$$\text{SPSC (mg P kg}^{-1}\text{)} = (\text{threshold} - \text{PSR}) * \text{PSM}$$

Where PSM is the P Storage Maximum (Equation 1-3), PSR is the P saturation ratio for a given soil sample calculated above, and “threshold” (molar ratio) is the breakpoint PSR of a segmented regression fit of PSR and WEP was determined using the R package `segmented` (Muggeo, 2008), with the starting breakpoint set to 0.1 (Dari 2018).

### Equation 1-3

$$\text{PSM (mg P kg}^{-1}\text{)} = 31 * (\text{Ox-Al}/27 + \text{Ox-Fe}/56)$$

I examined relationships among surface soil properties and prior land use. To do this I calculated averages of soil properties of the top 0-10cm layer for each site. For sites that had samples taken at 0-5cm, and 5-10cm, I calculated a bulk density weighted average of the two layers. I examined directional relationships between soil properties years since farming, and fraction farmed by calculating Spearman rank correlation matrices using the `rstatix` package (Kassambara, 2020). After an initial inspection of the data, I grouped soils by prior land uses using farming frequency thresholds of 40% and 80%. These thresholds are meant to reflect a rough estimate for groups of low (<40%) medium (40%-80%) and high (>80%) potential legacy P. I examined pairwise differences soil properties among groups of farming frequency using a non-parametric Kruskal-Wallace test, followed by a Dunn (1964) post-hoc test with Bonferroni adjustment for family-wise error rate using the `dunn.test` package in R (Dinno, 2017).

I calculated summary metrics for the intact core experiment by taking the mean and standard deviation of observations taken between the 10<sup>th</sup> and 15<sup>th</sup> day, for SRP, dissolved oxygen, pH, and temperature. To quantify how flux rates changed over the course of the experiment as concentrations increased, I estimated SRP flux ( $\text{g m}^{-2} \text{ d}^{-1}$ ) for each intact core for the first week (day 0 to day 7,  $\text{SRP flux}_{0:7}$ ) and for the course of the incubation (day 0 to day 14,  $\text{SRP flux}_{0:14}$ ) by fitting a zero-intercept linear least square regression model to the difference between the stock of SRP ( $\text{g/m}^2$ ). To verify differences between the aerobic and anaerobic intact core treatments I conducted an ANOVA on sampling plot and treatment using the Kruskal Wallace test with Dunn Bonferroni adjustment for multiple comparisons. Last, I fit linear

regression models to estimates of SRP flux against soil (in the top 0-5, 5-10 and 0-10cm) layers, and prior land use metrics to find the strongest predictors or proxies of flux using the `bestglm` package in R (McLeod et al., 2020). I used a test-statistic of 0.05 as the significance threshold in all statistical tests. Throughout the chapter I use the following significance codes: \* $0.05 \geq p > 0.01$ , \*\* $0.01 \geq p > 0.001$ , \*\*\* $0.001 \geq p$ .

## 1.3 Results

### 1.3.1 Land Use Classification

The google earth areal image classification method I developed had good accuracy and reproducibility for distinguishing between farmed and unfarmed sites. However, students were unreliable at reproducing land cover classifications beyond classifying points as farmed and unfarmed, especially for non-row crop and non-woody cover classes (Figure 1-5 in Appendix). For farmed and unfarmed classification, student classified points ( $n=389$ ) had good agreement (79%) with the 2016 0.5m Vermont landcover dataset and fair agreement (63%) with the NASS croplands data layer (Figure 1-6 in Appendix). For comparison, the NASS Croplands data layer had an agreement rate of 67% with the 2016 0.5m Vermont landcover data for student classified points ( $n=389$ ), and 74% agreement for all randomly generated points in potential wetland restoration sites ( $n=6,985$ ).

### 1.3.2 Soil Properties and Farming History

The soils I sampled varied in organic matter, soil texture, and indices of soil legacy P (Figure 1-1). Organic matter (LOI) averaged  $0.27 \pm 0.21$  g/g at sites with farming frequency  $< 40\%$  and was significantly greater than at sites with farming frequency of 40 - 80% and  $> 80\%$ , which both had mean LOI of 0.10 g/g (see Table 1-2 in Appendix of Chapter 1 for averages). The soils I collected were loamy. Clay content ranged from 4% to 30% while sand content ranged from 1% to 50%. As expected, many soil variables were significantly monotonically correlated (Table 1-1). I observed covariance between texture (sand, silt, clay, Ox-Al), organic matter (BD and LOI), and legacy P indices (HCl-[Pi:TP], PSR, MM-P) (Table 1-1). MM-Al did not correlate with Ox-Al and MM-Fe did not correlate with Ox-Al.

Ox-PSR and WEP exhibited a classic hockey stick relationship (Figure 1-2, e.g. Nair & Harris, 2004). The segmented regression model PSR threshold for the relationship between PSR and WEP was  $\sim 0.23$  ( $r^2=0.87$ ,  $n=170$ ). Ox-PSR ranged from 0.05 to 0.5, and WEP ranged from  $\sim 0.02$  to  $\sim 20$  mg P kg<sup>-1</sup>. Ox-SPSC (derived from the PSR threshold) ranged approximately from

-750 (over capacity) to 2500 (under capacity) mg P kg<sup>-1</sup>. There was a strong nonlinear relationship between MM-P and both PSR and SPSC, especially in soils with farming frequency greater than 75% (Figure 1-3). The PSR threshold of 0.23 corresponded to MM-P values of roughly 10 mg P kg<sup>-1</sup>.

The 42 sites I sampled varied in years since farming ranging (YSF) from 0 to 25+ years, with an even spread of farming frequency (FF) ranging from 0% to 100%. Farming frequency and years since farming correlated linearly and negatively with a Spearman correlation of -0.94 (Table 1-1, row 2, column 1). Many soil variables, including soil organic matter, texture and indices of legacy P were significantly correlated with farming frequency (Table 1-1). Sand, BD, PSR, WEP, MM-P, and HCl-[Pi:TP] correlated positively with farming frequency, while silt, Ox-Fe, MM-Al, and LOI correlated negatively with farming frequency (Table 1-1, column 1). These relationships are also evident in Table 1-2 which shows average soil properties of prior land use groups.

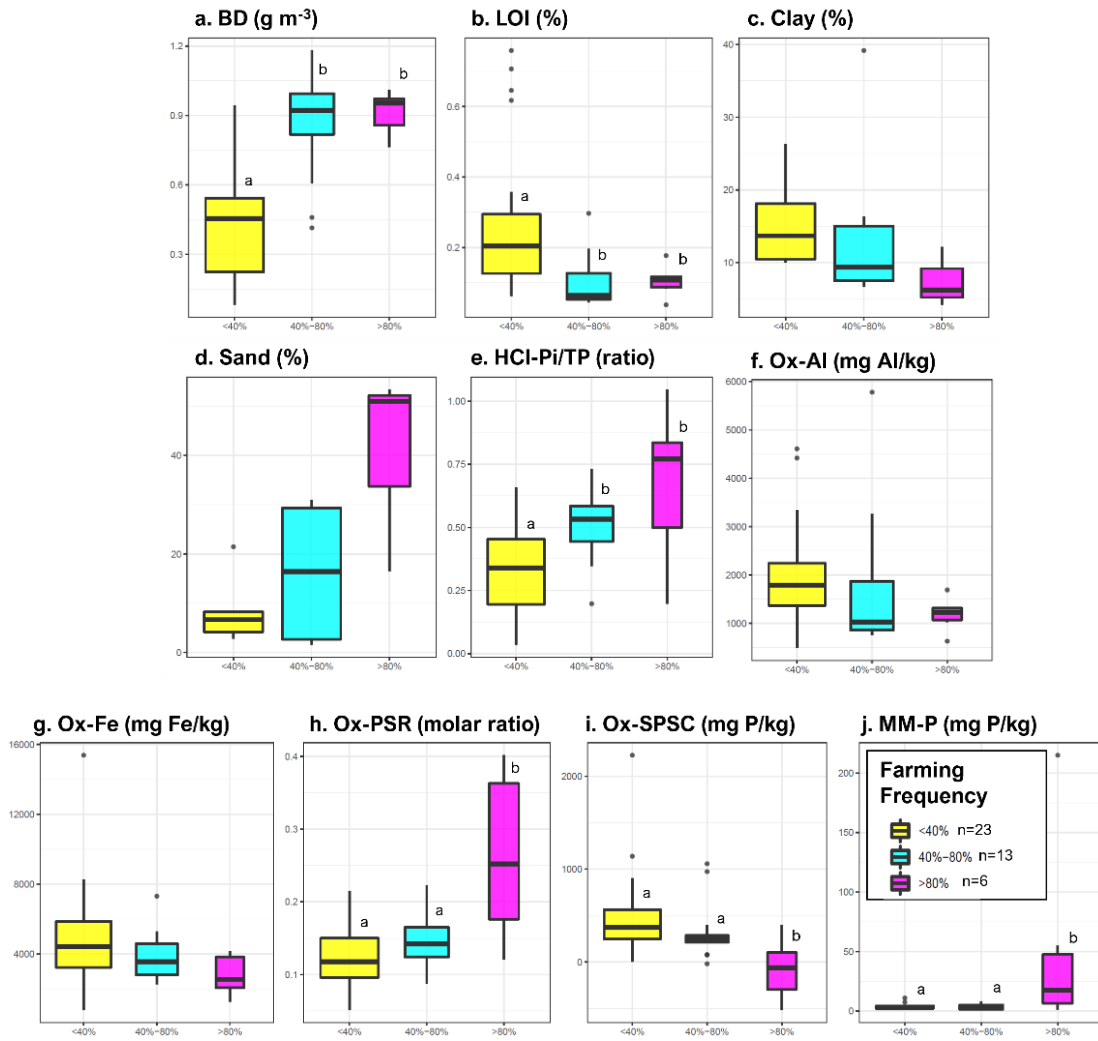


**Figure 1-1 Panel of box and whisker plots for soil properties of the top 0-10cm grouped by farming frequency. Letters denote significant differences with alpha>0.05 for the Dunn Kruskal-Wallace test with Bonferroni post-hoc adjustment. Plots with no letter show no significant differences among groups**

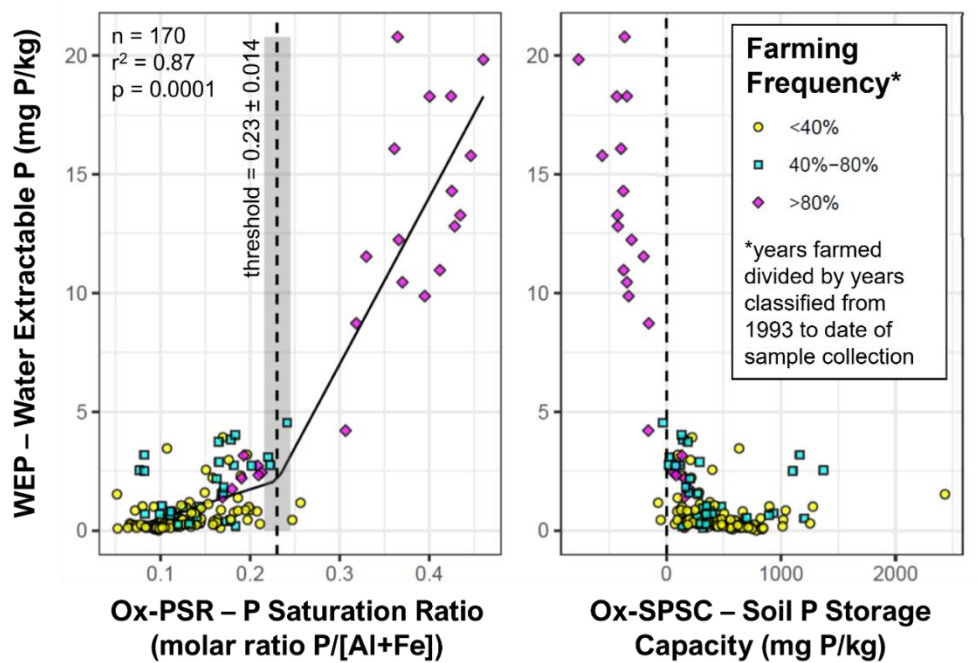


**Figure 1-2** Scatter plot of segmented regression fit of WEP and Ox-PSR (left) and WEP and Ox-SPSC (right), with color and shape corresponding to farming frequency between 1993 and the date of sample collection: less than 40% (yellow circles), between 40% and 80% (cyan squares), greater than 80% (magenta diamonds). Vertical dashed lines and shaded areas correspond to mean and standard error of breakpoints for segmented regression fit using the `segmented` package.

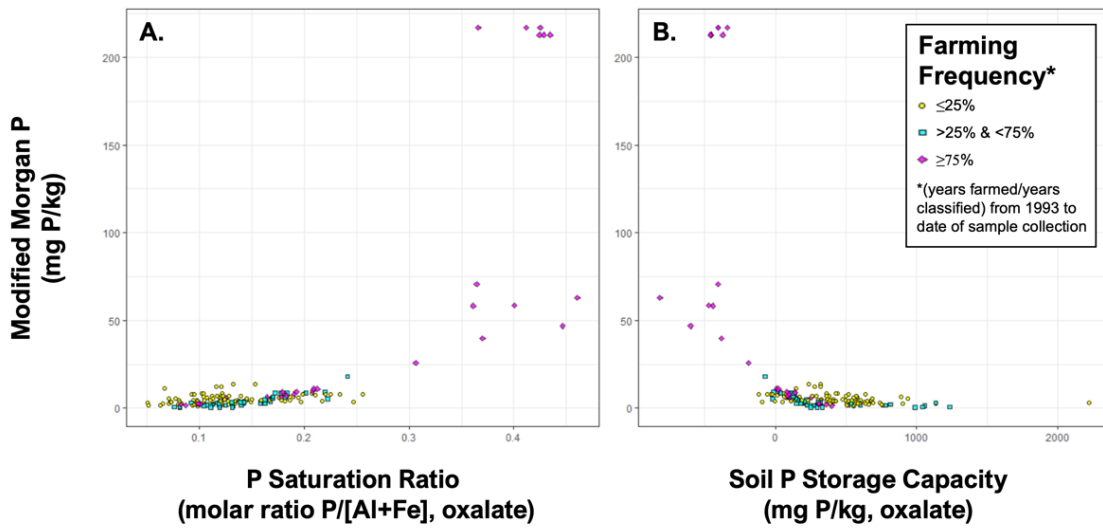


**Figure 1-3** Scatter plot of modified Morgan P (MM-P) versus Ox-PSR (A) and Ox-SPSC (B) with color and shape denoting different farming frequency groups.

**Table 1-1 Spearman rank correlation (r) matrix comparing bulk density weighted mean soil properties (0-10cm) for each sampling plot (n=42, unless specified otherwise). Variable names are listed on the top, left and diagonal of the matrix, variable definitions are given below the matrix. The upper right triangle shows the correlations significance code (\*0.05 > p ≥ 0.01, \*\*0.01 > p ≥ 0.001, \*\*\*0.001 > p), the lower left triangle shows r values. Negative r values are in red, positive are in black. Nonsignificant (p>0.05) correlations are left blank.**

Col	1	2	3	4	5	6	7	8	9	10	11	12	13	14	15	16	17	18	19
Row	FF	YSF	BD	LOI	sand <sup>§</sup>	silt <sup>§</sup>	clay <sup>§</sup>	WEP	<sup>†</sup> TP	<sup>†</sup> Pi	<sup>†</sup> Po	<sup>†</sup> Pi:TP	Ox-P	Ox-Al	Ox-Fe	<sup>‡</sup> PSR	MM-P	MM-Al <sup>ζ</sup>	MM-Fe <sup>ζ</sup>
1	FF	FF	***	***	***	**	*		**		***	**	***		*	***	*	**	
2	YSF	-0.94	YSF	***	***	*	*		*		**	*	***		*	**			
3	BD	0.75	-0.72	BD	***	**	*		*		***	***	***	***	**	***		*	
4	LOI	-0.5	0.5	-0.79	LOI	**	*	*		**	***	***	***	***	***	***	**		
5	sand <sup>§</sup>	0.68	-0.55	0.72	-0.76	sand <sup>§</sup>	***	*	***		***	***	***		**	*	**	**	**
6	silt <sup>§</sup>	-0.59	0.58	-0.55	0.54	-0.85	silt <sup>§</sup>		**		**	**	**				*	*	**
7	clay <sup>§</sup>			0.57	-0.54		clay <sup>§</sup>							***	*	*			
8	WEP	0.44	-0.37	0.38		0.8	-0.72		WEP		***		***	**		***	***	*	
9	<sup>†</sup> TP			0.42					<sup>†</sup> TP		***		***	***	***				
10	<sup>†</sup> Pi	0.52	-0.44	0.62	-0.54	0.77	-0.64		0.77		<sup>†</sup> Pi	**	***	**	*	***	***	*	
11	<sup>†</sup> Po	-0.4	0.38	-0.67	0.74	-0.83	0.71			0.77	-0.44	<sup>†</sup> Po	***	***	***	***	*		
12	<sup>†</sup> Pi:TP	0.57	-0.5	0.8	-0.75	0.82	-0.67		0.5		0.83	-0.75	<sup>†</sup> Pi:TP		***	*	***	*	
13	Ox-P							0.42	0.85	0.41	0.51		Ox-P	***	*	**			
14	Ox-Al			-0.57	0.57	-0.69		0.8		0.67	-0.34	0.84	-0.56	0.58	Ox-Al	***	*		
15	Ox-Fe	-0.39	0.37	-0.44	0.5	-0.53		0.64		0.54		0.65	-0.39	0.38	0.68	Ox-Fe	**		
16	<sup>‡</sup> PSR	0.54	-0.46	0.51	-0.44	0.72	-0.55	0.85		0.82	-0.36	0.66	0.42	-0.37	-0.42	<sup>‡</sup> PSR	***		
17	MM-P	0.35				0.69	-0.63		0.71		0.51		0.36			0.68	MM-P		
18	MM-Al <sup>ζ</sup>	-0.54		-0.4		-0.67	0.62		-0.46		-0.4						MM-Al <sup>ζ</sup>	***	
19	MM-Fe <sup>ζ</sup>					-0.64	0.76										0.65	MM-Fe <sup>ζ</sup>	

FF = farming frequency (y/y), YSF = years since farming, BD = bulk density (g cm<sup>-3</sup>), LOI = organic matter loss-on-ignition (g/g); WEP = water extractable P (mg P kg<sup>-1</sup>), Ox-X = acid ammonium oxalate X (mg X kg<sup>-1</sup>), MM-X = modified morgan X (mg X kg<sup>-1</sup>) § n = 15 for sand, silt, clay (%), † = HCl- (1M HCl extraction), ‡ Ox- (acid ammonium oxalate), ζ n = 26 for MM-Fe and MM-Al

### 1.3.3 Intact Core SRP Flux

Final SRP concentrations for sampling plots ( $\text{mg P L}^{-1}$ ) spanned evenly over two orders of magnitude, ranging from 0.02 to 1.8 and 0.055 to 2.01, respectively in the  $\text{O}_2$  and  $\text{N}_2$  treatments (Figure 1-4). Final SRP concentrations were higher on average in the  $\text{N}_2$  treatment than the  $\text{O}_2$  treatment with the percentage difference between the treatments decreasing with increasing final SRP. SRP concentrations in the intact cores increased throughout the experiment, with the rate of change declining over time as the water column approached an equilibrium SRP concentration with the soil (Figure 1-7 in Appendix). SRP flux rates ( $\text{mg m}^{-2} \text{ d}^{-1}$ ) over days 1 – 7 ranged from 1.6 to 225 and from 3.5 to 261, respectively in the  $\text{O}_2$  and  $\text{N}_2$  treatments. SRP flux rates calculated over days 0-14 were ~24% lower on average (mean) than over days 0-7, confirming that concentrations became more stable over time.

Modified Morgan P (MM-P), Ox-PSR, and Ox-SPSC were significantly correlated in the hypothesized directions with final SRP (see Table 1-3 in Appendix of Chapter 1). The top two best fitting predictors of final SRP were the Ox-[P:Fe] (power model) and Ox-SPSC (exponential model), both of which had nearly equivalent performance, with respective  $r^2$  of 0.67 and 0.66 (Figure 1-4). It seems that Ox-[P:Fe] had better correlation than Ox-SPSC with final SRP for soils with final SRP below 0.25 ( $\text{mg P L}^{-1}$ ) where dissolution of Fe-associated P may be a more important driver of SRP release. On the contrary, Ox-SPSC had better correlation than Ox-[P:Fe] at sites with higher final SRP above 0.25 ( $\text{mg P L}^{-1}$ ). After Ox-SPSC and Ox-[P:Fe], Farming frequency was the next best predictor ( $r^2=0.57$ , for exponential model) followed by the Ox-PSR ( $r^2 = 0.55$ , for power model) (Figure 1-4). The natural log of MM-P was a fair predictor SRP release ( $r^2=0.46$ ,  $p=9E-4$ ). Other soil variables had significant relationships with final SRP but had fair accuracy at best ( $r^2<=0.5$ ) (Table 1-3 in Appendix).

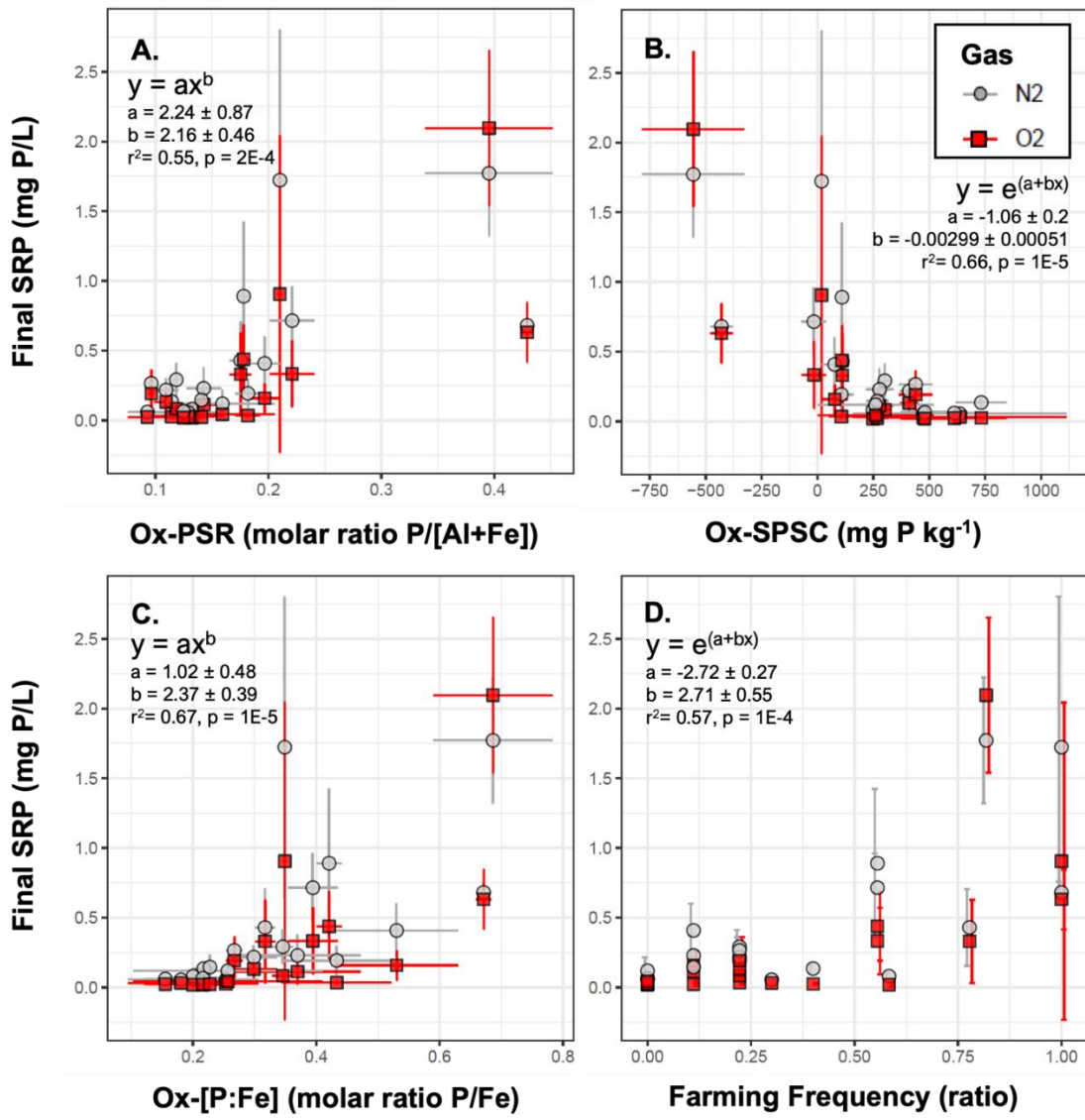


**Figure 1-4** Panel scatter plots showing of Final SRP (mean and SD of day 10 – 14) on the y axis against (a.) Ox-PSR, (b.) Ox-SPSC, (c.) Ox-[P:Fe] and (d.) Farming Frequency on the x axis. Grey circles = N<sub>2</sub> treatment, red squares = O<sub>2</sub> treatment. Vertical (y) and horizontal (x) bars are the standard deviation of mean estimates for a given variable at each sampling plot. The best fitting model and summary statistics are given in each plot.

## 1.4 Discussion

### 1.4.1 SRP Release, Soils and Farming Frequency

At the sites I sampled, more frequently and recently farmed soils tended to have coarser texture, lower organic matter, and greater amounts of inorganic P, resulting in higher PSR and lower SPSC than less frequently and less recently farmed soils (Figure 1-1). Concurrently I found higher SRP release in the intact cores of more frequently farmed soils and soils with high PSR and low SPSC (Figure 1-4). I found that intact core SRP tended to increase over time in intact cores and level off in the second week, indicating that SRP was approaching equilibrium. I also found that several soil variables correlate significantly to SRP Flux, with the strongest predictors being Ox-[P:Fe] and SPSC. While SPSC is commonly measured by researchers in Vermont, MM-P is much more widely measured on Vermont farms. MM-P was a fair predictor of SRP release. But MM-P was strongly and nonlinearly related to PSR and SPSC in soils with farming frequency >75% (Figure 1-3). In the future, MM-P could be used to estimate SPSC, PSR, and/or SRP release when oxalate data are unavailable. The use of MM-P to estimate PSR may be particularly helpful for parameterizing process models (see Chapter 3).

SRP flux declined exponentially with increasing time since farming and increased exponentially with increasing farming frequency. This is important because farming frequency for a given site was able to be accurately and reliably estimated by university students within minutes using free google software. Areal imagery classification was reliable for distinguishing between farmed and unfarmed sites and identifying row crops and woody areas. However, student classifications of farmed hay/pasture, unfarmed herbaceous, and unfarmed shrub cover types were unreliable. Therefore, I recommend that when soils data are absent, areal imagery classification be used to distinguish between farmed and unfarmed use at potential restoration sites and used to calculate farming frequency. The farming frequency metric, is simple, correlates with many soil properties and can predict SRP release with fair to good accuracy ( $r^2=0.57$ ), making it a useful a proxy metric for soil legacy P when soils data are not available.

While I saw a decrease in SRP flux with decreasing farming frequency and recency, sites that were farmed less than 80% and even 40% of the time still had potential to release substantial SRP, even when SPSC was above 0 and after over a decade after farming. This indicates historically farmed fields can release SRP for many years after farming stops and after wetland functioning returns. In fact, models I fit to my intact core data suggest that substantial SRP

release occur when SPSC is above 0 (Figure 1-4B), which is the threshold that has typically been used to distinguish between soils acting as P sinks vs. P sources (Nair et al., 2015).

I saw covariance observed between soil texture, organic matter, and farming recency and frequency. In this study, changes in soil properties attributable to farming history were confounded by changes in soil texture. Previous studies in Vermont have found similar patterns, wetlands and forests having finer soil texture than active cornfields within the same floodplain (Perillo et al., 2019; Young & Ross, 2016). Such patterns could be due to selective pressures that lead farmers to grow crops in only high elevation areas of floodplains where there is coarser textured soil with better drainage (Hudson et al., , 2006). Fine textured low-lying soils are more challenging for farmers to manage and tend to be as hayfields and pasture (Hudson et al., , 2006), which could be why those areas were restored and/or conserved earlier. Additionally, floodplain reconnection to stream channels can potentially lead to the trapping and accumulation of fine particles during flood events as well as the accretion of organic matter, altering surface soil properties (Noe et al., 2013). If so, it will be difficult to separate the effects of farming verses soil properties on SPSC with field studies. Nonetheless, I found a strong relationship between farming frequency and legacy P metrics across the sites I sampled.

PSR, inorganic P, and Modified Morgan P were all positively correlated with farming frequency and negatively correlated with years since farming. I attribute these relationships to several possible causes. (1) More recently farmed soils are more likely to have received recent input of organic amendments and/or P fertilizer. (2) Legacy P stocks are lost due to downstream transport and/or converted to stable forms of inorganic P and organic P over time. (3) Farm fields that are retired earlier also have conditions that promote higher SPSC and that also make farming more difficult, such as being inundated frequently and for long periods (and/or being poorly drained) allowing for accumulation of fine sediments and soil organic matter (both of which have high density of sorption sites).

Previous studies in Vermont have also found that soil properties relate to geographic metrics like soil drainage class and land use. Soils of poorer drainage class have been found to have finer texture and greater organic matter than more well drained soils, and actively farmed soils have been found to have greater soil P levels than unfarmed soil (Perillo et al., 2019; Young & Ross, 2016, 2018). A next step could be to conduct a meta-analysis using data from this chapter and others like it (e.g. Perillo et al., 2019) and test whether covariance between land use history and soil texture is also present. A parallel analysis could analyze the co-variability of soil

type and land use using state-wide geospatial data available in river corridors, such as NRCS soil survey units (NRCS, 2021), and the Croplands data layer (NASS, 2021).

If the patterns of soil texture among land use groups found state-wide reflect those found in existing soil studies (this chapter, Perillo et al., 2019; and others like it), then further steps could be taken to map SRP release based on widely available data by breaking SPSC into its component parts: P Saturation Ratio (PSR, Equation 1-1), and P Storage Maximum (PSM, Equation 1-3). A current example of this type of effort is given by Welikhe et al., (2020) who found significant relationships between PSM and more easily mapped soil variables like texture and organic matter in tile drained farm fields in Indiana.

In Vermont, areal imagery classification (e.g., this study) or the USDA croplands data layer (NASS, 2021) could be used to calculate farming frequency when the scale of analysis is case-by-case or statewide, respectively. NRCS soil survey data contains information on texture and drainage class that can be used to improve estimates of organic matter and soil texture from farming frequency (NRCS, 2021). Hydrologic metrics such as inundation depth, frequency, and duration that are being developed for floodplain segments across Vermont (Diehl et al., 2021; VTDEC, 2021). This hydrologic information could be incorporated along estimates of legacy P metrics to model the approximate impacts of floodplain management on net P balances using numerical models such as the one that I develop in Chapter 3.

#### **1.4.2 Intact Core Gas Treatments**

Intact soil core experiments have been used by a number of studies to approximate solute flux rates in wetlands and aquatic environments in laboratory settings (Anderson et al., 2018; Bhadha et al., 2010; Busse & Gunkel, 2002; Fisher & Reddy, 2001; Kinsman-Costello et al., 2014; Pant & Reddy, 2003; Roy et al., 2012; Upreti et al., 2019; Zak et al., 2017). With these experiments, temperature, light, oxygen availability, and hydraulics can be controlled to isolate the impacts of key mechanisms on the parameter of interest. Previous studies have used paired fully aerobic and anaerobic treatments in intact cores from the same location to establish lower and upper bound estimates for the effects of ferric metal reduction on P solubilization (e.g. Roy et al., 2012; Upreti et al., 2019). In this study, I use paired partially-aerobic and fully-anaerobic treatments to estimate a middle and upper bound flux rate.

During each 90 min purge cycle, the water columns of intact cores were being depleted of or saturated with dissolved oxygen (DO) for the 100% N<sub>2</sub> and 20% O<sub>2</sub> gas treatments,

respectively. The DO concentrations immediately after purging with gas were always below 0.4 mg/L (~5% atmospheric saturation) for the anaerobic treatment (purged 90 min/d with 100% N<sub>2</sub> gas) and were always above 8.4 mg/L (~90% atmospheric saturation) for the O<sub>2</sub> treatment (purged 90 min/d 20% O<sub>2</sub> room air). In the N<sub>2</sub> treatment, the mean DO of each intact core before sampling (~22.5 hrs after purging) averaged 0.6 mg/L and did not exceed 1.2 mg/L. In the O<sub>2</sub> treatment, mean DO before sampling averaged 5.6 mg/L, was as high as 7.67 and did not fall below 2.8 mg/L. I suspect that measured DO concentrations prior to sampling in the O<sub>2</sub> treatment relate to soil oxygen demand, with lower DO indicating higher soil oxygen demand (Smagin, 2018).

Given the range of DO concentrations I observed in the intact cores, some reduction of ferric metals was likely occurring in the soil during both treatments, however in the O<sub>2</sub> treatment reduced Fe could have precipitated upon reaeration of the water column each day, fixing SRP in the process. The DO regime in the O<sub>2</sub> treatment is comparable to conditions in shallow water ecosystems in the growing season, when diurnal cycling of photosynthesis and respiration add and remove DO from the water column (Reddy & Delaune, 2008). The DO regime in the N<sub>2</sub> treatment might more closely resemble winter when there is less sunlight for photosynthesis, temperature inhibits metabolism and growth of primary producers, and ice cover inhibits oxygen exchange from the atmosphere to floodwaters (see Chapter 2). The O<sub>2</sub> treatment is an estimate of the average potential soil to water SRP flux rate, while the N<sub>2</sub> treatment is an estimate for the maximum potential flux rate.

#### **1.4.3 Restoration and SRP Release**

My findings confirm that historically farmed wetland soils can release substantial amounts of SRP. The data from my intact core study and existing research indicates that hydrologic restoration and return to wetland functions in historically farmed site may promote solubilization of iron associated P (Aldous et al, 2007; Ardón et al., 2010; Hoffmann et al., 2012b). However, in my study the percent difference in SRP released in the anaerobic treatment compared to the aerobic treatment decreased as final SRP increased. In other words, soils that had the highest SRP release rates released large amounts of SRP regardless of soil redox conditions. It is also important to consider that historically farmed sites that are not hydrologically restored can still release substantial quantities of SRP, especially if they are subject to cycles of drought and re-wetting that promote rapid mineralization of microbial and colloidal P (S. Gu et al., 2018). SRP released from soil may not ultimately be exported downstream, especially if there is high

productivity of periphyton in the system (Dodds, 2003) and/or if water entering the system has the tendency to leave via evaporation rather than surface flow. Restoration projects designed to minimize SRP losses should promote water retention by including areas of near permanent ponding near outflows that have low risk of drying induced SRP release. It is critical to note that SRP release is only one flux influencing net P retention (Walton et al., 2020). Due to deposition of particle-bound P during floods, the net P balance of a wetland can still be positive even if a historically farmed site is releasing SRP (Audet et al., 2019), as I will show in Chapter 3.

## 1.5 Conclusions

In this chapter I examined how prior farming intensity and soil properties affect SRP release from riparian soils spanning restored wetlands to active farms. I established a threshold PSR needed to calculate SPSC, an important metric for estimating SRP release. I developed two metrics for farming history that are easily, accurately, and reliably calculated using free software. I found that these farming history metrics and soil properties including texture, organic matter, and metrics of legacy P (such as PSR and SPSC) were significantly correlated. These findings indicate that there is potential to map legacy P in Vermont from geospatial land use datasets. Future work should leverage existing geospatial datasets to examine relationships between soil texture and farming frequency. Such work could help inform efforts to map soil P storage capacity and SRP release in Vermont floodplains. For now, data and methods from this study can be used by land managers to evaluate SRP release risk on a site-by-site basis and select the appropriate restoration strategies in response.

The intact core experiment I conducted validates the use of SPSC for predicting the magnitude of potential SRP release in soils that are flooded for prolonged periods that allow anaerobic soil conditions to occur. High SRP release rates do not necessarily indicate that restoration will have negative impacts on downstream P loads and water quality. Soil potential SRP release rates are just one factor affecting net P balance in wetlands and floodplains. The net effects of management on sites with high legacy P should be evaluated contextually on a case-by-case basis, or using generalized modeling tools that adjust for local soil and hydrologic conditions. Examples of this are given in Chapters 2 and 3, where I further examine the various factors that influence net P retention.

## 1.6 Appendix

### 1.6.1 Supplemental Figures and Tables

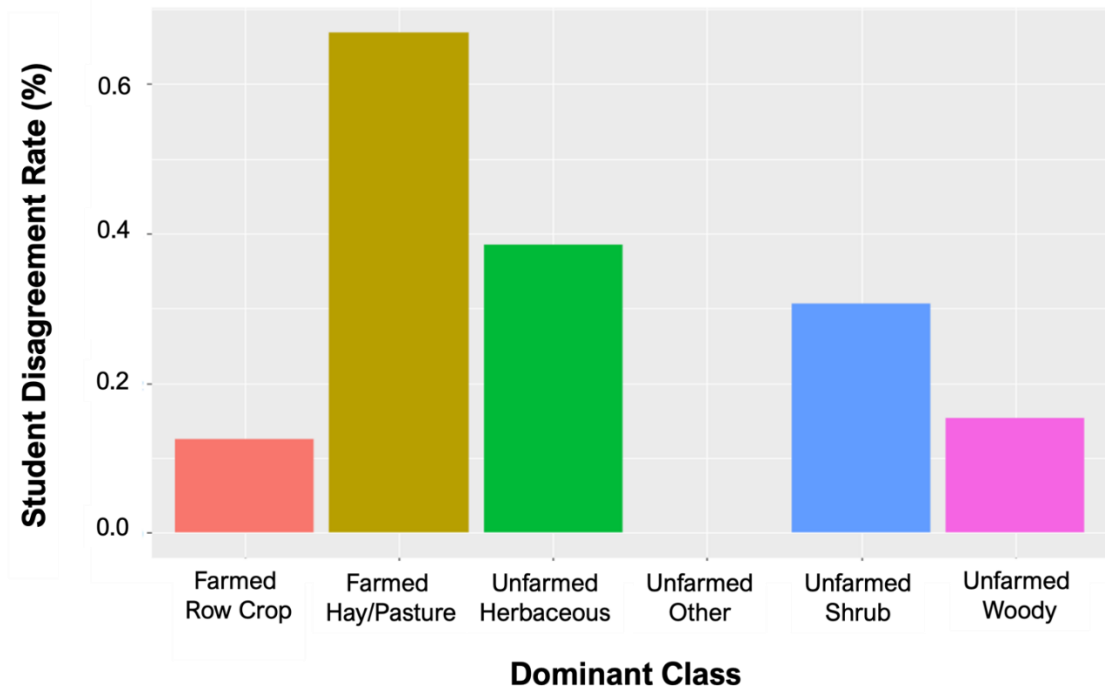


**Figure 1-5 Disagreement rate amongst student classified points by dominant class (the most frequently identified cover type).**

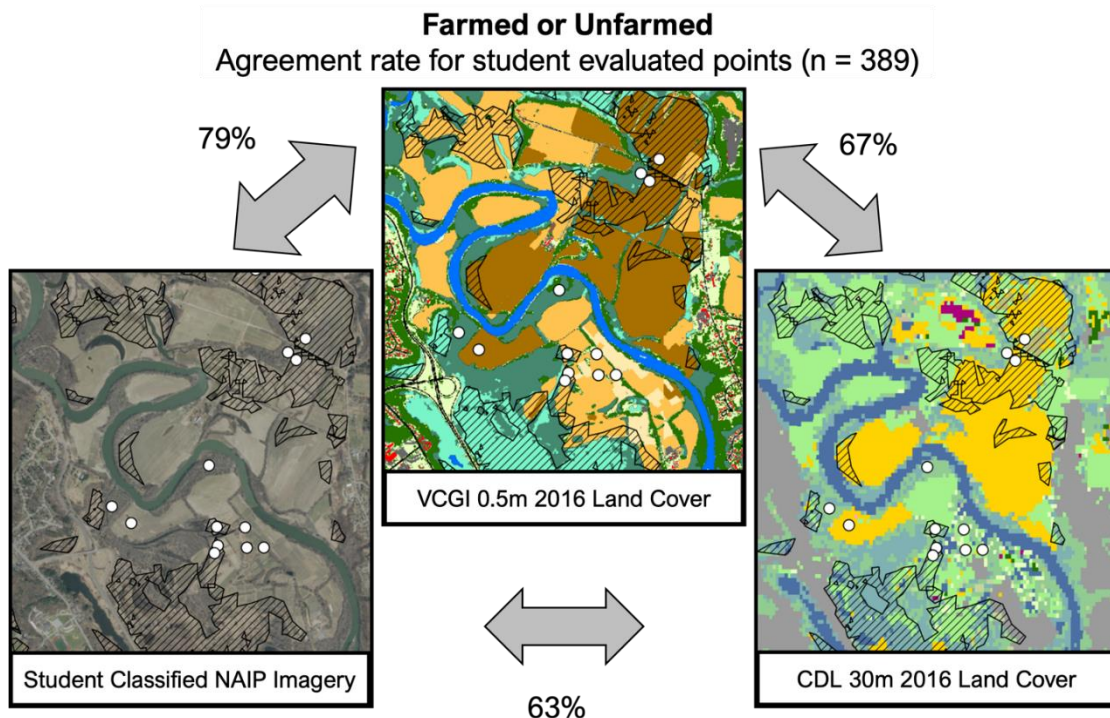


**Figure 1-6 Agreement rate for farmed vs unfarmed classification for all student evaluated points**

**Table 1-2 Average soil properties in the top 0-10cm soil layer for grouped by farming frequency. † sand and clay have respective n values of 6, 6, and 3; ‡ MM-Al and MM-Fe have respective n values of 12, 8, 6.**

Variable	Units	Farming Frequency Group		
		< 40% (n=23)	40% – 80% (n=13)	> 80% (n=6)
LOI	(g/g)	0.271 ± 0.21 a	0.104 ± 0.078 b	0.105 ± 0.046 b
clay	%	15.4 ± 6.4 a†	14.7 ± 12 a†	7.53 ± 4.1 a†
sand	%	8.29 ± 6.8 a†	16.2 ± 15 a†	40.3 ± 21 a†
HCl-[Pi:TP]	mass ratio	0.344 ± 0.18 a	0.518 ± 0.14 b	0.675 ± 0.31 b
Ox-Al	mg Al/kg	1980 ± 1000 a	1700 ± 1500 a	1190 ± 350 a
Ox-Fe	mg Fe/kg	4880 ± 2900 a	3800 ± 1400 a	2780 ± 1200 a
Ox-P	mg P/kg	554 ± 230 a	543 ± 220 a	700 ± 240 a
Ox-[P:Fe]	molar ratio	0.239 ± 0.1 a	0.263 ± 0.076 b	0.525 ± 0.26 b
Ox-PSR	molar ratio	0.12 ± 0.038 a	0.143 ± 0.04 b	0.263 ± 0.12 b
Ox-SPSC	mg P/kg	515 ± 460 a	329 ± 320 a	-75.7 ± 330 b
MM-Al	mg Al/kg	48.9 ± 25 a‡	37.8 ± 14 a‡	16.7 ± 9.6 b‡
MM-Fe	mg Fe/kg	61.6 ± 56 a‡	46.8 ± 47 b‡	13.9 ± 19 b‡
MM-P	mg P/kg	3.75 ± 2.2 a	3.9 ± 2.3 b	52.1 ± 82 b

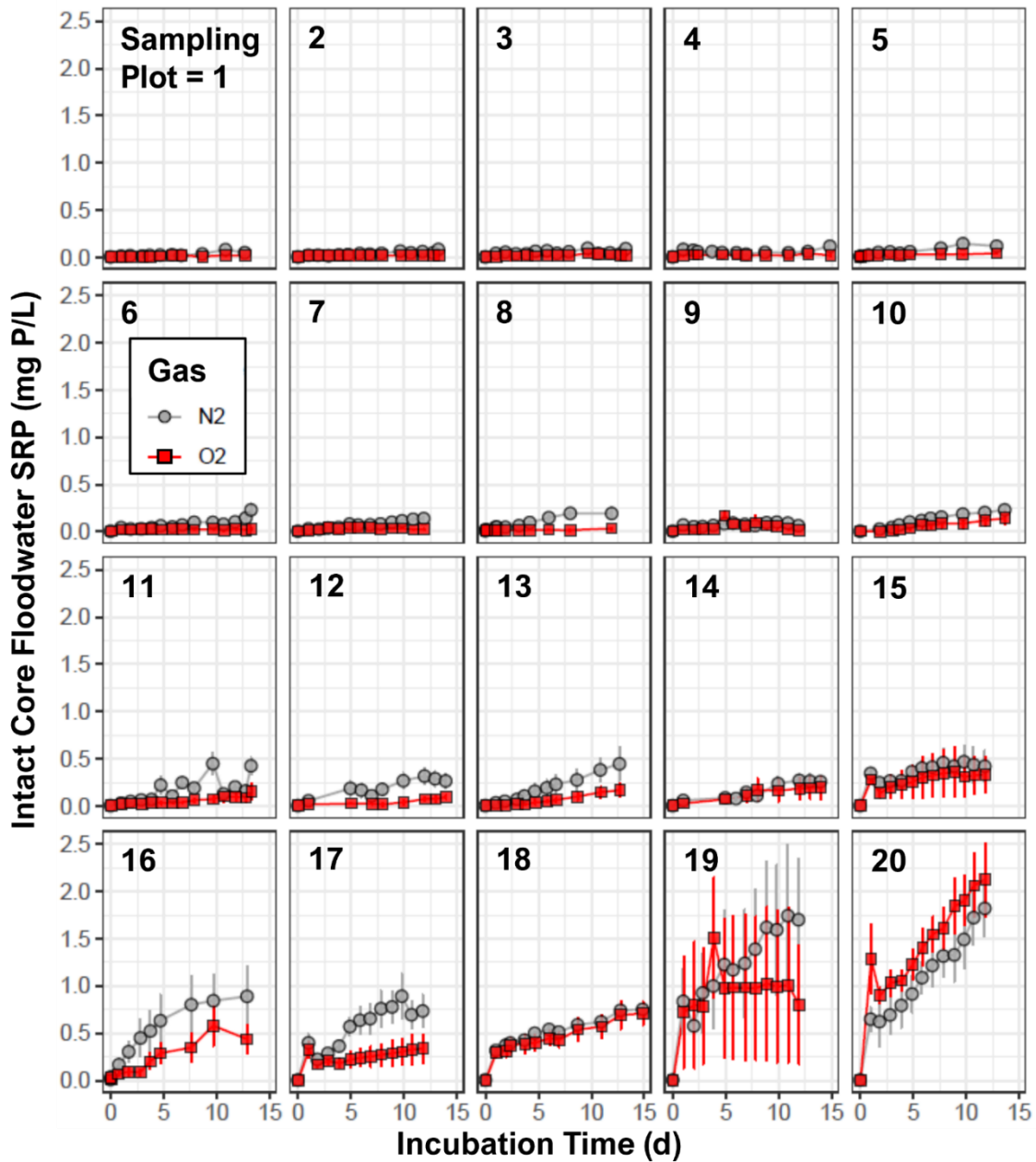


**Figure 1-7** Intact core incubation soluble reactive phosphorus (SRP) concentration over time for each site and plot, showing mean  $\pm$  1 standard deviation gas treatment, aerobic (O<sub>2</sub>) in red and anaerobic (N<sub>2</sub>) gas treatments in grey (n = 3 per plot per treatment).

**Table 1-3 Linear regression summary from the top 15 best fitting predictor (x) variables on the natural log of Final SRP (mean of both treatments at each sampling plot, n = 20). To translate the values in this table to final SRP (mg P L<sup>-1</sup>) use  $y = e^{\text{intercept} + \text{slope} \cdot x}$ . All models meet the assumptions of normality and homoskedasticity. Variables with the prefix “ln\_” were transformed using natural log. Homoskedasticity was verified with Breusch-Pagan test, and normality of residuals was verified with the Shapiro-Wilks test. Ox-P2Fe = Ox-[P:Fe], FF = farming frequency, YSF = years since farming**

x	r <sup>2</sup>	p	intercept	slope
ln_Ox-P2Fe	0.67	1E-05	1.02 ± 0.48	2.37 ± 0.39
Ox-SPSC	0.66	1E-05	-1.06 ± 0.2	-0.00299 ± 0.00051
Ox-P2Fe	0.62	4E-05	-3.86 ± 0.43	6.24 ± 1.2
FF	0.57	1E-04	-2.72 ± 0.27	2.71 ± 0.55
ln_Ox-PSR	0.55	2E-04	2.24 ± 0.87	2.16 ± 0.46
Ox-PSR	0.5	5E-04	-3.38 ± 0.43	9.44 ± 2.2
YSF	0.47	9E-04	-0.479 ± 0.38	-0.0853 ± 0.021
ln_MM-P	0.46	9E-04	-3.29 ± 0.44	0.744 ± 0.19
WEP	0.39	0.003	-2.15 ± 0.25	0.149 ± 0.044
ln_WEP	0.37	0.005	-1.72 ± 0.22	0.515 ± 0.16
ln_MM-P-ICP	0.31	0.011	-3.96 ± 0.81	0.797 ± 0.28
BD	0.3	0.012	-2.99 ± 0.5	2.46 ± 0.88
sand	0.26	0.023	-2.41 ± 0.36	0.0375 ± 0.015
ln_LOI	0.22	0.036	-3.16 ± 0.67	-0.804 ± 0.35
ln_BD	0.2	0.046	-1.01 ± 0.42	0.866 ± 0.4

### 1.6.1 Farming History of Wetland Restoration Candidates

I calculated the percent overlap of restoration sites with the 2016 Vermont agricultural land use layer by overlaying the parcels of the restoration candidates with land cover data from the Vermont Center for Geographic Information (VTADS, 2021), I calculated that 96% and 94% of restorable wetland area was farmed as recently as 1992 and 2016, respectively.

## **CHAPTER 2. PHOSPHORUS CYCLING IN RIPARIAN WETLANDS RESTORED ON FORMERLY DRAINED AND FARMED LAND IN THE VERMONT PORTION OF THE LAKE CHAMPLAIN BASIN**

### **Abstract**

Riparian wetland P balances are largely a function of particulate P capture (e.g., deposition of particle-attached P during floods) and internal soluble reactive P (SRP) loss (e.g., release of SRP from soils). It is very difficult to precisely measure net phosphorus (P) balances for riparian wetlands with field studies due to complex hydrology and internal biogeochemical cycling. In this Chapter, I applied several methods to gauge the magnitude of particulate P deposition and internal SRP loss in three restored riparian wetlands on former agricultural land in the Lake Champlain Basin. All three sites had not been farmed for over 10 years at the start of the study and fall into the category of low energy floodplains characterized by inundation from flood pulses lasting days to weeks. At wetland sampling plots, I observed inorganic sediment gain and decreased water column total suspended solids concentrations relative to the river/inflow, which indicated wetlands were effectively trapping particles. Inorganic P accretion (i.e., best estimate for mineral P deposited during floods) ranged from ~0.1 to ~1 g P m<sup>-2</sup> yr<sup>-1</sup> depending on site and elevation. Elevated SRP concentrations in wetland water columns relative to the river sources indicated internal SRP release from soils, and high frequency data indicated that factors such as temperature, dissolved oxygen, and primary production likely influence internal SRP dynamics.

### **2.1 Introduction**

Excessive phosphorus (P) loading to freshwater lakes and the resultant symptoms of eutrophication, including harmful cyanobacteria blooms, remains a critical environmental problem around the world (Chapra et al., 2017). In Vermont, the U.S. Environmental Protection Agency has established a total maximum daily load (TMDL) for the state's portion of the Lake Champlain watershed, which requires substantial reductions in P loading to the lake from non-point agricultural and urban sources (US EPA, 2015). Generally, created and restored wetlands tend to be net sinks of P due to high particle trapping, high primary productivity, and low decomposition (Walton et al., 2020). For this reason, floodplain wetland restoration is being considered as a strategy to reduce P loading to Lake Champlain (Singh et al., 2019). A potential issue is that most of the thousands of wetland restoration candidates in the region lay atop historically farmed soils that may contain “legacy P”, accumulated from additions of fertilizer and manure over time.

The surface water P budget in riparian wetlands on soils containing legacy P are primarily determined by two factors: particulate P gain and soluble P loss (Ready et al., 1999). Restoring hydric conditions on former agricultural land can potentially mobilize soil legacy P in dissolved forms, partially or completely offsetting the P retained via particle deposition (Hoffmann et al., 2009). However, little information is available to quantify this trade-off and mitigate it through site selection and design to maximize P retention benefits. Only a handful of the hundreds of studies dedicated to wetland nutrient retention examine restored riparian wetlands overlying historically farmed soils (Land et al., 2016b; Walton et al., 2020), and no such studies have occurred in the Lake Champlain Basin.

Previous studies of restored riparian wetlands overlying historically farmed soils have shown that hydrology, along with soil, vegetation, and land use factors contribute to considerable variability in nutrient retention efficiencies reported in the literature (Audet et al., 2020; Land et al., 2016b; Walton et al., 2020). In floodplains, hydraulic loading rate, river depth, velocity, and proportion of discharge that flows through floodplains are negatively correlated with P retention efficiency (Noe and Hupp, 2009; Venterink et al., 2003). Systems with deep fast-moving water can reduce P retention efficiency because (a) sediment particles tend to remain in suspension rather than being deposited, and/or (b) the constant flushing with river water maintains steep concentration gradients between soil porewater and overlying water leading to greater rates of soluble P flux from soils. The retention rate of TP and SRP tends to correlate positively to their respective influent concentrations (Johannesson et al. 2017; Noe & Hupp, 2009; Walton et al., 2020). Negative values for P retention were found in Danish alder fens that had high soil P concentrations due to agricultural legacies (Hoffmann et al., 2012b). In these systems, P retention was correlated with the soil equilibrium P concentration as determined by adsorption isotherms and the molar ratio of oxalate extractable P and Fe in soil (Hoffmann et al., 2012b).

Redox chemistry is an important factor affecting soluble P release from sediments. Lab and field studies on riparian wetlands of agricultural regions in France have shown that when the saturated soil of a wetland becomes anaerobic, the solubility of iron-phosphorus compounds and increases in pH lead to soluble P release from sediments (Gu et al., 2018; Gu et al., 2019). The timing of flooding has also been identified as an important factor affecting soluble P release from riparian wetlands, with wetlands releasing more P when re-wetting after prolonged dry periods (Gu et al., 2018).

The bulk of previous studies on wetland P mass balance have scaled their unit of analysis so that the system in question has clear inflow and outflow channels (Audet et al., 2020; Land et al., 2016b; Walton et al., 2020). But in Vermont floodplains, restoration is being done at the scale of individual farm fields, where flows during flooding are often unconfined by channels. Such complex hydrology necessitates the use of numerical models to estimate P mass balances and account for project benefits (Paudel & Jawitz, 2017; Preiner et al., 2020; Trentman et al., 2020). However, models need to be informed by field data on P cycling. Such data are lacking in historically drained and farmed riparian wetlands, especially in the northeastern United States.

Given current monitoring technology, complex hydrology and internal biogeochemical cycling in riparian wetlands make it impractical to precisely measure the rates of imported particulate P deposition and net export of SRP in the field (let alone net P retention). However, by looking at multiple lines of evidence, it is possible to gauge the approximate magnitudes of these fluxes and estimate the degree to which riparian wetlands are acting as P sources or P sinks. In this study, I applied an array of methods to assess evidence of particulate P deposition and internal SRP release in three wetlands through a 2-year field monitoring campaign by measuring P stocks in soil, water, and vegetation, as well as net fluxes among them, guided by the following research questions:

- (1) Is there evidence of particulate P deposition in the study wetlands?
- (2) Is there evidence of internal SRP release in the study wetlands?
- (3) What factors influence particulate P deposition and internal SRP release?
- (4) What combination of methods are most useful for estimating particulate P deposition and internal SRP release?

## 2.2 Methods

### 2.2.1 Study Area

I studied three historically farmed wetlands in the Vermont portion of the Lake Champlain Basin (Figure 2-1). The study sites occupy two common settings for potential wetland restoration candidates with a history of farming in the region. The ecosystems studied in this chapter fall in the category of low energy (low gradient) floodplain systems which are characterized by lentic (slow moving) waters and inundation time on the order of days to weeks for a given flood pulse.

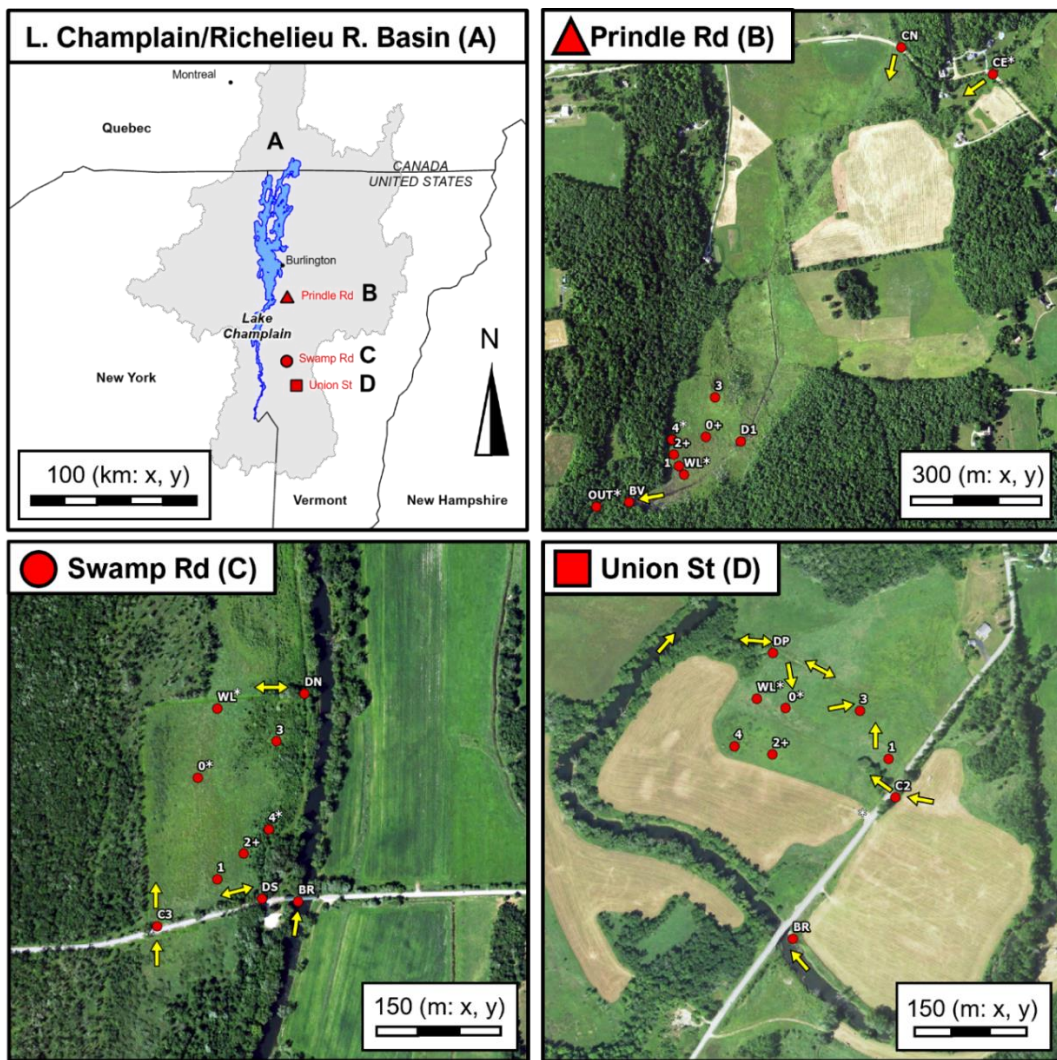


**Figure 2-1** Map of the Lake Champlain and Richelieu River basin (A, grey area) showing sampling plot locations at each of the three study sites at Prindle Rd (B), Swamp Rd (C), Union St (D). Yellow arrows indicate observed water flow directions. USDA national areal imagery color imagery from 2016; Plot label key: 0-4 = soil and vegetation sampling plots, C = culvert, D = drainage ditch, BR = bridge, + = ISCO 6712 automatic water samplers and miniDOT dissolved oxygen and temperature logger, \* = HOBO MX2100 water level logger.

One site was located along Prindle Brook, a small tributary of Lewis Creek near Prindle Rd in the Town of Charlotte at Lewis Creek Hill Preserve owned by The Nature Conservancy (Prindle Rd henceforth). The two other sites are located along Otter Creek which is the longest river draining to Lake Champlain in Vermont. One is located north of Swamp Rd and west of Otter Creek in the Town of West Salisbury at Otter Creek Swamps Preserve, owned by the Nature Conservancy (Swamp Rd henceforth). The other is north of Union St and east of Otter Creek in the Town of Brandon on an NRCS wetland reserve easement (Union St henceforth).

Prindle Rd is a headwater depression wetland that receives inflow from two first order streams from the northeast at two culverts that pass under Prindle Rd (Figure 2-1B). The site is underlain by a clay pan soil (NRCS hydrologic group D) and drains at a beaver dam near an outcropping of bedrock in the southwest. The Prindle Rd site drains a 2.5km<sup>2</sup> catchment of low intensity development, and low to moderate intensity agriculture. There are wetlands upstream of the culverts that drain into the Prindle Rd study area. The stream channel of Prindle Brook had been ditched and straightened to improve agriculture use in the 1960s and 1970s. Agriculture stopped within the sampling zone by 2006, and by my first site visit in 2018, beavers had recolonized the site and plugged the ditch with a dam that raised water levels ~1 to ~2 m above the eroded stream bed.

Otter Creek sites are in a large drainage area (HUC8) floodplain and show patterns of flow through ditches that reverse when the floodplain is filling or draining relative to the river. The Otter Creek sites are positioned 25km apart along an un-dammed reach of well-connected floodplain swamp that was once intensively ditched, logged and farmed, but now with help from conservation and restoration efforts the forest is regenerating. The Swamp Rd site was cleared and ditched for farming as early as 1942, farming stopped by 2003 (Figure 2-1C), and as of 2021 the ditches remain unplugged. The section of Otter Creek near Swamp Rd is characterized by annual flooding that ranges from weeks to months during the wet seasons (October through May). The floodplain at Union St is narrower and flood peaks are higher but shorter compared to the Swamp Rd downstream site (Trueheart et al., 2020). The sampling zone at Union St was ditched and farmed conventionally as early as 1942, by the late 1990s the site was used only as a hay field, and by 2004 the sampling zone was no longer being farmed. In 2018 a ditch plug was placed on the ditch of the northside of the sampling zone draining to Otter Creek (Eikenberry, personal communication).

To define the sampling zones within each site, I delineated a polygon that had uniform prior land use and perennial emergent vegetation based on available areal imagery in Google Earth Pro. I then removed areas from each sampling zone that were not likely to receive floodwater at-least once during the 2yr monitoring campaign. At the Otter Creek sites, the sampling zone was clipped with a polygon of the maximum inundation extent for the spring flood of 2018 (which was roughly a 1.5-year recurrence probability flood). The aforementioned polygon was produced by a 2D HEC-RAS model (Trueheart et al., 2020) of the Otter Creek floodplain between Rutland and Middlebury. I verified the model estimated flooding extent in the field in 2018 by examining the predicted flooding depth against the high-water mark on trees. At

Prindle Rd, I did not have a model to estimate the maximum flooding extent, so I collected GPS points of the flooding extent during the spring flood in May of 2019 and adjusted the sampling zone not to exceed the elevation of the high-water mark. At each site, I distributed 5 circular plots of 5m radius within each sampling zone along an elevation gradient based on 0.5m resolution LiDAR elevation data (VTADS, 2021). This was done by reclassifying the sampling zone at each site into five equal area pentile groups based on elevation, with each group accounting for 20 percent of the area inside the sampling zone. One sampling plot was randomly placed within each pentile. I also set up additional sampling plots for taking water samples from the river upstream of each site and at ditches and other likely water flow paths during flooding and draining. Figure 2-1 shows the location of sampling plots and instruments within each site.

## 2.2.2 Field Sampling and Laboratory Analysis

### 2.2.2.1 Soil

In July of 2019, duplicate soil samples (surficial 0-5 and 5-10cm, excluding surface litter) were collected from each plot in each system using 7-cm diameter polycarbonate coring tubes, transported to the lab in a cooler, and then stored at 4°C until processing. At the lab, 20-30g subsamples of each soil sample was analyzed for gravimetric moisture content by drying at 60°C (Reddy, et al. 2013), and additional subsamples were air-dried (25°C) for certain protocols. Dried subsamples were then sieved (<2mm), and a subsample of sieved soil was ground with a mortar and pestle. Dried, processed soils were sealed in water-tight polypropylene containers and stored in the dark at room temperature until further extraction and analysis.

Within the first week of sample collection, I extracted moist soils for water extractable P (WEP) [2g dry equivalent of field-moist soil in 20 mL DDI H<sub>2</sub>O extraction for 1h, analyzed for SRP]. Within one week of collection, I also initiated a sequential P fractionation that separates five operational fractions of soil P (Reddy et al. 1998; Roy et al. 2017) using 1-2 g field-moist soil samples: (1) readily available P [20 mL 2 M KCl extraction for 1h, analyzed for SRP], (2) Fe/Al-bound Pi [20 mL 0.1 M NaOH extraction for 17h, analyzed for SRP], (3) alkali extractable Po [= 0.1 M NaOH TP – 0.1 M NaOH-Pi], (4) Ca/Mg-bound Pi [20 mL 0.5 M HCl extraction for 24 h, analyzed for SRP] and (5) residual P [nitric acid digestion on residue from step 4, analyzed on ICP, Perkin-Elmer Avio 200 ICP-OES] (Richardson & Reddy, 2013). I calculated total P (frac-TP) as the sum of all five fractions, Organic P (frac-P<sub>o</sub>) as the sum of fractions 3 and 5, and inorganic P (frac-P<sub>i</sub>) as the sum of fractions 1, 2, and 4 (Figure 2-2).

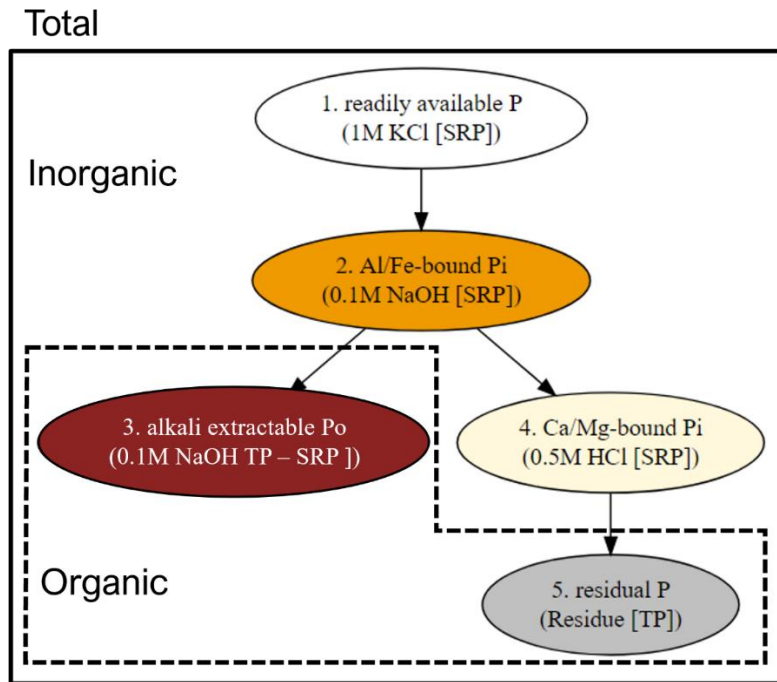


**Figure 2-2 Flow diagram of sequential P fractionation showing inorganic and organic pools.**

I determined oxalate-extractable forms of Al, Fe, Mn, and P (Ox-Al, Ox-Fe, Ox-Mn, Ox-P, respectively) by extracting air dried soil samples, 2mm sieved and ground, with acid ammonium oxalate for 3hrs in the dark following Courchesne & Turmel (2008). I diluted the extracts 5x in 0.1 M nitric acid before analysis by ICP. With data from the oxalate extraction, I calculated the molar ratio of P to Al (Ox-P:Al], and P to Fe (Ox-[P:Fe]), P saturation ratio (PSR, molar ratio of P to the sum of Al and Fe), P storage maximum (PSM), and soil P storage capacity (SPSC) following methods described in (Chapter 1). Total minerals, including P, Fe, Al, Ca, and Mg were determined using nitric acid microwave digestion following EPA method 3051 and analysis by ICP. Particle size analysis was run on 2mm-sieved air-dried soils after overnight dispersion in Calgon solution. Clay was determined by the hydrometer method (Bouyoucos, 1962; Day, 1965). Sand was determined gravimetrically by wet sieving to <53µm (sieve No. 270). Silt was calculated as the remainder. Particle sizes and texture class are from the USDA Soil Survey Manual (Soil Science Division Staff, 2017).

I conducted a three-pool parallel fractionation for total, inorganic, and organic P (Levy & Schlesinger, 1999; Richardson & Reddy, 2013) to compare with the five-pool sequential P fractionation described above. For total P (HCl-TP), 0.3g dried and ground soil subsamples were placed into pre-weighed borosilicate glass 15ml conical bottom extraction tubes then ashed and

reweighed to estimate organic content via loss on ignition (LOI, at 550°C for 4 hours). Ashed samples were then extracted with 15ml (1:50 m/v) of 1 M HCl for 16 hrs. For inorganic P (1 M HCl-P<sub>i</sub>), 0.3g dried and ground soil subsamples were placed in HDPE centrifuge tubes and extracted in the same fashion as for 1 M HCl-TP. Organic P (1 M HCl-P<sub>o</sub>) was calculated as the difference between 1 M HCl-TP and 1 M HCl-P<sub>i</sub>. Active-C was determined via analysis of permanganate oxidizable carbon following Culman et al. (2012), who refined the method of Weil et al. (2003).

I conducted batch incubations of phosphate sorption isotherms following Graetz & Nair (2009) to compare with metrics produced from the ammonium oxalate extraction described above. Briefly air dried, sieved soils were composited volumetrically at each plot and depth, then ~1g aliquots of soil were equilibrated for 24hrs in the dark at 4°C in 20ml of 0.01 M KCl solution with concentrations (C) of phosphate as KH<sub>2</sub>PO<sub>4</sub>: 0, 0.1, 0.5, 0.1, 1, 10, 75 mg P L<sup>-1</sup>. The amount of sorbed P (S) was calculated from the difference in concentration before and after each incubation. The initially sorbed P (S\_0) was determined as the y-intercept parameter to a linear regression fit of S and C, at values of C below 1 mg P L<sup>-1</sup>. The Equilibrium P concentration where net sorption and desorption equal zero (EPC-0) was determined by solving for y equals zero using the linear regression fit to S and C, at values of C below 1 mg/L. I used a nonlinear Langmuir model determine the bond energy (K<sub>L</sub>) and maximum P sorption (Smax) for the S-C relationship using all concentrations (Bolster & Hornberger, 2007). I also calculated a single point sorption index, that approximates Smax, from the 75 mg P L<sup>-1</sup> extraction (Roy et al., 2017).

Following extraction, I immediately centrifuged (4066 x g for 10 minutes) and filtered (0.45 µm) samples for WEP, P sorption isotherms, sequential, and parallel P fractionations into scintillation vials for frozen storage. For SRP measurements, I diluted samples with DDI H<sub>2</sub>O as needed and analyzed samples for SRP at 660 nm using a microplate reader (BioTek Synergy HT) following the malachite green method for colorimetric orthophosphate analysis (D'Angelo et al., 2001b; Ringuet et al., 2011).

### 2.2.2.2 Diffusion of SRP from soils

I estimated diffusive SRP movement between wetland soils and the overlying water column using a two-week incubation of intact cores under aerobic and anaerobic treatments (refer to Chapter 1 for the intact core sampling and incubation methods). Briefly, intact cores were collected from the low, average, and high elevation plots at each site, plot numbers 0, 2, and 4 respectively in Figure 2-1. Intact cores were topped with 20cm of filtered water (collected from

the adjacent stream) and incubated for two weeks. Each day technicians collected water samples (for SRP analysis) and measured temperature, pH, and dissolved oxygen (to confirm O<sub>2</sub> presence/absence) in the floodwater of each intact core.

### **2.2.2.3 Biomass**

In Early September 2019, I collected aboveground biomass (AGB) of herbaceous plants from triplicate 0.5 m x 0.5 m (0.25 m<sup>2</sup>) quadrats by clipping vegetation 1-2 cm above soil or water surface (Dunne et al., 2007). At the same time, belowground biomass was collected in each herbaceous sampling quadrat by collecting the top 10cm of soil with a 7-cm diameter core tube. Biomass samples were placed in a cooler for transport and stored at 4°C until processing, which occurred within 1 month of sample collection. Belowground biomass samples were wet sieved with tap water through a 1 Mm mesh to remove soil from roots and then dried at 60°C until constant weight (Dunne et al., 2007). Aboveground herbaceous biomass samples were clipped into 10cm pieces dried and weighed to determine dry mass per unit area (g m<sup>-2</sup>). Woody biomass stocks, if present, were estimated using allometric equations (Chojnacky et al. 2014) with data from stem counts and diameter measurements (at breast height for trees, 30cm for shrubs) conducted in July 2021. The herbaceous plant biomass collected in year 2019 was then analyzed for LOI and TP using methods described above for soil, TP content for woody biomass was estimated to be 750 mg kg<sup>-1</sup> based on literature values (Bedford et al., 1999; Cronk & Fennessy, 2001).

### **2.2.2.4 Litterfall and Litter Decomposition**

I estimated annual litterfall production by measuring the stock of end of season herbaceous biomass plus freshly fallen litter in triplicate at each plot. This was done by clipping standing herbaceous biomass to within 1-2 cm of the soil surface (Dunne et al., 2007), then also carefully collecting freshly deposited litter within each 0.25m<sup>2</sup> quadrat October of 2019 and 2020 (prior to flooding). Litterfall was transported, stored, dried, weighed and homogenized in the same fashion as aboveground biomass.

Litter mass decay and net P mineralization were estimated using a litterbag decomposition experiment. Briefly, litterbags were constructed from fiberglass window screen (20 cm x 20 cm; 2-mm mesh) and stainless-steel staples. Bags were filled with 10-20 g of dry clipped and homogenized litter and labeled with the site, plot, time increment and replicate. In late fall of 2019, five groups of triplicate litterbags were placed at each sampling plot by fastening

each to the soil surface with stainless steel landscaping staples (15 cm). Litterbags were retrieved in triplicate after incubating for periods of 0, ~100, ~150, ~250, and ~365 days (Chimney & Pietro, 2006). Retrieved litter samples were dried at 60°C for 72 hr and weighed to determine mass loss and analyzed for total P and organic content using the LOI and 1M HCl-TP method described above.

#### **2.2.2.5 Accretion**

Accretion is the vertical accumulation of material, including litter, detritus, and sediment, over the soil surface (Callaway et al., 2013). I measured accretion rates in the riparian wetlands using ceramic tiles (30.5 x 30.5 cm) (McMillan & Noe, 2017), three per plot placed in early October 2019. Accumulated sediment and litter were collected carefully from tiles and bagged during dry conditions in July of 2020. Accreted material was stored in pre-weighed and labeled zip-lock bags and then composite samples of accreted material were created (separately for tiles and feldspar). At the lab, live biomass and other inert contamination (plastic, tile debris) was removed, samples were dried at 60°C and weighed, and then analyzed for loss-on-ignition, total P (HCl-TP), inorganic P (HCl-P<sub>i</sub>), and organic P, following the 3-pool parallel P fractionation method described above for soils (Richardson & Reddy, 2013). Organic mass or P accretion was calculated from the difference between total mass or P accretion and inorganic mass or P accretion. I estimated mass or P in accumulated sediment and detritus (periphyton, invertebrates, etc.) by subtracting macrophyte from total mass or P accretion.

#### **2.2.2.6 Flood Monitoring**

I placed water level recorders at high and low elevation plots of each site (HOBO MX2001-04, Onset Computer). The water level recorders were housed inside vented PVC pipes and installed into the ground as shallow groundwater wells. The water level recorders had two pressure transducers separated by 5ft, which allowed for real time local correction for changes in atmospheric pressure. One pressure transducer was kept aboveground at the high elevation plot of each site and was used to calculate water levels if the water depth above the low elevation recorder exceeded 5ft. At the median elevation plot of each site, I placed optical dissolved oxygen and temperature loggers (miniDOT, PME) equipped with anti-fouling plates and an automated lens wiper (miniWiper, PME).

To capture dynamics of the initial flood pulse with high temporal resolution the median elevation plot of each site had one ISCO autosampler (Model 6712, Teledyne Technologies, Inc.)

that collected discrete water samples during the first 24 hrs of inundation. Due to drought conditions in 2020, I moved the ISCO at Prindle Rd from the median elevation plot (plot=2) to the lowest elevation plot (plot=0). ISCOs were programmed to collect floodwater samples hourly over 24 hrs after water levels exceeded 10 cm above the soil surface. The ISCOs were placed outside the perimeter of the sampling plot and were fastened 1.5 m above the sediment surface to a wooden frame. Each ISCO had a 25 ft suction-line and strainer that was held at 10 cm above the sediment surface at the center of the sampling plot. An actuator triggered sampling when water levels rose above the strainer (Model 1640, Teledyne Technologies, Inc.).

To capture the spatial variability of the initial flood pulse, each wetland sampling plot also hosted replicate USGS-designed first flush (passive siphon) samplers that collected floodwater samples upon inundation (Diehl, 2007). The siphon samplers consisted of a 1 L narrow mouth amber Nalgene bottle sealed at the top with a no. 7 two-hole rubber stopper. The stopper held a siphon made from copper tubing, and a vent tube made from vinyl tubing that enabled water flow into the bottle after water levels rose above the crest of the copper tubing. The siphons were fixed sideways, attached to a pole at each plot center, and were positioned to trigger when water exceeded 10 cm above the sediment.

To capture longer term dynamics across the sites, 1 L grab samples were collected from the river and inflow and outflow channels at each site, as well as at all wetland plots (5 per site) on the rising and falling limbs of flood events. To collect grab samples, wide mouth amber Nalgene bottles were attached to an extendable pole fitted with hose clamps. Water temperature, dissolved oxygen ( $\text{mg L}^{-1}$ ), oxidation reduction potential (mV), specific conductivity ( $\mu\text{s cm}^{-1}$ ) and pH were recorded each time a grab sample was taken using a YSI Professional Plus. Each YSI parameter was calibrated daily before each sampling trip and verified with a reference solution. During the three flood pulses that were captured by ISCOs, the sites were monitored daily during the rising limb of floods or until ISCO programs had finished, this allowed collection of each sample within the U.S. EPA recommended maximum hold time for SRP of 24hrs (O'Dell, 1993).

All water samples were stored on ice during transport and processed immediately at the University of Vermont Aiken Forestry Sciences Lab. Subsamples of 5 mL volume were filtered ( $0.45 \mu\text{m}$ ) and frozen until analysis for SRP, while subsamples of 20 mL volume were pipetted into pre-cleaned (acid washed, and 3x rinsed with DDI  $\text{H}_2\text{O}$ ) 60 mL borosilicate glass digestion vials and stored in the dark at room temperature for digestion and analysis of total P (TP). The

remaining water samples were analyzed for total suspended solids (TSS), as well as mineral and organic fractions of TSS based on ignition at 550°C (Roy et al., 2016). SRP was analyzed at 660 nm using a microplate reader (BioTek Synergy HT) following the malachite green method for colorimetric orthophosphate analysis (D'Angelo et al. 2001; Ringuet et al. 2011). TP samples were digested following the alkaline persulfate digestion (Patton & Kryskalla, 2003), and analyzed using colorimetric orthophosphate analysis at 880 nm on a Lachat QuickChem 8500 using the ascorbic acid method for molybdenum blue (Murphy & Riley, 1962).

### 2.2.3 Calculations and Statistics

I calculated stocks of P in soil, biomass, litter, and accreted material by multiplying the mass stock by P content of the material for a given P pool (Equation 2-1).

#### Equation 2-1

$$P_x = C_x * M_x$$

where,  $P_x$  is the stock of phosphorus contained in material X (e.g., g P m<sup>-2</sup>),  $C_x$  is content of P per dry unit material X (e.g., g P g<sup>-1</sup> dry soil), and  $M_x$  is dry mass stock of material X (e.g., g dry soil m<sup>-2</sup>). For water, P stock was calculated as the product of P concentration (e.g., mg P L<sup>-1</sup>) and water volume (e.g., L).

Flux rates (e.g., litter decomposition, accretion) were calculated as change in mass or P stock between two time points. Flux rates of P in the water column were quantified as the difference in water column P stocks between time increments, divided by the change in time (Fisher & Reddy, 2001; Roy et al., 2012). It is important to note that rates measured in this chapter are net fluxes that represent the difference between additive and subtractive processes. For soil, biomass, litter, and accreted material stocks, I calculated summary statistics (mean, standard deviation), at the plot level by averaging replicates for a given plot, and at the site level by averaging means for all 5 wetland sampling plots. Because the sampling plots were distributed randomly within equal area elevation percentile bins at each site, site level averages from sampling plots represent estimates of spatially weighted averages across the entire sampling zone. I examined correlations amongst different P stocks across all sites using Spearman rank correlation tests. Additionally, I assessed patterns in soil properties, P flows, and P stocks along elevation gradients in each site by performing Spearman rank correlation tests and multiple regression with hydrologic metrics, including fraction of time inundated (ind) and the 90<sup>th</sup> and 99<sup>th</sup> percentile flooding depth (D90%, D99%, respectively). I compared site-level spatially

weighted mean P stocks and fluxes for soil, biomass, litter, and accreted material using the non-parametric Kruskal-Wallace test, followed by a Dunn (1964) post-hoc test with Bonferroni adjustment for family-wise error rate using the `dunn.test` package in R (Dinno, 2017).

For analysis of field water quality data, I classified the water samples based on three categories: the site, the sample origin (inflow/outflow, river, or wetland), and the condition (filling or draining). At Prindle Rd, samples were classified as inflow if they were collected at the culverts along Prindle Rd and samples were classified as outflow if they were collected from below the beaver dam. At Otter Creek sites (Swamp Rd and Union St), samples were classified as having river origin if they were collected in the river or from ditches when the flow was from the river into the wetland. Samples that were not classified as river, inflow or outflow were defined as having wetland origin. Samples were classified as having the condition of filling if the rate of change in the water level was positive and classified with the condition of draining if the rate of change in the water level was negative. I determined differences in water quality parameters (TSS, ISS, OSS, DO, pH, ORP, SPC, SRP, TP) among the following groupings: (first) origin only, (second) origin and condition, (third) site and origin, and (fourth) site, origin, and condition, using the Dunn method for the Kruskal-Wallace test with Bonferroni p-value adjustment using the `dunn.test` package in R (Dinno, 2017). I also fit simple linear regressions to water quality parameters. I used a test-statistic of 0.05 as the significance threshold in all statistical tests. Throughout the paper I use the following significance codes: \* $0.05 > p \geq 0.01$ , \*\* $0.01 > p \geq 0.001$ , \*\*\* $p < 0.001$ . All calculations and statistics were performed using R version 4.0.3 (R Core Team, 2020).

## 2.3 Results

### 2.3.1 Soil Analyses

The soil properties of the study sites shared many similarities. The three sites did not differ in levels of soil moisture (MC), bulk density (BD) and organic matter (LOI) in both soil layers (Table 2-1). Site-wide averages in the 0-5cm layer ranged from 57% to 67% for MC, 0.32 to 0.38 g cm<sup>-3</sup> for BD, and 22% to 30% for LOI. The soil layers differed in some cases in terms of MC, BD, and LOI, with lesser MC, greater BD, and lesser LOI in the 5-10 cm layer compared to the 0-5 cm layer (differences especially pronounced for Prindle Rd). Flooding depth was well correlated to each of MC, BD and LOI at each study site.

Soil aluminum (Al) and iron (Fe) can play important roles in wetland P cycling. There were significant differences in the levels of total and oxalate extractable Al and Fe between sites, notably Al-3051a, Fe-3051a, and Ox-Fe (Table 2-1). Union St had significantly lower levels of total Al (Al-3051a = ~20 g Al kg<sup>-1</sup>) compared to Prindle Rd (Al-3051a = ~29 g Al kg<sup>-1</sup>). At Swamp Rd, Al-3051a was slightly higher than Union St and lower than Prindle Rd, but not significantly different from either site. At Union St, both total and oxalate extractable Fe were greater than at Swamp Rd and Prindle Rd (Table 2-1).

The sites did not differ significantly in terms of mean inorganic P (HCl-P<sub>i</sub>), organic P (HCl-P<sub>o</sub>), or total P (HCl-TP). HCl-P<sub>i</sub> (mg P kg<sup>-1</sup>) ranged from 313 to 396 and did not differ by site or sample depth (0-5cm vs 5-10cm). HCl-P<sub>o</sub> (which ranged from 476 to 861, mg P kg<sup>-1</sup>) and HCl-TP (which ranged from 788 to 1260, mg P kg<sup>-1</sup>) differed in some cases by depth within sites but did not differ significantly between sites for either soil depth layer. The two Otter Creek sites both had similar levels of oxalate extractable P (Ox-P, mg P kg<sup>-1</sup>) near ~600, which were greater than at Prindle Rd at ~400 (Table 2-1).

Soil P in both 0-5 cm and 5-10 cm layers was mostly contained within organic fractions, with the relative size of NaOH-Po versus residual P varying across sites (Figure 2-3). The relative proportion in residual P pool was greater at Lewis Creek compared to the two Otter Creek sites. For most plots, the 0.5 M HCl-P<sub>i</sub> pool from the sequential fractionation, which has been operationally defined to contain primarily Ca- and Mg-bound P, was the largest inorganic P pool. However, the NaOH-Pi pool, which contains Al- and (redox sensitive) Fe-associated P was also prominent at the two Otter Creek sites, especially at lower elevation plots. The sum of P fractions with the most potential to eventually become bioavailable (Exchangeable P + NaOH-Pi + NaOH-Po) as a percentage of frac-TP, equaled 29±18% and 30±21% at Prindle Rd, 50±8.1% and 52±11% at Union St, and 54±7.6 % and 53±4.6% at Swamp Rd, in the 0-5cm and 5-10cm layers, respectively.

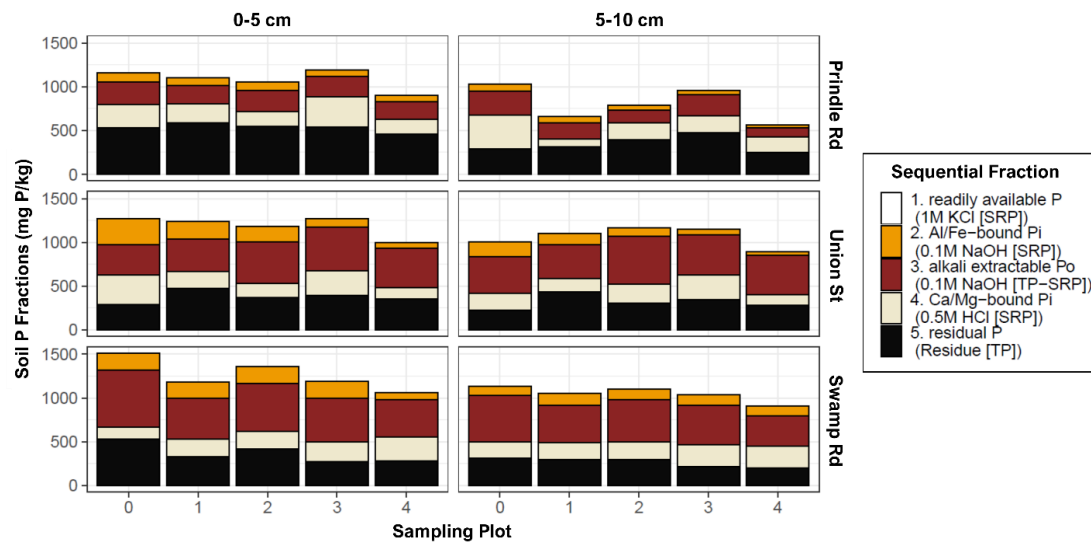


**Figure 2-3 Soil P fractions of soil at each sampling plot faceted by depth (columns) and site (rows). Fraction 1, readily available P (1 M KCl [SRP]), is smaller than the minimum plotting resolution.**

Plot-level mean total P estimated by the sum of all sequential P fractions (frac-TP, mg P kg<sup>-1</sup>) ranged from ~900 (Prindle Rd, plot 4) to ~1500 (Swamp Rd, Plot 0) and ~560 (Prindle Rd, plot 4) to 1160 (Union St, plot 2) for the 0-5 cm and 5-10 cm layers, respectively. There was some evidence of increasing total P with decreasing elevation (multiple regression on frac-TP vs. D99% and site, adj- $r^2 = 0.43, p = 4.2\text{E-}7$ ). The three methods used to measure soil total P (frac-TP, 1 M HCl-TP, and 3051a-TP) were in good agreement (see Figure 2-11 in Appendix). The sum of organic pools in the sequential fractionation (frac-P<sub>o</sub>) correlated well with organic P estimated using the 3-pool parallel fractionation (1 M HCl-P<sub>o</sub>) ( $y=0.994x + 24.6, r^2 = 0.67, p = 4\text{E-}17$ ). Similarly, the total inorganic P estimated by the sequential (frac-P<sub>i</sub>) and parallel (1 M HCl-P<sub>i</sub>) schemes generally aligned well ( $y = 0.647 + 147, r^2 = 0.52, p = 7.9\text{E-}11$ ), however, the regression fit deviated significantly from a 1:1 line even after removing outliers and leverage points (Figure 2-11). This suggests that the 1 M HCl-P<sub>i</sub> method might overestimate inorganic P in some cases, especially when present in relatively low amounts.

The P stock in the top 0-10 cm of soils averaged on the order of ~50 g P m<sup>-2</sup> at each site (Table 2-3 in Appendix). Stocks of soil TP (g P m<sup>-2</sup>) were  $44.4 \pm 10.5$  at Prindle Rd,  $52.3 \pm 10.9$  at Union St, and  $53.7 \pm 13.6$  at Swamp Rd. At each site, organic P made up most of the TP stock. The difference in TP stocks between Prindle Rd and the Otter Creek sites was explained by Prindle Rd having 20% lower stocks of HCl-P<sub>o</sub> than the Otter Creek sites. Of the Otter Creek

sites, Swamp Rd and Union St had similar stocks of TP but were differentiated by Swamp Rd having slightly higher stocks of HCl-P<sub>i</sub> despite having similar or lower stocks of HCl-P<sub>o</sub>.

### 2.3.2 Diffusion of SRP from soils

SRP flux rates ( $\text{g P m}^{-2} \text{ d}^{-1}$ ) ranged from 0.002 for the intact aerobic treatment at the plot 2 of Union St to 0.031 for the anaerobic treatment at plot 2 of Swamp Rd (see Table 2-2 in Appendix of). In all cases the anaerobic treatment (cores purged 90 min/d with 100% N<sub>2</sub>) yielded higher flux rates than the aerobic treatment (cores purged 90 min/d with 20% O<sub>2</sub>). For the anaerobic treatment, Swamp Rd had the highest SRP flux rates ( $\text{g P m}^{-2} \text{ d}^{-1}$ ) at ~0.023, followed by Prindle Rd at ~0.02, then Union St at ~0.006. For the aerobic treatment, Prindle Rd had the highest flux rates ( $\text{g P m}^{-2} \text{ d}^{-1}$ ) at ~0.009, followed by Swamp Rd at ~0.006, then Union St at ~0.003. SRP flux was correlated to some soil properties for the 0-5cm soil layer. The anaerobic SRP flux rates correlated significantly and most strongly with the molar ratio of oxalate extractable P to Fe (Ox-[P:Fe],  $r = 0.97, p = 0.00017$ ), followed by Ox-SPSC ( $r = -0.82, p = 0.011$ ) and Ox-Fe ( $r = -0.72, p = 0.037$ ). Anaerobic flux rates did not have significant correlations with WEP, Ox-[P:Al], Ox-PSR, S<sub>max</sub>, K<sub>L</sub>, or EPC<sub>0</sub>. Aerobic SRP flux rates were significantly correlated only with Ox-Fe 0-5cm ( $r = -0.72, p = 0.037$ ).

### 2.3.3 Vegetation Biomass

Aboveground woody biomass was not present at any of the Prindle Rd plots but was present at high elevation zones of the Otter Creek sites. Woody biomass was present at plot 4 of Union St, which was dominated by *Salix spp.* (willow). Union St site average dry mass of woody biomass was on the order of 362 ( $\text{g dw m}^{-2}$ ), with stocks of woody biomass P around  $0.27 \pm 0.09$  ( $\text{g P m}^{-2}$ ) (Table 2-3). At Swamp Rd, woody biomass was present at plots 3 and 4, and comprised of *Fraxinus pennsylvanica* (green ash), *Acer rubrum* (red maple), and *Acer saccharinum* (silver maple). Swamp Rd site average dry matter stocks of woody biomass ~17,500 ( $\text{g dw m}^{-2}$ ) and P stocks of woody biomass were  $\sim 13.1 \pm 4.4$  ( $\text{g P m}^{-2}$ ). Across all sites, the aboveground herbaceous biomass TP stock ranged from ~0.4 – 1.25  $\text{g P m}^{-2}$  and was greatest at Union St, followed by Swamp Rd and then Prindle Rd. The stocks of TP in belowground biomass ( $\text{g P m}^{-2}$ ) were greatest at Union St at  $2.20 \pm 1.58$ , followed by Prindle Rd at  $1.31 \pm 0.45$ , then Swamp Rd at  $1.03 \pm 0.51$  (Table 2-3).

### 2.3.4 Litterfall and Litter Decomposition

Litterfall production, collected in Fall 2019, was on average  $\sim 400 \text{ g dw m}^{-2} \text{ y}^{-1}$  and did not differ significantly between sites (Table 2-3). The corresponding P stocks ( $\text{g P m}^{-2}$ ) at Prindle Rd, Union St, and Swamp Rd were  $0.6 \pm 0.4$ ,  $0.47 \pm 0.18$ , and  $0.61 \pm 0.32$ , respectively. For samples collected in Fall 2020, litterfall production ( $\text{g dw m}^{-2} \text{ y}^{-1}$ ) was  $419 \pm 220$  at Prindle Rd,  $795 \pm 324$  at Union St, and  $559 \pm 212$  at Swamp Rd, resulting in greater litter P stock estimates for the two Otter Creek sites in 2020 compared to 2019.

Litter bags were incubated at the sampling plots for a maximum of 297, 351, and 354 days at Prindle Rd, Union St, and Swamp Rd, respectively. The percent mass loss over that period was  $56.1 \pm 16\%$ ,  $71.4 \pm 20\%$ , and  $61.7 \pm 14\%$  at Prindle Rd, Union St, and Swamp Rd, respectively. The litter TP content ( $\text{mg P kg}^{-1}$ ) decreased markedly over the first incubation period in the winter, then increased or stayed constant in each successive incubation period at each site (Figure 2-4). Final litter TP stocks were highest at Union St, followed by Swamp Rd, and Prindle Rd. The ratio of HCl-P<sub>i</sub> to HCl-TP (HCl-[P<sub>i</sub>:TP]) for litterbags decreased on average at all sites from a mean of  $0.55 \pm 0.12$  initially to  $0.23 \pm 0.09$  at the end of the last incubation period, with HCl-P<sub>i</sub> significantly increasing relative to HCl-TP at higher elevation plots after adjusting for incubation time (multiple regression on HCl-[P<sub>i</sub>:TP] vs. incubation time and D99%,  $p=0.008$ ,  $r^2=0.77$ ).

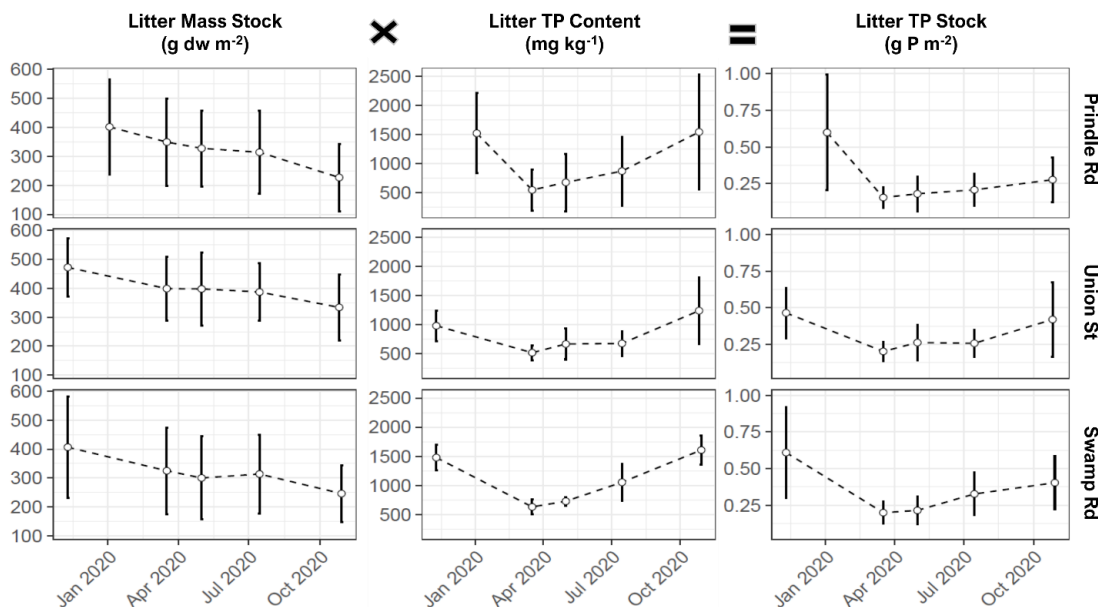


**Figure 2-4 Site level averages for litter stocks over time estimated from the litterbag decomposition experiment, with (A) stock of dry mass, (B) total P content of litter, and (C) stock of total P. Error bars denote standard deviation.**

### 2.3.5 Accretion

Dry mass accretion rates ranged from 200 to 600 g dw m<sup>-2</sup> and were positively correlated with flooding depth (Figure 2-5a,  $r^2 = 0.27$ ,  $p < 0.05$ ). Macrophyte litter made up a substantial fraction of accreted mass at 180 – 500 g dw m<sup>-2</sup> and was not significantly correlated with flooding depth (Figure 2-5b,  $r^2 = 0.06$ ,  $p = 0.36$ ). The mass of sediment and detritus – estimated as the difference between total accretion and litter – ranged from 0 to 400 g dw m<sup>-2</sup> and was positively correlated with flooding depth (Figure 2-5c,  $r^2 = 0.31$ ,  $p < 0.05$ ). Inorganic mass accretion ranged from 50 to 200 g dw m<sup>-2</sup> and was well correlated with flooding depth (Figure 2-6b,  $r^2 = 0.48$ ,  $p < 0.01$ ). Organic matter accretion ranged from 200 to 500 g dw m<sup>-2</sup> and was not correlated with flooding depth (Figure 2-6c,  $r^2 = 0.05$ ,  $p = 0.4$ ). Despite having similar magnitudes, accretion rates of organic matter and macrophyte litter were not correlated ( $r^2 = 0.01$ ,  $p = 0.66$ ).

The rate of total P accretion ranged from 0.25 to 1.7 g P m<sup>-2</sup> and was highly and positively correlated with flooding depth (Figure 2-5d,  $r^2 = 0.81$ ,  $p < 1e-5$ ). Macrophyte litter P in accreted material, ranging from 0.1 to 0.5 (g P m<sup>-2</sup>), was positively correlated with flooding depth (Figure 2-5e,  $r^2 = 0.6$ ,  $p < 0.001$ ), but it made up a relatively small amount of total P accretion. Sediment and detritus made up most of the stock of total P in accreted material (0 to 1.25 g P m<sup>-2</sup>) and was highly and positively correlated with flooding depth (Figure 2-5f,  $r^2 = 0.80$ ,  $p < 1e-5$ ). Both inorganic and organic P accretion had similar magnitudes, 0.05 – 1.1 and 0.2 – 1 g P m<sup>-2</sup>, respectively, and were positively correlated with flooding depth (Figure 2-6e and f,  $r^2 = \sim 0.6-0.7$ ,  $p < 0.0001$ ).

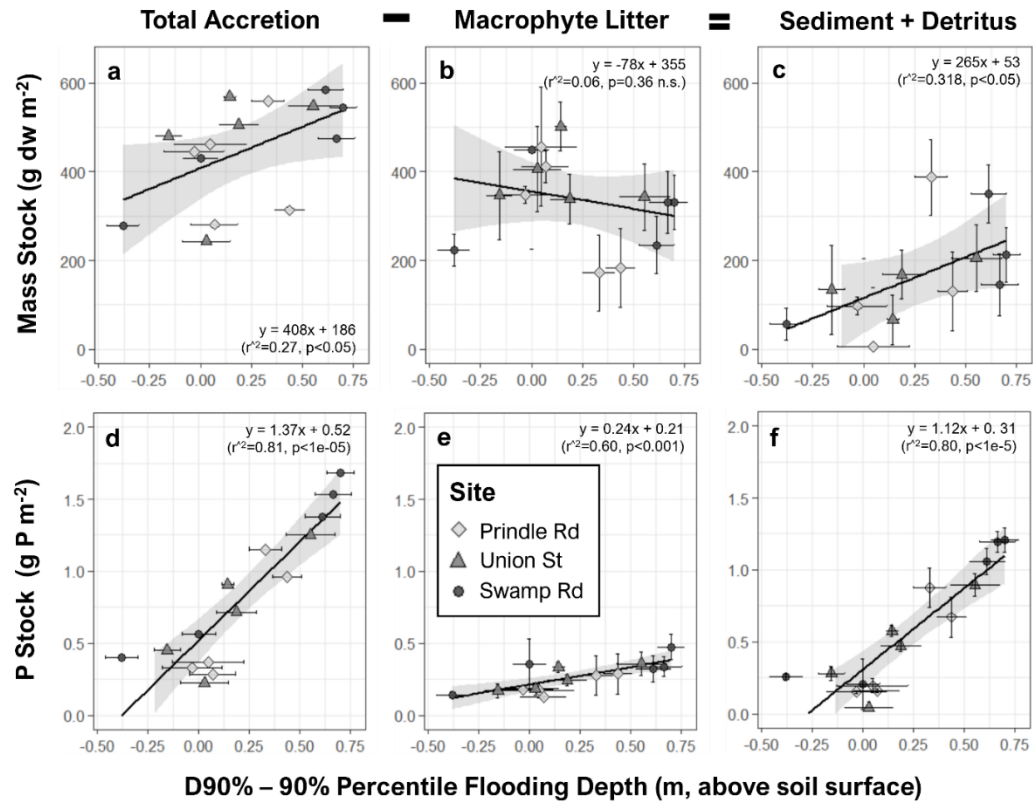


**Figure 2-5** Accretion (including litter, sediment and detritus) over ceramic tiles plotted against fraction the 90% percentile flooding depth for each site, showing mass stocks (top row), P stocks (bottom row) for total accretion (a & d), macrophyte litter (b & e) and sediment and detritus (c & f). Sediment + detritus is calculated as the difference between total accretion and macrophyte litter. Black bars around points indicate standard deviation. Black lines and shaded areas show best fit lines for regressions, fit statistics are given on the top right of each sub-plot.

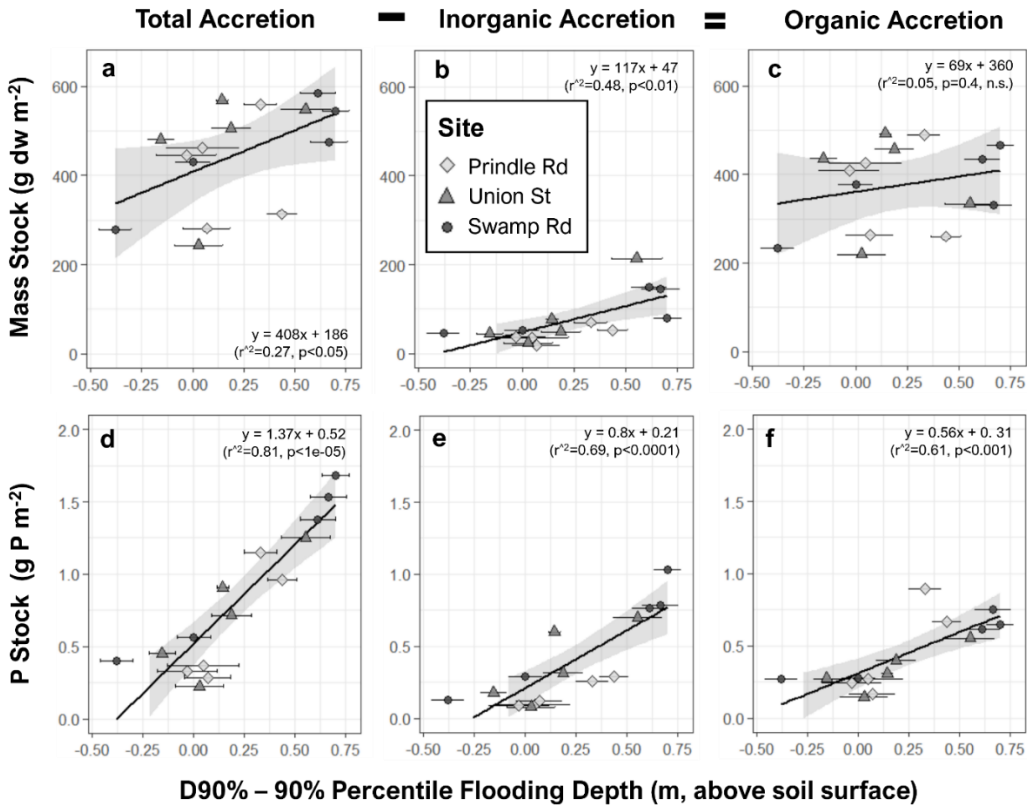


**Figure 2-6 Accretion (including litter, sediment and detritus) over ceramic tiles plotted against 90<sup>th</sup> percentile flooding depth for each site, showing mass stocks (top row), P stocks (bottom row) for total accretion (a & d), inorganic accretion (b & e) and organic accretion (c & f). Organic accretion is calculated as the difference between total and inorganic accretion. Black bars around points indicate standard deviation. Black lines and shaded areas show best fit lines for regressions, fit statistics are given on the top right of each subplot.**

### 2.3.6 Floodwater Monitoring

#### 2.3.6.1 Grab Samples

I collected a total of 522 grab samples that were analyzed for SRP and had valid YSI readings. Of those, I analyzed 448 for TP and 329 for TSS. At Prindle Rd, DO ( $\text{mg L}^{-1}$ ) was greatest at the outflow during the filling condition and DO was not significantly different between the inflow and wetland. SRP at Prindle Rd was greatest at the inflow, followed by the wetland then the outflow. TP and TSS at Prindle Rd did not differ significantly between the inflow, wetland, and outflow, except for filling outflow samples, which had lower TP and higher TSS than other groups (Figure 2-7). At both Otter Creek sites, Union St and Swamp Rd, there were significant differences between the river and wetland with DO being higher in the river, SRP being lower in the river, TP being lower in the river, and TSS being higher in the river (Figure

2-7). In the wetlands of the Otter Creek sites, DO, TP, TSS, and (for Swamp Rd only) SRP were significantly greater on the rising limb of floods when the floodplain was filling with river water than on the falling limb when wetlands were draining to the river (Figure 2-7). The river at both Otter Creek sites had higher TSS and TP on the rising limb (river filling wetlands) compared to the falling limb (wetlands draining to the river), while differences in river DO and SRP between limbs were not significant (Figure 2-7).

In the wetlands of Otter Creek sites and in samples of any origin at Prindle Rd, TSS was a poor predictor of variability in TP. In these areas, there was weak correlation and heteroskedasticity in the TSS-TP relationship (Figure 2-8a). Conversely, TP was explained well by TSS in river samples of both Otter Creek sites: Union St river samples had a very strong linear TSS-TP relationship ( $r^2 = 0.82$ ,  $n = 20$ ,  $p = 5.2\text{e-}8$ ) and Swamp Rd river samples had a strong linear TSS-TP relationship ( $r^2 = 0.63$ ,  $n = 21$ ,  $p = 1.8\text{e-}5$ ) (Figure 2-8b and Figure 2-8c). The inorganic fraction of TSS was ~80% in the river at Otter Creek sites and ~50% at Otter Creek wetlands and at Prindle Rd. In the Otter Creek wetlands and the inflow of Prindle Rd, variability in TP was explained by SRP well at higher concentrations ( $\text{SRP} > 0.05 \text{ mg P L}^{-1}$ ), where TP increased ~1:1 with SRP, and less well when SRP was below  $0.05 \text{ mg P L}^{-1}$  where the TP-SRP slope tended to be greater than 1:1 (Figure 2-9). At the wetland and outflow of Prindle Rd, the variability in TP was poorly explained by both SRP and TSS (Figure 2-8, Figure 2-9). At all three sites, SRP was significantly related to DO according to a negative exponential model. This relationship was strongest at Swamp Rd, followed by Union St, then Prindle Rd (Figure 2-10).

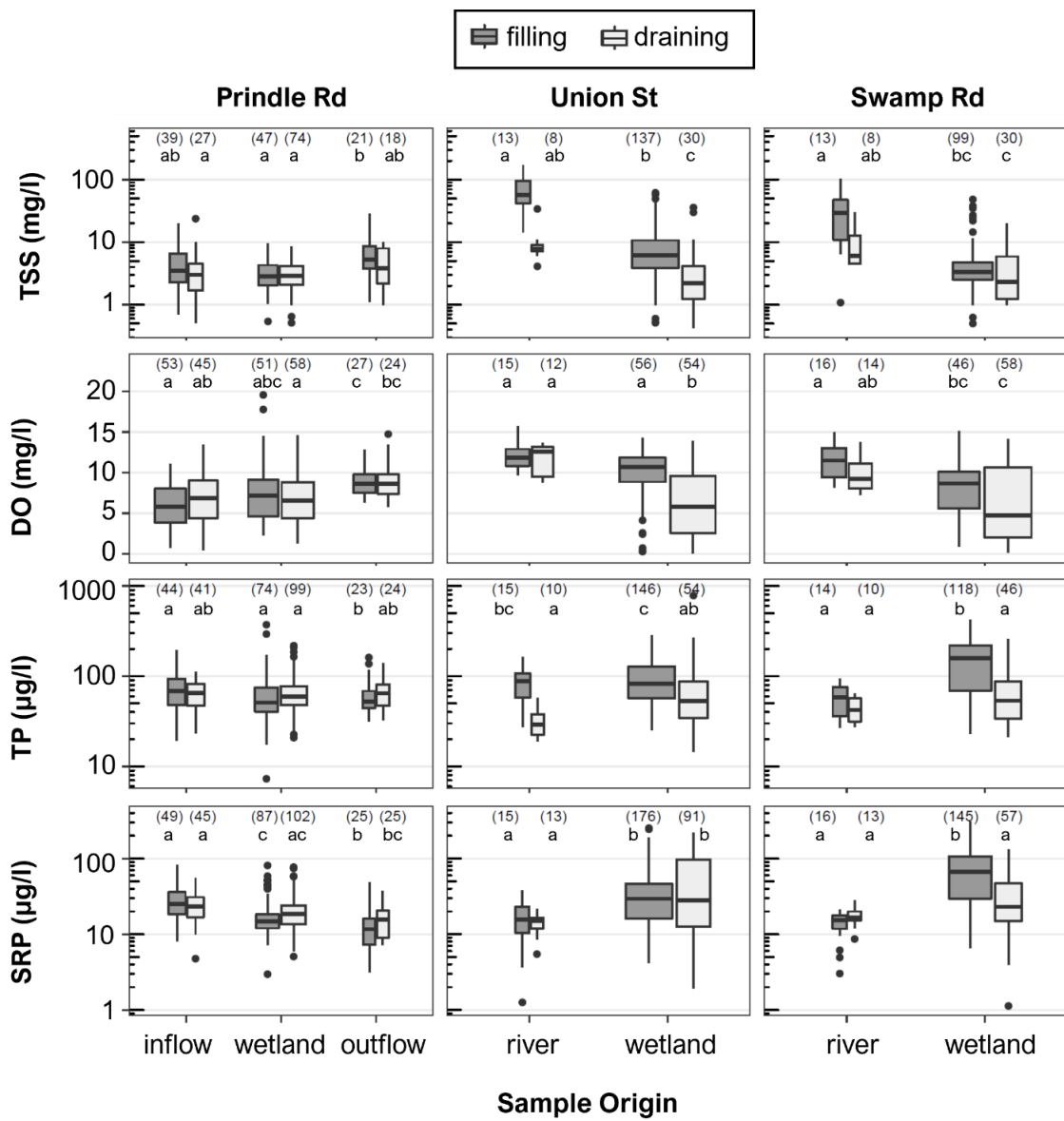


**Figure 2-7** Panel showing box-and-whisker plots of concentrations of total suspended solids (TSS), dissolved oxygen (DO), SRP, and TP, in grab samples at each site. Shading of boxes denotes the condition of the system when samples were collected, dark grey for filling (water level rising) and white for draining (water level falling). The number of observations is given in parentheses above each group. Letters denote significant differences among groups (origin and condition) within sites (Dunn-Bonferroni,  $\alpha = 0.05$ ).

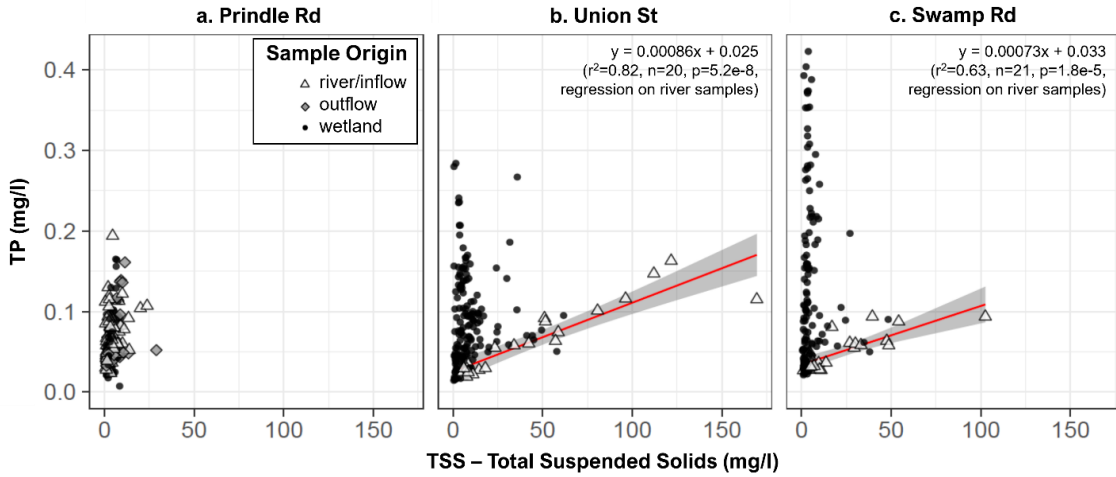


**Figure 2-8 Scatterplot of TSS and TP in grab samples taken at each sample site: Prindle Rd (a, left), Union St (b, center), Swamp Rd (c, right); shapes correspond to sample origin: river/inflow (white triangles), outflow (grey diamonds), wetland (black circles); the black line shows the best fit regression line and the shaded grey area shows the 95% confidence interval for the best fit line, model fits are shown for river samples at Union St and Swamp Rd fit statistics are given on the upper right.**

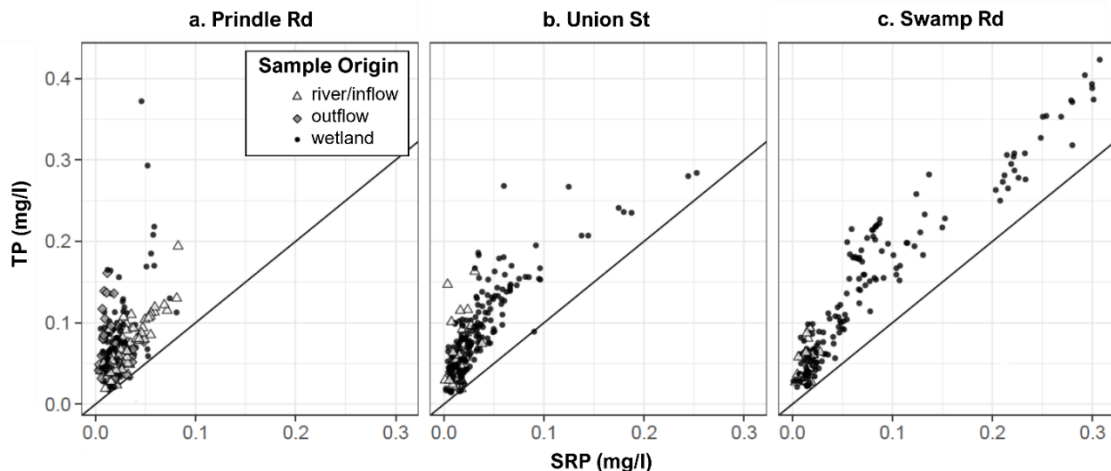


**Figure 2-9 Scatterplot of TP and SRP water samples (including grabs, siphons and ISCOs) taken at each sample site: Prindle Rd (a, left), Union St (b, center), Swamp Rd (c, right); shapes correspond to sample origin: river/inflow (white triangles), outflow (grey diamonds), wetland (black circles); the black line shows the 1:1 line.**

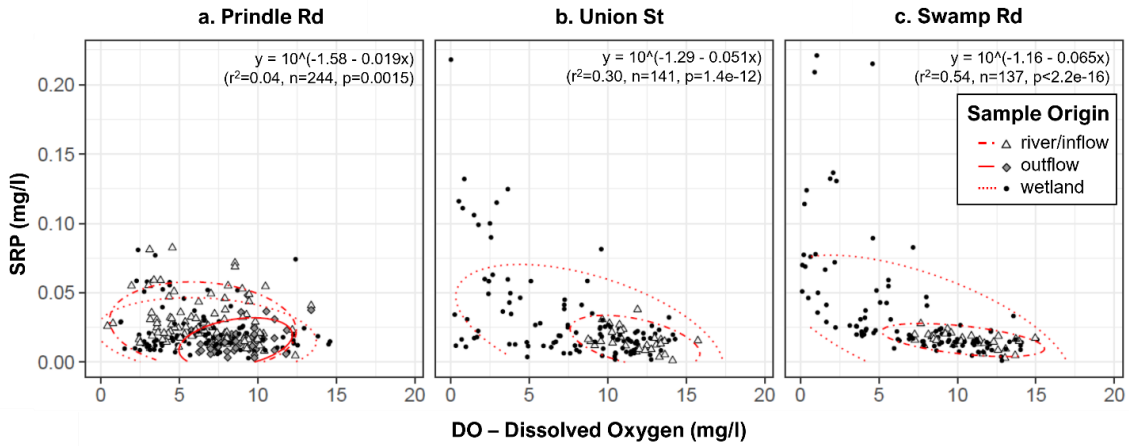


**Figure 2-10 Scatterplot of DO and SRP in grab samples taken at each sample site: Prindle Rd (a, left), Union St (b, center), Swamp Rd (c, right); shapes correspond to sample origin: river/inflow (white triangles, dot-dash ellipse), outflow (grey diamonds, solid ellipse), wetland (black circles, dotted ellipse); red ellipses are plotted to show differences in clusters between sample origins, log-linear regression fit statistics of SRP vs DO are given on the upper right for each site.**

### 2.3.6.2 Flood Pulse Dynamics

I captured one flood pulse in late October of 2019 at Prindle Rd. For this event, the water levels peaked near ~20cm above the median elevation plot, temperature ranged from ~5 to ~15°C and DO ranged from ~20% to ~80% (Figure 2-12 R1, C1). In 2021, I captured two events at Prindle Rd. One snow-melt driven event occurred in March 2021, with peak depth (relative to plot 0) of ~32cm, temperature ranging from ~0°C to ~12°C, and DO ranging from ~20% to ~100% (Figure 2-12 R1, C2). Another rain driven pulse came in late-April/early-May 2021, with peak depth of ~45cm (relative to plot 0), temperature ranging from ~7 to 15°C, and DO ranging from ~0% to over 100% (Figure 2-12 R1, C3).

The first event captured in Otter Creek was a rain driven event in late October 2019 that was preceded by an unusually wet year in the region (NOAA, 2021). For this event, Union St had a peak depth of ~55cm on 10/21, there was a power failure for the miniDOT sensor at Union St, and therefore no data were collected for temperature and DO at the soil-water interface (Figure 2-12 R1, C4). At Swamp Rd, the late October flood pulse produced a peak depth of ~45cm, temperature was consistently near 10°C, while DO dropped from 100% initially to 0% after 4 days then DO fluctuated between 0% and 30% for the remainder of the pulse (Figure 2-12 R1, C7). The second pulse captured in Otter Creek was a snowmelt and rain driven event that began on December 26<sup>th</sup> 2020, this event was preceded by a year of drought in the region (NOAA, 2021). For this event, Union St had a peak depth of ~85cm on 12/28/21, temperature was flat near

$\sim 2^{\circ}\text{C}$ , and DO fell from 75% to 0% over three days then fluctuated between ~0% and 40% for the remainder of the event (Figure 2-12 R1, C5). At Swamp Rd the peak flood depth was ~60cm on 1/1/21, temperature was flat near  $\sim 2^{\circ}\text{C}$ , and DO fell from 95% initially to 0% after  $\sim 3.5$  days and then ranged from 0%-10% for the remainder of the pulse (Figure 2-12 R1, C8). The third event captured in Otter Creek was driven by rain and mountain snowmelt that began on March 25 of 2021. At Union St, the peak depth was ~80cm on 3/31/21, temperature ranged from  $6^{\circ}\text{C}$  to  $20^{\circ}\text{C}$ , and DO started at 95% then dropped to  $\sim 10\%$  after three days then rose to  $\sim 80\%$  and remained above 50% for most of the rest of the pulse (Figure 2-12 R1, C6). Meanwhile, at Swamp Rd, the flood peak occurred on 4/5/21 with a depth of ~95cm, temperature ranged from  $6^{\circ}\text{C}$  to  $20^{\circ}\text{C}$ , and DO initially declined from 95% to 0% over the first 4 days then increased to above  $\sim 20\%$  but below  $\sim 90\%$  for about 1 week then declined to 0% and fluctuated between ~0% and  $\sim 80\%$  for the remainder of the flood (Figure 2-12 R1, C9).

At Prindle Rd, the concentrations of SRP, TP and TSS in floodwater on the wetland ranged from  $\sim 0.01$  to  $0.04 \text{ mg SRP L}^{-1}$ ,  $0.02$  to  $0.16 \text{ mg TP L}^{-1}$ , and  $0$  to  $8 \text{ mg TSS L}^{-1}$  (Figure 2-12). Peak concentrations at Prindle Rd, typically coincided with the peak water level and tended to be within or below the shaded area denoting river (i.e., stream) concentrations (Figure 2-12, R2-R4 and C1-C3). At Union St, the SRP and TP concentrations ranged from  $0.01$  to  $0.13 \text{ mg SRP L}^{-1}$  and  $0.01$  to  $0.27 \text{ mg TP L}^{-1}$ . At Swamp Rd, SRP and TP concentrations ranged from  $0.02$  to  $0.31 \text{ mg SRP L}^{-1}$  and  $0.02$  to  $0.42 \text{ mg TP L}^{-1}$ . TP and SRP concentrations at Otter Creek sites followed similar patterns, tending to peak above levels observed in the river on the rising limb of the flood, then decline to near the levels predicted by the river at the crest and falling limb of floods. During the flood pulse beginning on 12/27/20, concentrations of TP and SRP at both Otter Creek sites remained above levels predicted by the river on both the rising and falling limbs of the pulse (Figure 2-12, R4 and C4-C9). At both Otter Creek sites, TSS concentrations in the wetlands were largely less than  $20 \text{ mg TSS L}^{-1}$  and consistently lower than concentrations measured in the river (Figure 2-12 R4 and C4-C9), thus providing evidence that river suspended solids were being captured on site.

## 2.4 Discussion

### 2.4.1 Particle Trapping

In Otter Creek, TSS concentrations were significantly greater in the river (when filling) than in wetlands during filling or draining conditions, which provided evidence that Otter Creek wetlands trapped and removed particulates from floodwaters (Figure 2-7). Evidence for particle

trapping was less clear at Prindle Brook. At Prindle Brook, TSS concentrations in the inflow were quite low, averaging less than 10 mg/l on the rising limb of floods (when concentrations are normally highest, Figure 2-7). Nonetheless, the TSS concentrations in the wetland were still lower (though not significantly so) than the inflow on the rising limb.

Accretion data also indicated that the wetlands were effective sediment traps. Inorganic matter accretion ranged from 10 to ~200 g dw m<sup>-2</sup> y<sup>-1</sup> and increased with depth. Inorganic accretion increased with flooding depth (Figure 2-6), and depth adjusted inorganic accretion rates were higher at Otter Creek sites which had influent TSS than the Prindle Rd site. At least 70% of the sampling plots at Otter Creek (where TSS was higher) fell above the regression lines of inorganic (mass and P) accretion with depth, while all five Prindle Rd (where TSS was lower) plots tended to fall below the same regression lines (Figure 2-6 b and e); this indicates that Otter Creek received higher exogenous inputs of inorganic sediments and particulate P than Prindle Rd.

Unexpectedly, TSS concentrations in the outflow of Prindle Rd were higher than in the inflow or the wetland. This could be explained by one of several factors: flow by-passing the wetland, internal generation of organic TSS via primary production, or erosion of the beaver dam. Three pieces of data suggest that the latter explanation is the most likely. First, TSS concentrations collected in the open water portion of the wetland (“D1” and “WL” in figure 2-1B) were closer to wetland samples (“0”-“4” in figure 2-1B) than outflow samples (“BV” and “out” in figure 2-1B). Given this, the odds of flow by-passing and/or endogenous primary production as explanatory factors for higher TSS in the outflow are low. Second, flow velocities below the beaver dam increased as a function of depth in the wetland and approached 1 m/s at peak flow. Flows of this velocity could erode the beaver dam. Third, the slope of the relationship between flow velocity (y) and water level (x) increased over time, which indicates that the beaver dam was becoming less effective at retaining water over the course of the two-year monitoring period.

#### 2.4.2 SRP Dynamics

The high-resolution data (Figure 2-12) revealed several important dynamics relevant to riparian wetland P cycling. Diurnal oscillations in DO and temperature occurred within flood water ~5 cm above the sediment-water interface, with both measures commonly reaching daily maximums in late afternoons and daily minimums in early mornings. These patterns in DO suggest photosynthesis-respiration dynamics common for shallow water bodies and flooded wetlands (Reddy & Delaune, 2008). These data also suggest that my “aerobic” intact core

experiments in the laboratory – where room air was bubbled into core water columns 90 min per day for reaeration and then turned off, allowing DO declines due to sediment oxygen demand until reaeration the following day – better represent average conditions in the field during floods than when more fully anaerobic conditions were imposed using N<sub>2</sub> gas (see Chapter 1 section 1.4.2). The exceptions were winter floods (middle column for each site in Figure 2-12), when DO remained depressed during the majority of the flood pulse, a condition caused either by the inhibition of photosynthesis in the water column by low temperatures and/or inhibition of oxygen diffusion into the water column by ice at the water surface.

My grab sampling data suggest that elevated SRP concentrations correspond with lower DO, especially in the Otter Creek wetlands (Figure 2-10) where soils had higher amounts of redox sensitive Fe (Ox-Fe). Therefore, winter flood pulses with less primary productivity appear likely to result in prolonged anaerobic conditions and increased internal SRP loading to the water column from soils. Furthermore, less SRP can be assimilated into plant biomass (including macrophytes, periphyton, and phytoplankton) during these cold flood pulses.

Intriguingly, I generally observed the greatest SRP concentrations at my Otter Creek sites early in the flood pulses. My laboratory incubations suggest that diffusive flux of SRP reaches maximum (i.e., equilibrium) SRP concentrations after ~1 week (see Chapter 1 Figure 1-7). However, my field data suggest maximum SRP concentrations in the water column occur more quickly during flood pulses. I hypothesize that this is due to rapid mineralization upon initial rewetting of organic material on top of and within surface soils, along with the liberation of very loosely held inorganic P (e.g., accreted litter, organic sediment and detritus, Figure 2-5 and 2-7) (Gu et al., 2018; Schönbrunner et al., 2012b; Surridge et al., 2012). The surface layer of litter was removed from the soil before sampling intact cores, which might explain why I did not see this rapid initial release during the intact core experiment. Future intact core experiments could examine differences in SRP fluxes from soil cores with and without surface litter to test the hypothesis above. Further, it seems likely that influent river water (having lower SRP concentrations) provides a dilution effect at the peak of the flood pulse, after which SRP diffusion from soils can continue to occur (as evidenced by the winter flood pulse dynamics I observed in Figure 2-12 C5 and C8). SRP concentrations in the water column might stay suppressed due to biologically mediated removal of SRP from the water column during warmer periods (Figure 2-12 C6 and C9), either through assimilation in biomass or precipitation of SRP with oxidizing Fe and Mn (Ardón et al., 2010a; Kinsman-Costello et al., 2016).

My findings suggest that some SRP in floodwaters may be retained through biological uptake and deposited onto the soil surface. In Otter Creek, wetland floodwater SRP-DO and SRP-TP relationships were strong while the TP-TSS relationship was weak (FiguresFigure 2-8,Figure 2-9 and Figure 2-10). This indicated that floodwater P concentrations in Otter Creek wetlands werewetlands were regulated strongly by biochemical processes (e.g., organic P mineralization, biomass uptake, and precipitation with Fe). These patterns were less clear at the Prindle Rd site. Accretion data at all sites indicated that there were sources of non-herbaceous plant litter organic P (e.g., slime, carcasses, feces) to sediments in addition to that increased with flooding depth. Organic and inorganic P captured through these pathways could eventually re-release SRP following drying and rewetting (Gu et al., 2018; Kinsman-Costello et al., 2016). A rapid cycling pattern of this type is common for eutrophic systems (Ardón et al., 2010a; Kinsman-Costello et al., 2016).

In Otter Creek floodwaters of wetlands, SRP-DO and SRP-TP relationships were strong while the TP-TSS relationship was weak. This indicated that floodwater P concentrations in Otter Creek wetlands were regulated strongly by biochemical processes (e.g., organic P mineralization, biomass uptake, and precipitation with Fe). These patterns were less clear at the Prindle Rd site. More research is needed to enhance understanding of the role of biology (especially surface litter and periphyton) and oxygen dynamics in regulating wetland internal loading of SRP during flood pulses, and why some ecosystems behave differently than others (e.g., Prindle Rd vs. Otter Creek). Future studies could measure chlorophyll and Fe in floodwaters to estimate the respective impacts of primary production (Weigelhofer et al., 2015) and redox changes on SRP dynamics (Gu et al., 2019b). Nitrogen dynamics may also be important (Maberly, et al., 2002). Data driven approaches that use high frequency sensors to measure DO, conductivity, turbidity, and more may also help elucidate the various factors that influence SRP concentrations in wetlands during floods (e.g., Rode et al., 2016).

#### **2.4.3 Hydrogeomorphic Controls on P Cycling**

Previous studies indicate that local variability in hydrogeomorphology influences biogeochemical cycling of P and other nutrients (Moser et al., 2009; Noe et al., 2013). The soil, biomass, accretion, and litter data from this chapter suggest that flooding depth exerts strong controls over ecosystem structure and rates of internal P cycling. Several soil parameters correlated significantly with flooding depth, such as organic matter (positively), bulk density (negatively), and total P (positively). Woody biomass was only present at the highest elevation

plots. In litterbags, the ratio of inorganic P to total P increased with flooding depth across all sites (after adjusting for incubation time). Flooding depth strongly and positively correlated with all forms of P accretion. Approximately 50% of P accretion was inorganic. Given the substantial amounts of inorganic P in litterbags, some of accreted inorganic P was likely held within cells of decomposing plants and other detritus. Organic P accretion correlated strongly with depth, of which endogenous macrophyte P made up about 50%. Exogenous inputs of organic P were not likely a substantial contributor to non-macrophyte organic P accretion. Inputs of organic P in suspended solids were minor in Otter Creek, where organic matter made up just 20% of TSS. While at Prindle Rd inflow TSS was 50% organic but concentrations were very low in the wetland, often near the detection limit of 2 mg/L.

#### **2.4.4 Landscape Position**

Numerous studies have demonstrated the important influence of landscape position and geomorphology on stream corridor and wetland nutrient retention (Cheng & Basu, 2017; Records et al., 2016; Walton et al., 2020). The patterns in water quality data collected in the river/inflow at my wetlands reinforce the idea that landscape is important. For example, the Prindle Rd beaver dam complex drained pastures, hay fields and residential homes that were buffered by wetlands. As a result, TSS, TP, and DO levels were relatively low, while SRP was relatively high. In Otter Creek, the Union St site was on the upstream portion of a floodplain wetland complex and subject to greater flooding depth but shorter duration relative to Swamp Rd downstream. At Union St, the TSS, TP, and DO levels in the river were higher than Swamp Rd, while SRP was not different between sites.

The relationships in the water quality data also indicate that Prindle Rd functions differently from the Otter Creek sites. In Otter Creek, TSS explained most of the variability in river/inflow TP, while at Prindle Brook the TP-TSS relationship in the inflow was not significant and not different from the wetlands (Figure 2-8). Conversely, TP variability in the inflow of Prindle Rd was well explained by SRP, which is a pattern that was seen in the wetlands of Otter Creek but not the river (Figure 2-9). These patterns suggest that stream corridors that fall below functioning wetlands will tend to have relatively low incoming concentrations of TSS and DO, while TP and SRP levels may vary depending on soils, upstream land use, and a variety of event-based factors (discussed in section 2.4.2 above).

## 2.5 Conclusions

In this study I applied an array of methods to examine evidence of particulate P deposition and internal SRP loss – which are two important factors affecting net P balances – at three restored riparian wetlands on agriculturally impacted soils. The study sites had not been farmed for over 10 years at the start of the study and were positioned in low energy floodplains characterized by inundation from flood pulses lasting days to weeks. The data in this study revealed methodological insights and key drivers of particulate P deposition and SRP release:

1. **Water data and inorganic P accretion rates indicated that the three study wetlands were effective at trapping sediment.** Differences in TSS concentrations between the river and wetlands in Otter Creek provided strong evidence that wetlands trapped and removed particulates from floodwaters. My comparison of different P fractionation methods suggests that a 16 hr 1 M HCl extraction is suitable for assessing inorganic P in wetland sediments. Inorganic accretion (material deposited over ceramic tiles) provided an approximate measurement of allochthonous inputs of mineral sediment and P to my study wetlands. However, this approach may slightly overestimate allochthonous P inputs for long incubation periods (1 yr or more) because it also detects recently mineralized P and loosely held P in detritus.
2. **I saw mixed evidence of SRP release from wetlands to floodwaters.** My simulated floods inside intact soil cores suggested that the soils of each site were capable of releasing SRP; metrics derived from the acid ammonium oxalate were good predictors of intact core SRP release while metrics derived from P sorption isotherms were not. In the field wetland SRP concentrations sometimes rose above inflow/river concentrations over the course of a flood, but sometimes fell below the river/inflow concentrations before the floodwaters receded; this suggests that local biogeochemical factors affect wetland SRP loss on an event-by-event basis. More research is needed to investigate the role of biology and dissolved oxygen dynamics in regulating SRP balances during floods in these settings.
3. Flooding depth significantly correlated with soil, biomass, litter, and accretion data, which suggests that **local variability in hydrogeomorphology exerts strong control over wetland functioning.**

4. The differences between sites in SRP, TP, TSS, and DO concentrations of river/inflow waters suggests that **landscape position impacts influent water quality and the subsequent interactions of that water with the wetlands.**

At my three sites, inorganic accretion ranged from ~0.1 to ~1 g P m<sup>-2</sup> y<sup>-1</sup>. These rates fall on the low end of the range of ~1 to >100 g P m<sup>-2</sup> y<sup>-1</sup> for floodplain P deposition within the Lake Champlain Basin estimated by Diehl et al. (2021). The relatively low sediment inputs, long periods of inundation, and recent history of farming that were present at each of my sites are typical conditions where internal SRP loss and negative TP balances have been reported in the literature (Walton et al., 2020). In the field, wetlands did release SRP at times, but there was mixed evidence that this SRP was exported during floods. On the contrary, water data from each study site showed that TP concentrations at river/inflow locations (when filling) were greater than in the wetlands (when draining) (Figure 2-7), which suggests that the wetlands may be net TP sinks on average. However, modeling is needed to formally estimate P retention rates and confirm source-sink behavior of the study wetlands (and this will be done in Chapter 3).

## 2.6 Appendix

### 2.6.1 Supplemental Figures and Tables

**Table 2-1 Averages ( $\pm 1$  standard deviation) for soil properties at each site by depth. Letters in common across rows (site and depth) indicate no significant difference in median value (Dunn-Bonferroni).**

site	Prindle Rd		Union St		Swamp Rd	
depth	0-5cm	5-10cm	0-5cm	5-10cm	0-5cm	5-10cm
MC (g/g)	a $0.67 \pm 0.11$	b $0.44 \pm 0.11$	ab $0.57 \pm 0.12$	b $0.47 \pm 0.094$	ab $0.60 \pm 0.19$	b $0.44 \pm 0.11$
BD (g cm <sup>-3</sup> )	a $0.32 \pm 0.15$	b $0.73 \pm 0.22$	ac $0.38 \pm 0.095$	bc $0.58 \pm 0.11$	ac $0.36 \pm 0.18$	b $0.64 \pm 0.15$
LOI (g/g)	a $0.27 \pm 0.062$	b $0.16 \pm 0.037$	ab $0.22 \pm 0.086$	ab $0.20 \pm 0.094$	ab $0.30 \pm 0.20$	b $0.17 \pm 0.08$
Active-C (g kg <sup>-1</sup> )	ab $1.89 \pm 0.77$	a $1.28 \pm 0.81$	c $1.48 \pm 0.56$	c $0.72 \pm 0.27$	bc $1.29 \pm 0.94$	abc $0.64 \pm 0.5$
Al-3051a (g kg <sup>-1</sup> )	a $27.8 \pm 3.6$	ab $30.8 \pm 5.2$	bc $20.2 \pm 1.4$	c $20.1 \pm 1.4$	bc $22.7 \pm 3.0$	bc $25.2 \pm 5.0$
Ca-3051a (g kg <sup>-1</sup> )	a $8.07 \pm 1.1$	ab $6.23 \pm 1.1$	b $4.51 \pm 0.68$	b $3.65 \pm 0.37$	a $4.73 \pm 1.1$	ab $4.44 \pm 0.90$
Fe-3051a (g kg <sup>-1</sup> )	ab $20.2 \pm 3.6$	a $23.8 \pm 4.8$	abc $28.4 \pm 2.6$	bc $28.1 \pm 3.1$	c $22.4 \pm 2.9$	bc $23.7 \pm 2.1$
Mg-3051a (g kg <sup>-1</sup> )	a $6.95 \pm 1.0$	a $7.61 \pm 1.2$	a $6.01 \pm 0.55$	a $5.75 \pm 0.52$	a $5.63 \pm 0.005$	a $5.86 \pm 0.76$
HCl-P <sub>i</sub> (mg kg <sup>-1</sup> )	a $333 \pm 60$	b $313 \pm 85$	a $388 \pm 120$	ab $332 \pm 93$	a $396 \pm 44$	ab $357 \pm 39$
HCl-TP (mg kg <sup>-1</sup> )	a $1140 \pm 160$	b $788 \pm 180$	a $1140 \pm 150$	ab $1060 \pm 140$	a $1260 \pm 230$	ab $1050 \pm 180$
Ox-Al (mg kg <sup>-1</sup> )	a $2090 \pm 480$	a $2500 \pm 680$	a $1960 \pm 220$	a $1910 \pm 230$	a $1910 \pm 480$	a $1920 \pm 610$
Ox-Fe (mg kg <sup>-1</sup> )	a $2550 \pm 460$	a $2640 \pm 660$	b $6110 \pm 1500$	b $5790 \pm 1200$	a $3090 \pm 710$	a $3080 \pm 1600$
Ox-P (mg kg <sup>-1</sup> )	ab $407 \pm 57$	a $342 \pm 86$	c $644 \pm 120$	bc $577 \pm 75$	c $662 \pm 150$	c $625 \pm 130$

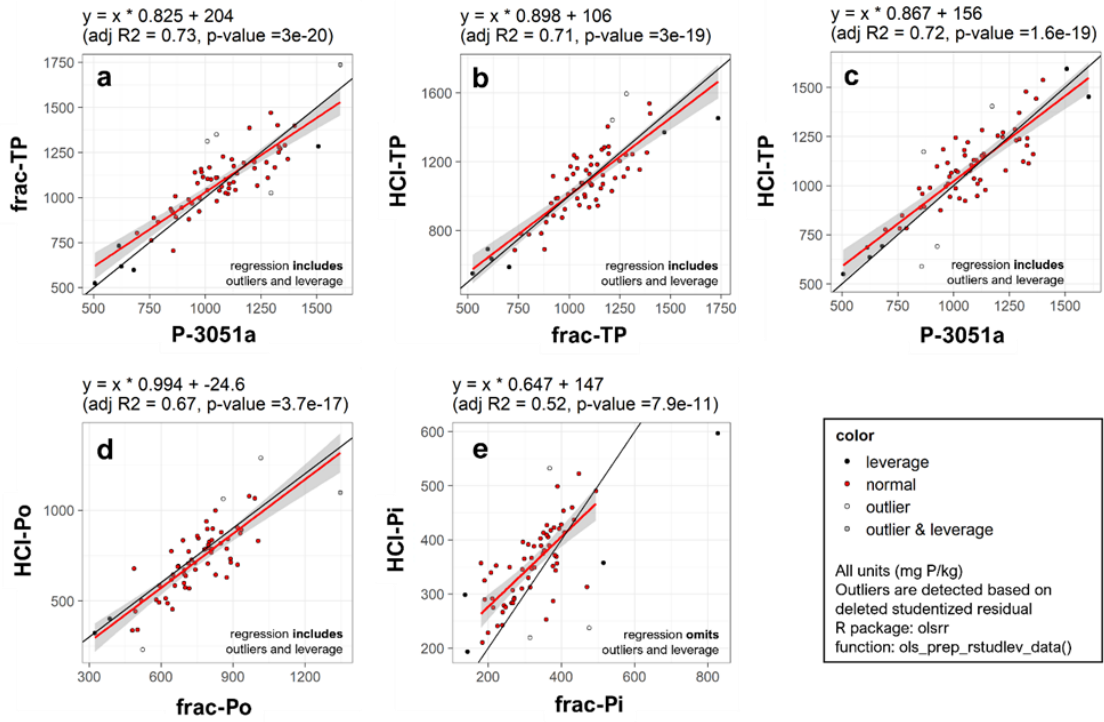


**Figure 2-11 Comparison of soil P fractions estimated from different methods.** The top row compares total P methods: P-3051a vs frac-TP (a), frac-TP vs HCl-TP (b), and P-3051a vs HCl-TP (c). The bottom row compares organic (d) and inorganic (e) P measures from the sequential and parallel schemes used. All regressions include leverage and outlier points except for inorganic P (e). In each scatter plot the red line is the regression fit and black line is the 1:1 line.

**Table 2-2 Soil to water SRP flux rates observed in simulated floods inside intact cores (average flux rate over the first 7 days after flooding) and related soil properties (reported as averages for the top 0-5cm).**

site	Prindle Rd			Union St			Swamp Rd		
plot	0	2	4	0	2	4	0	2	4
<i>Intact Core SRP flux rates (g P m<sup>-2</sup> d<sup>-1</sup>) - Day 0 to 7</i>									
Anaerobic	0.024 ± 0.017	0.019 ± 0.008	0.017 ± 0.003	0.009 ± 0.005	0.004 ± 0.001	0.005 ± 0.002	0.029 ± 0.015	0.031 ± 0.024	0.01 ± 0.005
Aerobic	0.004 ± 0.002	0.008 ± 0.006	0.015 ± 0.016	0.003 ± 0.001	0.002 ± 0.001	0.003 ± 0.001	0.006 ± 0.003	0.007 ± 0.004	0.004 ± 0.001
<i>Soil Properties - Depth 0 to 5cm</i>									
WEP (mg/kg)	0.47 ± 0.25	0.13 ± 0.13	0.18 ± 0.27	0.57 ± 0.29	0.07 ± 0.11	0.06 ± 0.09	2.45 ± 2.35	0.27 ± 0.41	0.44 ± 0.22
Ox-[P:Fe] (mol/mol)	0.35 ± 0.02	0.3 ± 0.04	0.27 ± 0.01	0.25 ± 0.05	0.22 ± 0.03	0.16 ± 0.03	0.37 ± 0.1	0.53 ± 0.1	0.23 ± 0.01
Ox-[P:Al] (mol/mol)	0.18 ± 0.2	0.17 ± 0.25	0.15 ± 0.14	0.26 ± 1.28	0.29 ± 0.25	0.23 ± 0.95	0.24 ± 0.22	0.31 ± 0.25	0.37 ± 0.22
Ox-PSR (mol/mol)	0.12 ± 0	0.11 ± 0.01	0.1 ± 0	0.13 ± 0.02	0.12 ± 0.01	0.09 ± 0.02	0.14 ± 0.02	0.2 ± 0.01	0.14 ± 0.01
Ox-SPSC (mg/kg)	339 ± 35	457 ± 40	484 ± 82	539 ± 155	543 ± 113	672 ± 97	324 ± 61	127 ± 60	311 ± 55
S <sub>max</sub> (mg/kg)	635 ± 23	558 ± 25	438 ± 8	652 ± 7	653 ± 5	586 ± 30	925 ± 9	644 ± 23	405 ± 21
K <sub>L</sub> (L/mg)	0.035 ± 0.003	0.063 ± 0.009	0.082 ± 0.005	0.328 ± 0.015	0.282 ± 0.009	0.056 ± 0.009	0.054 ± 0.001	0.144 ± 0.02	0.101 ± 0.019
EPC <sub>0</sub> (mg/L)	2.47	0.46	0.2	0.05	0.06	0.27	1.16	0.23	0.09

**Table 2-3 Total mass and P stocks by site (mean  $\pm$  standard deviation, units given in table).**

Significant differences across rows are denoted by lowercase letters, differences are determined based on the Kruskal-Wallace test with Dunn-Bonferroni post-hoc adjustment.

Abbreviations: TM = total mass, IM = mass of inorganic material, OM = mass of organic material, C = P content of material, dw = dry weight.

Site	Prindle Rd	Union St	Swamp Rd
<i>Above Ground Woody Biomass (live, diameter measurements, 2021-08-13)</i>			
TM (g dw m <sup>-2</sup> )	0	362	17456
TP (g P m <sup>-2</sup> )	0	0.27 $\pm$ 0.09	13.1 $\pm$ 4.4
<i>Above Ground Herbaceous Biomass (live, clipped to 1cm of soil, 2019-09-02)</i>			
TM (g dw m <sup>-2</sup> )	386 $\pm$ 292 <sup>ab</sup>	704 $\pm$ 352 <sup>a</sup>	374 $\pm$ 262 <sup>b</sup>
C (mg P kg <sup>-1</sup> )	1135 $\pm$ 335	1854 $\pm$ 415	2892 $\pm$ 877
TP (g P m <sup>-2</sup> )	0.385 $\pm$ 0.286	1.25 $\pm$ 0.543	0.891 $\pm$ 0.519
<i>Below Ground Biomass (Roots, 0-10cm, wet sieved to &gt;1 Mm, 2019-09-02)</i>			
TM (g dw m <sup>-2</sup> )	1135 $\pm$ 397 <sup>ab</sup>	1390 $\pm$ 737 <sup>a</sup>	812 $\pm$ 409 <sup>b</sup>
C (mg P kg <sup>-1</sup> )	1164 $\pm$ 179	1536 $\pm$ 297	1269 $\pm$ 176
TP (g P m <sup>-2</sup> )	1.314 $\pm$ 0.454	2.202 $\pm$ 1.583	1.033 $\pm$ 0.513
<i>Aboveground Litter Production (Live herbaceous &amp; fresh surface litter, 2019-10-14)</i>			
TM (g dw m <sup>-2</sup> )	402 $\pm$ 169	472 $\pm$ 103	406 $\pm$ 180
C (mg P kg <sup>-1</sup> )	1524 $\pm$ 705	979 $\pm$ 269	1477 $\pm$ 222
TP (g P m <sup>-2</sup> )	0.6 $\pm$ 0.4	0.47 $\pm$ 0.18	0.61 $\pm$ 0.32
<i>Aboveground Litter Production (Live herbaceous &amp; fresh surface litter, 2020-10-15)</i>			
TM (g dw m <sup>-2</sup> )	419 $\pm$ 220 <sup>a</sup>	795 $\pm$ 324 <sup>b</sup>	559 $\pm$ 212 <sup>ab</sup>
C (mg P kg <sup>-1</sup> )	1524 $\pm$ 705	979 $\pm$ 269	1477 $\pm$ 222
TP (g P m <sup>-2</sup> )	0.61 $\pm$ 0.56	0.78 $\pm$ 0.37	0.83 $\pm$ 0.36
<i>Surface Accretion (30cm<sup>2</sup> tiles, incubated 2019-10-01 to 2020-07-15)</i>			
TM (g dw m <sup>-2</sup> yr <sup>-1</sup> )	412 $\pm$ 102	469 $\pm$ 117	463 $\pm$ 106
IM (g dw m <sup>-2</sup> yr <sup>-1</sup> )	43 $\pm$ 17	81 $\pm$ 68	94 $\pm$ 44
OM (g dw m <sup>-2</sup> yr <sup>-1</sup> )	369 $\pm$ 92	388 $\pm$ 99	369 $\pm$ 82
TP (g P m <sup>-2</sup> yr <sup>-1</sup> )	0.62 $\pm$ 0.36	0.71 $\pm$ 0.36	1.11 $\pm$ 0.53
IP (g P m <sup>-2</sup> yr <sup>-1</sup> )	0.17 $\pm$ 0.09	0.37 $\pm$ 0.24	0.6 $\pm$ 0.34
OP (g P m <sup>-2</sup> yr <sup>-1</sup> )	0.45 $\pm$ 0.28	0.34 $\pm$ 0.14	0.51 $\pm$ 0.2
<i>Soil (0-10cm, sieved to &lt;2mm, ground, 2019-07-15)</i>			
TM (g dw m <sup>-2</sup> yr <sup>-1</sup> )	52100 $\pm$ 16900	48300 $\pm$ 9800	49500 $\pm$ 15400
IM (g dw m <sup>-2</sup> yr <sup>-1</sup> )	42300 $\pm$ 15200	38700 $\pm$ 10500	40200 $\pm$ 14600
OM (g dw m <sup>-2</sup> yr <sup>-1</sup> )	9800 $\pm$ 2100	9600 $\pm$ 3000	9300 $\pm$ 3700
TP (g P m <sup>-2</sup> yr <sup>-1</sup> )	44.4 $\pm$ 10.5	52.3 $\pm$ 10.9	53.7 $\pm$ 13.6
IP (g P m <sup>-2</sup> yr <sup>-1</sup> )	15.8 $\pm$ 3.3	16.3 $\pm$ 2.7	18.6 $\pm$ 6.7
OP (g P m <sup>-2</sup> yr <sup>-1</sup> )	28.6 $\pm$ 8.5	36 $\pm$ 9.8	35 $\pm$ 8.4

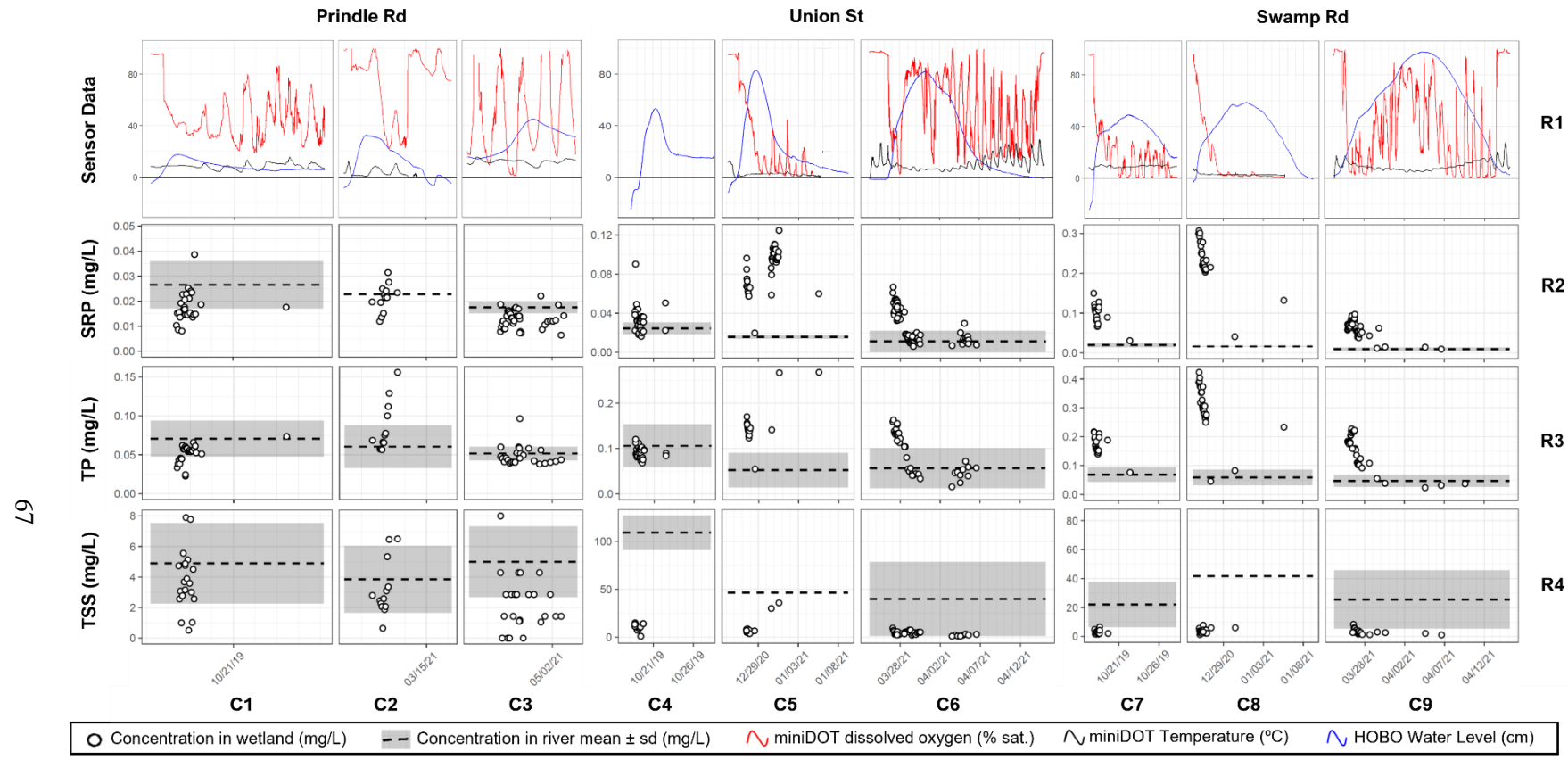


**Figure 2-12** High frequency sensor data including water level, dissolved oxygen, and temperature (R1), and concentrations of SRP (R2), TP (R3), TSS (R4) at Prindle Rd (C1-C3), Union St (C4-C6), and Swamp Rd (C7-C9). Points show values measured in each wetland, while dashed lines and shaded area show the mean and standard deviation, respectively, of the river concentrations for each pulse. All data for Union St and Swamp Rd correspond with the median elevation plot at each site (plot 2). The data first column at Prindle Rd was collected at plot 2, while the second and third columns were collected at plot.

## **CHAPTER 3. NUMERICAL MODELING OF PHOSPHORUS RETENTION IN RESTORED RIPARIAN WETLANDS HAVING AGRICULTURAL LEGACIES**

### **Abstract**

Modeling is needed to estimate the phosphorus (P) retention benefits of riparian wetland restoration in watersheds having agricultural legacies. Existing wetland models are unable to easily simulate dynamics of particulate P and soluble reactive P (SRP) across numerous sites of varying soil characteristics and hydrology. Here I developed a dynamic wetland P model capable of simulating net P retention from a simple set of soil and hydrologic inputs. The model uses three key inputs for soil: (1) organic matter content, (2) soil P saturation ratio, and (3) P storage maximum, with the latter two being inputs for determination of soil P storage capacity. These three metrics are simple and inexpensive to measure and are commonly quantified in contemporary studies focused on soil legacy P. I simulated three wetlands over two years, leveraging monitoring data from Chapter 2 for calibration and verification, and ran scenarios where inflow concentrations and flood magnitude and discharge were changed within plausible ranges. Simulated net total P balance was typically positive (-0.04 to 0.24 g P m<sup>-2</sup> yr<sup>-1</sup>), with an average total P retention efficiency of approximately 40%, although retention efficiency varied substantially depending on site and scenario. P balances and retention efficiency were especially sensitive to changes in influent P and total suspended solids (TSS) concentrations. Greater concentrations of P and TSS in influent floodwater led to greater net P retention. Lower influent SRP concentrations promoted increased SRP release from soils and net SRP export, suggesting that SRP buffering could be a persistent issue for water quality in riparian zones characterized by agricultural legacies. In the future, the model can be applied more broadly to investigate the potential P retention benefits of wetland restoration at sites across Vermont.

### **3.1 Introduction**

Wetland restoration has numerous potential ecological and societal benefits, one of which is the retention of phosphorus (P) and consequent protection of downstream water bodies from eutrophication (Meli et al., 2014). Over 4000 potential wetland restoration sites have been identified in the Vermont portion of the Lake Champlain Basin, which is subject to a TMDL for phosphorus (US EPA, 2015). Targeted restoration of these sites has potential to be a cost-effective strategy for the State of Vermont to meet EPA mandated P load reductions to Lake Champlain (Singh et al., 2019). However, most of the potential wetland restoration sites in the

region are located on current or former agricultural fields and little useful information is available to guide estimates of P retention in these settings.

Past studies have documented net P retention for a variety of wetland types by measuring influents and effluents (Land et al., 2016b). In riparian wetlands, net TP balance is very difficult and costly to estimate with field studies, especially for individual fields within a larger floodplain, due to a variety of complicating factors, such as unconstrained hydrologic flow paths, temporal variation in inflow concentrations and spatial variation in biogeochemical cycling rates (see Chapter 2). The few existing studies on P retention in restored riparian wetlands on former agricultural soil report a wide range of retention efficiency values with net P release on average due to loss of SRP from soils (Land et al., 2016b; Walton et al., 2020). However, P retention rates from the literature tend to be estimated during the first few years after restoration and may not reflect long term averages because retention efficiency can likely change over time as vegetation grows and organic soils develop (Ardón et al., 2010a; Hoffmann et al., 2012a). Wetland P retention efficiency varies based on soil properties, water chemistry, and hydrology (Land et al., 2016b; Walton et al., 2020), and therefore, literature values cannot be simply transferred to Vermont. Thus, numerical models are needed to estimate P balances in riparian settings, let alone the impact of wetland restoration on downstream P loads. In this Chapter, I address these gaps by developing, documenting, and demonstrating the use of a process-based wetland phosphorus model that can estimate net TP retention for a wide array of potential restoration sites using a relatively small number of input parameters.

There are multiple existing wetland and water quality models (DHI, 2004; Jackson-Blake et al, 2017; Kalin & Hantush, 2017; Neitsch et al, 2002). However, there are several reasons why I pursued the development of a new and different P model for riparian wetlands. First, the available models are either overly simple for my intended use – e.g., assuming that all wetlands retain some fixed percentage of incoming P flows (Redhead et al., 2018; Singh et al., 2019) – or overly complex – requiring users to collect data on and/or make assumptions about dozens of spatial, meteorological, and hydrologic input parameters and variables (DHI, 2004; Hantush et al., 2013; Marois & Mitsch, 2016). Furthermore, the most widely collected and available metrics and data that inform legacy P risk assessment, such as soil P saturation ratio (PSR), P Storage Maximum (PSM), Soil P Storage Capacity (SPSC) (which is a function of PSR and PSM), or soil P tests (such as Modified Morgan P in Vermont) are not directly transferrable to the existing models. Here I developed the first process-based wetland P model that I am aware of that uses PSR and PSM directly as input parameters and state variables (that are calculated each iteration).

The model has sufficient complexity to simulate key processes affecting P retention and release in riparian wetlands, but I distilled the list of required inputs down to a handful of local soil and hydroclimatic parameters that are either widely available or simple to estimate.

Second, the ability to simulate dynamic soil conditions is important to estimate the long-term net P balances of wetland restoration projects, and the potential effects of changing water quality and quantity on P retention. Few wetland models that resolve key dissolved P dynamics (e.g., adsorption onto sediments, assimilation in biomass, decomposition of organic matter) also resolve soil evolution (e.g., changing adsorption kinetics as particulate inorganic P is lost or converted to organic P) which is necessary to estimate the long-term impacts of wetland management and soil legacy P on net P retention. To do this, the model in this study adapts and combines two types of wetland models, (1) a P dynamics model from Marois & Mitsch (2016), with origins tracing to Wang et al. (2003) and Christensen et al. (1994), that simulates dissolved inorganic P changes in response to various ecosystem processes – and (2) an Eco-geomorphic model from Wiegman et al. (2019) originally developed by Morris & Bowden (1986) that simulates long-term inorganic and organic soil accretion in tidal wetlands. By merging these two models, I have created a model capable of simulating interactions between soil development and P dynamics for estimation of wetland net P retention as soil evolves over the course of many years to decades. Such information may be important for guiding incentive programs and P load reduction crediting systems. However, in this dissertation I will be focused on a 2-year time period corresponding to the data collection used for model calibration (year 1) and verification (year 2).

Third, many models run on proprietary software like MATLAB (Chowdhury et al., 2016) or STELLA (Marois & Mitsch, 2016), or are written in compiled coding languages like Fortran or C/C++. Compiled languages, while computationally efficient, have a steep technical barrier for entry and are not easily manipulated, due to the lack of interactive development environments and the need to declare data types for each variable (Soetaert et al., 2010). There is a need for a more malleable, open source, and user-friendly wetland model. I chose to develop the model in R, using the package `deSolve` because R is the most widely used statistical software and programming environment in the ecological sciences (Soetaert et al., 2010). This opens the model up to the maximum pool of potential users.

Forth, a numerical model serves as a formalization of hypotheses about the system it represents (Hall & Day 1977; Guide, 2009; van Groenendael, 1997). This model is meant to

support the development and testing of hypotheses about wetland and floodplain soil development and P cycling that can help guide decision-making about watershed land use and management. By creating a model that is interactive, malleable, and embedded in R – the statistical environment that most wetland scientists are familiar with – I am building a link between those who collect and analyze data, and those who use data to practice simulation modeling.

The primary objectives of this Chapter were to develop, document, and demonstrate the use of the novel Wetland P Model in the R programming environment. I completed the following tasks in service to these primary objectives: (1) I parameterized the model for use in Vermont riparian wetlands using data from peer reviewed literature and data from the previous chapters. (2) I calibrated the model against simulations of one year of data observed in the field at the three wetland sites from Chapter 2 and verified performance against the second year of data. (3) With the calibrated model, I simulated 2 years of observed conditions at the field sites in chapter 2, and addressed the following research questions:

1. What is the mass balance and retention efficiency for total P (TP) and SRP (i.e., DIP) for the three wetlands studied in Chapter 2?
2. Will potential changes in hydrology due to climate or land use have a substantial impact on net P balances in restored riparian wetlands?
3. How might P balances in restored riparian wetlands be affected by changes in upstream water quality?

## 3.2 Methods

### 3.2.1 Model Documentation

The Wetland P Model simulates a spatially averaged wetland unit on a daily time step using ordinary differential equations and is integrated using the `lsoda` integration function for stiff and non-stiff problems from the R package `deSolve` (Petzoldt, 2018; Soetaert et al., 2010). The model scripts, are hosted on GitHub (available upon request, <https://github.com/arhwiegman>). A model documentation file and user manual containing tables that describe the model parameters, state variables, rate calculations, and differential equations is will be attached as a supplemental file in the electronic version of this thesis.

The model documentation file is also available on GitHub at the following permanent link:  
[https://github.com/arhwiegman/wetlandP\\_manual\\_dissertation/blob/7b106d43465a38e6e5746247c759fe33eec3eda4/Documentation%20%80%93wetlandP\\_v2.1.pdf](https://github.com/arhwiegman/wetlandP_manual_dissertation/blob/7b106d43465a38e6e5746247c759fe33eec3eda4/Documentation%20%80%93wetlandP_v2.1.pdf)

Figure 3-1 shows the mass stocks and biogeochemical processes (flows) represented by the model. The mass stocks resolved by model include: aboveground live biomass P (shootP) and belowground live biomass P (rootP), aboveground litter/detritus (litterP), labile (fast-decomposing) organic sediment (LOP, and belowground), and refractory (slow-to-non-decomposing) organic sediment (ROP, above and belowground), inorganic sediment (IM, above and belowground), particulate inorganic P (PIP, above and belowground), and dissolved inorganic (DIP, above and belowground). Processes simulated in the model include assimilation and mortality of biomass and decomposition of litter, decomposition of organic matter, settling of particles from aboveground to belowground, adsorption of DIP on to PIP, and diffusion of DIP from belowground to aboveground.

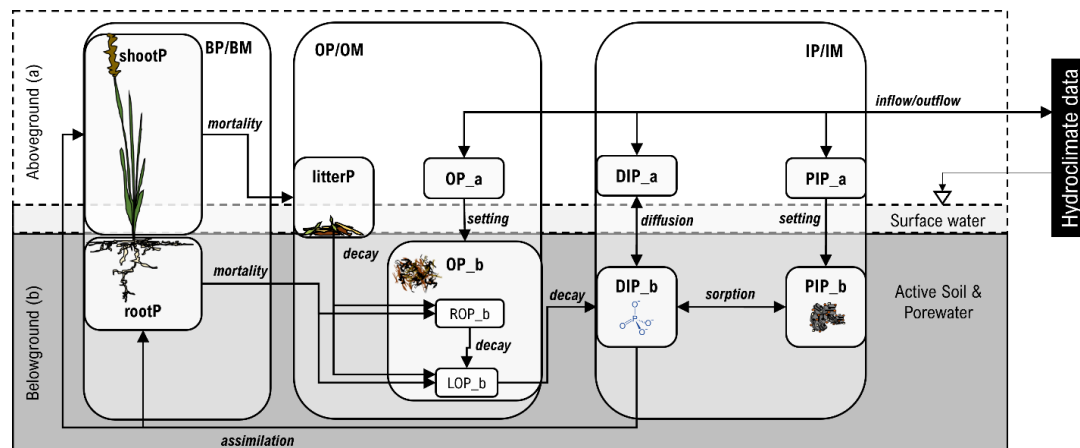


**Figure 3-1 Diagram of the mass stocks and flows represented by the wetland P model.**  
**Model compartments include belowground (\_b) surface soil and porewater, and aboveground (\_a) surface water. Inflows and outflows are determined by externally generated forcing hydroclimate data. BP/BM = biomass P/mass, OP/OM = organic P/mass, IP/IM = inorganic P/mass, LOP = Labile Organic P (fast decomposing), ROP = Refractory Organic P (lignin/humic substances), DIP = dissolved inorganic P (aka orthophosphate, aka SRP), PIP = particulate organic P.**

Other than soils, the key input parameters in the model are hydraulic retention time (HRT), simulated wetland water level, and influent water quality, specifically concentrations of TSS, TP, and SRP. Hydraulic retention time or residence time is the measure of the average amount of time a molecule of water will spend in a control volume before leaving (Mitsch & Gosselink, 2013) and is a powerful parameter for explaining nutrient processing rates in aquatic

ecosystems (Cheng & Nandita, 2017). HRT is calculated by dividing the system water volume by the volumetric outflow rate. Changes in HRT and water level both affect discharge through the wetland. The model's time units are days (d), the mass units are in grams (g), and the distance, area, and volume units are meters (m), square meters ( $m^2$ ), and cubic meters ( $m^3$ ), respectively. The model takes two types of input table as ` .csv` files, one for parameters and one for forcing hydroclimate variables. During initialization the model reads the input files, creates a linear approximation function for each forcing variable in time, changes parameters from default values, and then initializes the value of state variables based on the parameters and values of the forcing variables at time zero.

With the intention of reducing the amount of site information needed to run the model, I made many simplifying assumptions about the equations of wetland soil and P dynamics and data informing parameters in those equations. The simplifying assumptions are listed below.

### **3.2.2 Simplifying Assumptions**

#### **1. DIP adsorption**

- a. Oxalate extractable Al plus Fe represents the P storage maximum (PSM) for exchangeable P in the soil [PSM = 31/(Al/27+Fe/56)]. In this chapter, PSM is referred to as Ex\_max, the variable name used in the Wetland P Model. Oxalate extractable P represents the exchangeable inorganic P pool (Ex). Therefore, the product of the Oxalate P Saturation Ratio (PSR) [PSR = (P/31)/(Al/27 + Fe/56)], and Ex\_max can be used to initialize the model.
- b. Based on my observations in Chapter 2, riparian/floodplain wetland water columns experience intermittent spells of aerobic and anaerobic conditions, so I assume that P adsorption dynamics will be adequately simulated without including the effects of oxygen dynamics (e.g. Wang et al., 2003).
- c. Langmuir model parameters are commonly used to simulate equilibrium dynamics (e.g. Wang et al., 2003). However, In Chapter 2, I found poor correlation between my intact core data and Langmuir model parameters (see sections 3.6.2.1 and 3.6.7 in Appendix). Consequently, I decided to impose an equilibrium DIP value based on the final SRP concentration observed during the O<sub>2</sub> treatment of intact cores for simulating field sites.

In future applications of the model equilibrium DIP can be calculated from the regression equation for final SRP concentration in intact cores versus SPSC (with SPSC derived from input parameters PSR and PSM).

2. Inorganic soil accretion (settling, outflows)
  - a. There is no significant bioturbation effect.
  - b. Wetlands retain (trap) 100% of incoming sediments. This appears to be a reasonable assumption for low energy riparian wetland systems based on the low TSS concentrations (0-3 mg/L) measured in the wetlands towards the later periods of flood pulses. However, this may result in overestimates of particulate P retention. This assumption will be evaluated in more detail below.
  - c. Adsorption occurs only below the soil surface and does not occur in the water column.
  - d. Inflow concentrations of inorganic sediments and dissolved and particulate inorganic P are derived from inflow/stream concentrations of TSS and TP (see section 3.6.3 in Appendix).
3. Organic soil accretion (growth/decay, inflows)
  - a. Herbaceous vascular plants (macrophytes) are currently the only primary producer represented in the model. They synthesize above and below ground biomass in equal proportion, but with differing turnover rates – above ground biomass turns over at least once per year with winter senescence, while belowground biomass can take many years to turnover.
  - b. Primary production rates are affected by temperature and nutrient limitation only.
  - c. Concentrations of P are the same across all forms of organic matter: live biomass, or litter, labile or refractory organic matter and do not vary based on soil nutrient status or average water depth. In reality, organic tissue P contents vary depending on species (which may change in response to hydrologic gradients), soil nutrient levels (Güsewell & Koerselman, 2002; Tessier & Raynal, 2003) (See Figure 3-12 in Appendix) and stage of decomposition (Rejmánková & Houdková, 2006).

- d. The decomposition rate coefficient of labile organic matter is affected only by temperature. Refractory organic which represents lignin (phenolic compounds, Morris et al., 2016) matter does not decompose when the wetland is inundated (Freeman et al., 2001), but when water falls below the wetland surface refractory decomposes in the same fashion as labile organic matter, but with a much smaller rate coefficient.
- e. Inflow concentrations of labile and refractory organic sediments and P are derived from median stream/inflow concentrations of TSS and TP (see section 3.6.3 in Appendix).

### **3.2.3 Parameterization (Calibration and Verification)**

Model input parameters fall into three groups: (A) local (measured) parameters, (B) stochastic (unmeasured) parameters, and (C) universal parameters. Universal parameters are precisely known, and do not vary within the model scope (e.g., the viscosity of freshwater water at 20°C, the particle density of inorganic sediments). The values for universal parameters were taken directly from literature values. The distinction between local and stochastic parameters is the feasibility of their measurement/derivation. Local parameters vary from site to site and are feasibly measured or derived across many sites; these include parameters that define the initial conditions of state variables (soil, water, vegetation), hydrologic flows, and inflow concentrations. The values for local parameters were taken from field/lab measurements from Chapters 1 and 2. Stochastic parameters may or may not vary from site to site but are impractical to measure at a wide number of potential wetland restoration sites (many thousands have been identified in Vermont). Stochastics in the model tend to be rate coefficients that affect process flows, or partitioning coefficients that relate the size of one pool to the size of another (the rate of decay of macrophyte litter, and the labile fraction of decomposing litter).

For the purposes of this Chapter, calibration and verification dealt with estimating likely values for stochastic parameters. I set a range for stochastic parameter values based on the literature and, where-possible, leveraged statistical fits to direct measurements made in the lab or field using data from Chapters 1 and 2 (see section 3.6.2 in Appendix of Chapter 3). I then calibrated the default (“center” or “best guess”) value of the stochastic parameters using data and experiments conducted in the previous chapters. I started by calibrating parameters with metrics that were affected by the fewest processes then moved to more and more complex ones (progressing in this manor helped reduce uncertainty in estimates). First, I calibrated the value of

parameters affecting soil water SRP fluxes (adsorption and diffusion) by simulating an intact soil core experiment (identical to the one conducted at 20 plots in Chapter 1) (see section 3.6.2.1). Then I investigated assumptions and calibrated model parameters to inorganic accretion data, then biomass and litter stocks from the three intermittently flooded wetland ecosystems in Chapter 2 (see section 3.6.2.2).

I ran the model at sampling plots 0, 2, and 4 of the study wetlands for calibration and verification (see section 3.6.2 in Appendix). Briefly, I set equilibrium DIP (DIP\_E) to the final SRP concentration from the intact core experiments. I set the dry mass and P stocks of biomass (aboveground shoots and belowground roots) and soil input parameters the mean value from samples collected in summer of 2019. I set parameters for adsorption, assimilation, and decomposition to my best guess by adjusting their values within their range reported in the literature. Then I estimated inflow concentrations of various P stocks from median values of TSS (mg d.w./L), TP (mg P L<sup>-1</sup>), the organic fraction of TSS (mg d.w./mg d.w.), soluble-reactive fraction of TP (mg P/mg P) (see section 3.6.3). I preprocessed the hydroclimatic data for each site and plot based on measured water levels and data from local meteorological stations (see section 3.6.4). I then forced hydroclimate variables in the model and calibrated the parameters for adsorption, assimilation, and decomposition with data from the first year (7/15/19 – 7/15/20) by tweaking their values within their range reported in the literature until the criteria listed below were met (see Appendix). Finally examined the simulation results from year 2 (7/16/20 and 7/15/21) to verify performance.

The calibration and verification criteria were as follows:

1. Biomass (d.w.), inorganic sediment deposition (d.w.), litter P (d.w.), were all clustered near the 1 to 1 line (+/- 100%)
2. DIP and total P stocks (g/m<sup>2</sup>) and concentrations (mg/L) were within the range observed in the field during floods (not more than double or less than half of the averages reported in Figure 2-7).
3. Stocks of soil organic matter were relatively stable (not increasing or decreasing by more than 1 – 2% per year).

### **3.2.4 Baseline Simulations**

I simulated the three wetlands from Chapter 2 for the two-year monitoring period at plots 0, 2 and 4 and estimated mass balance and retention efficiency of TP and SRP (i.e., DIP).

Wetland water levels were measured on site and used to solve water balances (section 3.6.4 in Appendix). I utilized an existing 2D HEC-RAS model for Otter Creek (Trueheart et al., 2020) to determine the relationship between water level and HRT at Union St and Swamp Rd for flood inundation depths of ~1-2 m. HRT data generated from the HEC-RAS model were well predicted by negative power law models using water elevation (Figure 3-9). For the Prindle Rd site, I calculated HRT based on water volume (estimated by water level measurements and site DEMs) and measured system outflow (Figure 3-10, section 3.6.5 in Appendix). Changes in the relationship between HRT and wetland water level over time were evident at Prindle Rd, which I assume were caused by changes in the beaver dam controlling outflow (Figure 3-10, section 3.6.5 in Appendix). I determined negative power law equations to predict HRT based on water elevation for each site (best fit lines shown in Figure 3-3, data are shown for Otter Creek and Prindle Rd in Figure 3-9 and Figure 3-10, respectively). To estimate influent water chemistry for model simulations, I analyzed inflow stream (i.e., river) grab samples collected during flood conditions over the course of the 2-year monitoring campaign. I determined the organic fraction of TSS and the SRP fraction of TP, which I used to estimate inputs of organic P, dissolved inorganic P, and particulate inorganic P to the control volume during modeling.

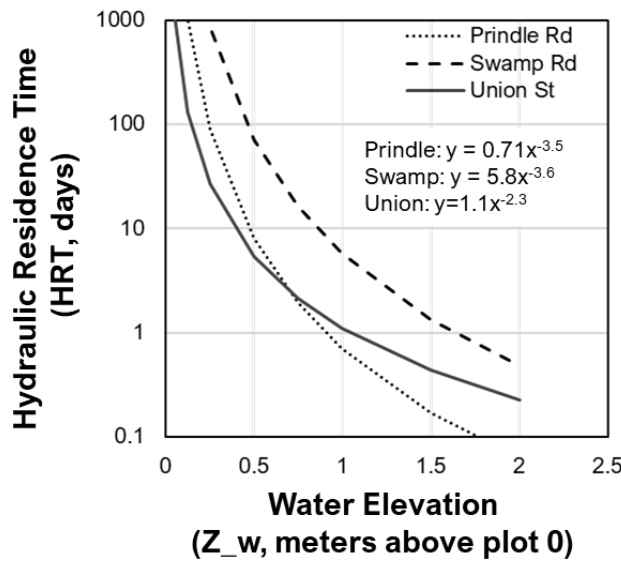


**Figure 3-2 Power model of Hydraulic Residence Time (HRT), as a function of Water Elevation relative to the lowest elevation plot in the wetland. The parameters for each site were generated from data points extracted for system wide volume and discharge at various flood stages.**

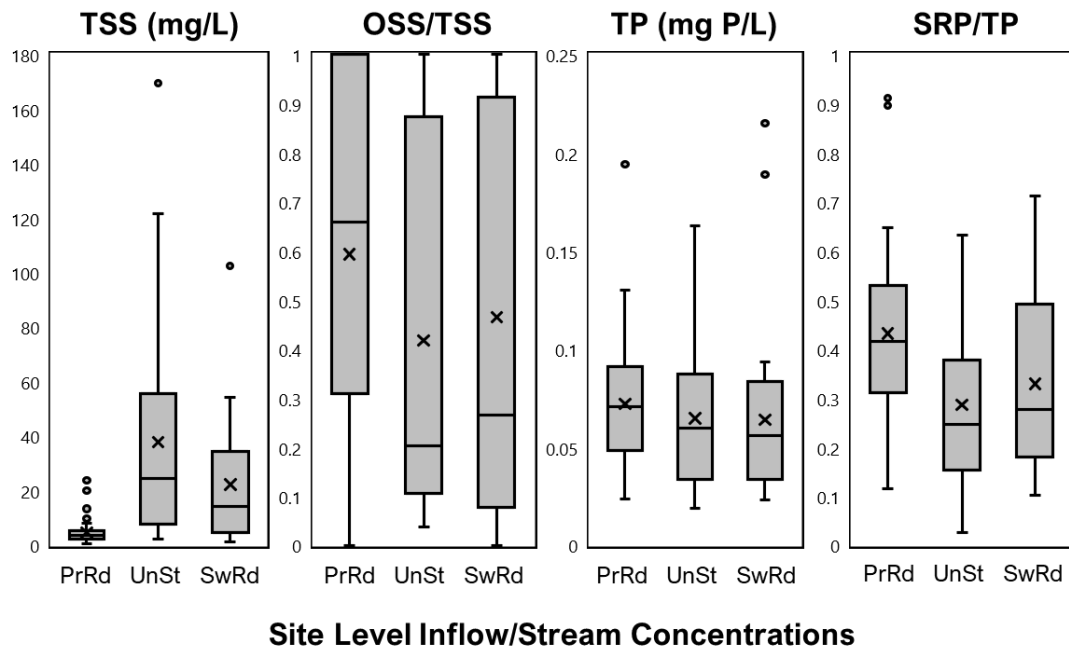


**Figure 3-3 Box and whisker plots showing concentrations measured in the stream or inflow locations of each site. Median concentrations are marked by horizontal lines in the middle of each box, the mean concentration is marked by x. Pr = Prindle Rd, Sw = Swamp Rd, Un = Union St.**

### 3.2.5 Scenarios

Because riparian wetlands and floodplains have a wide range of hydrologic conditions that affect sediment deposition, I also evaluated simulations that assumed 100% particle retention within the wetland as well as those where particle settling is modeled using Stokes' law and thus particulate export from the system is possible. For the simulations that applied Stokes' law, settling velocity was estimated based on particle density and radius, with particle density based on soil texture for inorganics and literature values for organics (Marois & Mitsch, 2016). This was an important assumption to investigate explicitly in this chapter since the power model for HRT and flooding depth dictates that flow rates (and particulate P loads) are highest when water levels are highest. When Stokes' law and the power model for HRT are applied together, some sediment may bypass the system before being deposited, especially at the highest flooding depths.

In addition to varying settling assumptions, I conducted simulations in which I varied the and influent water quality (i.e., concentrations of TSS, TP, and SRP) hydraulic retention time (HRT), and wetland water level, at each site and sampling plot. This served two purposes: (1) to estimate upper and lower uncertainty bounds for mass balance and retention efficiency, and (2) to identify the magnitude and direction of the effect each parameter had on the results. The latter is

important because each of the parameters above could vary in the future due to changing site hydrology, upstream land and watershed management, and/or climate (Guilbert et al., 2014).

Inflow concentrations were doubled and halved, to represent respective reductions and improvements in upstream water quality. Wetland water levels were increased by a factor of 1.2, which represents a high-end estimate increases in average flows in the next several decades due to wetter climate in the Lake Champlain Basin (Guilbert et al., 2014). Preliminary results using stream concentrations showed that the power models for HRT (i.e., dynamic HRT predicted based on water level) produced very similar results to the fixed 10d HRT scenario for Prindle Rd, and to the fixed 100d HRT scenarios for both Otter Creek sites. HRT was varied between 10d and 100d to reflect potential changes in discharge through the wetland.

### 3.3 Results

Net P retention estimates ranged from -0.04 to 0.24 g P m<sup>-2</sup> yr<sup>-1</sup> (-0.36 to 2.2 lbs P acre<sup>-1</sup> yr<sup>-1</sup>) across all simulations, with net P retention near 0.1 g P m<sup>-2</sup> yr<sup>-1</sup> (~1 lb P acre<sup>-1</sup> yr<sup>-1</sup>) for my baseline simulations (median stream concentrations, dynamic HRT based on power model) (Figure 3-4 B and E). Very few baseline simulations resulted in net P export, suggesting that the wetlands investigated in this study generally function as P sinks on the landscape. Simulations that modeled particle settling resulted in net P retention values ranging -0.04 to ~0.12 g P m<sup>-2</sup> yr<sup>-1</sup> (-0.36 to 1 lbs P acre<sup>-1</sup> yr<sup>-1</sup>) (Figure 3-4 B), while simulations that assumed 100% particle trapping resulted in net P retention values ranging from 0.05 to 0.24 g P m<sup>-2</sup> yr<sup>-1</sup> (0.4 to 2.2 lbs P acre<sup>-1</sup> yr<sup>-1</sup>) (Figure 3-4 E).

Across all sites and plots and scenarios that varied stream concentrations and HRT, median/mean TP retention efficiency was 38% (Figure 3-5). TP retention efficiency was substantially higher when I assumed 100% particle trapping (mean = 55%), verses when I modeled particle settling using Stokes' law (mean = 23%) (Figure 3-5). For 100% particle trapping scenarios, all P export is SRP (Figure 3-4 A-C), whereas when particle trapping is estimated based on settling velocity some particulate P can also be exported from the control volume (Figure 3-4 D-F). In all cases, particulate P import was greater than particulate P export (Figure 3-4 o's). However, the balance between DIP imports and exports tended to be negative, though it varied depending on site and inflow concentration (Figure 3-4 x's). While net TP retention tended to be positive, on average retention efficiency of DIP was negative (mean = -23%) in the each of the wetlands (Figure 3-6).

Wetland net TP balance was sensitive to variations in stream concentrations. Greater influent concentrations led to enhanced net P retention, while reduced influent concentrations decreased net P retention. For example, net TP balances for Stokes' Law simulations ranged from -0.06 to ~0.05 g P m<sup>-2</sup> yr<sup>-1</sup> (-0.5 to 0.4 lbs P acre<sup>-1</sup> yr<sup>-1</sup>) and ~0.1 to ~0.5 g P m<sup>-2</sup> yr<sup>-1</sup> (0.9 to 4 lbs P acre<sup>-1</sup> yr<sup>-1</sup>) for 0.5x stream concentrations and 2x stream concentrations, respectively (Figure 3-4 D and E). Changes in stream concentrations had substantial effects on DIP balance and retention efficiency, with DIP retention efficiency having a positive correlation with inflow concentrations (Figure 3-6).

While changing water levels and HRT also had noticeable effect on TP and DIP balances for a given site, the model was more sensitive to changes in inflow concentration than water level or HRT. For example, a base 2 order of magnitude increase in concentration (0.5x to 1, or 1 to 2x) had a greater effect on net TP retention than a base 10 increase in HRT (10 days to 100 days) (see Figure 3-11 in Appendix of Chapter 3). Assuming shorter fixed 10 day HRT – which increased discharge through the wetland – led to greater net P retention compared to fixed 100 d HRT for all site-influent combinations. Potential future increases in discharge (water levels increased by 1.2 x) had minimal effects on P balances when compared to potential changes in influent concentrations (Figure 3-7).

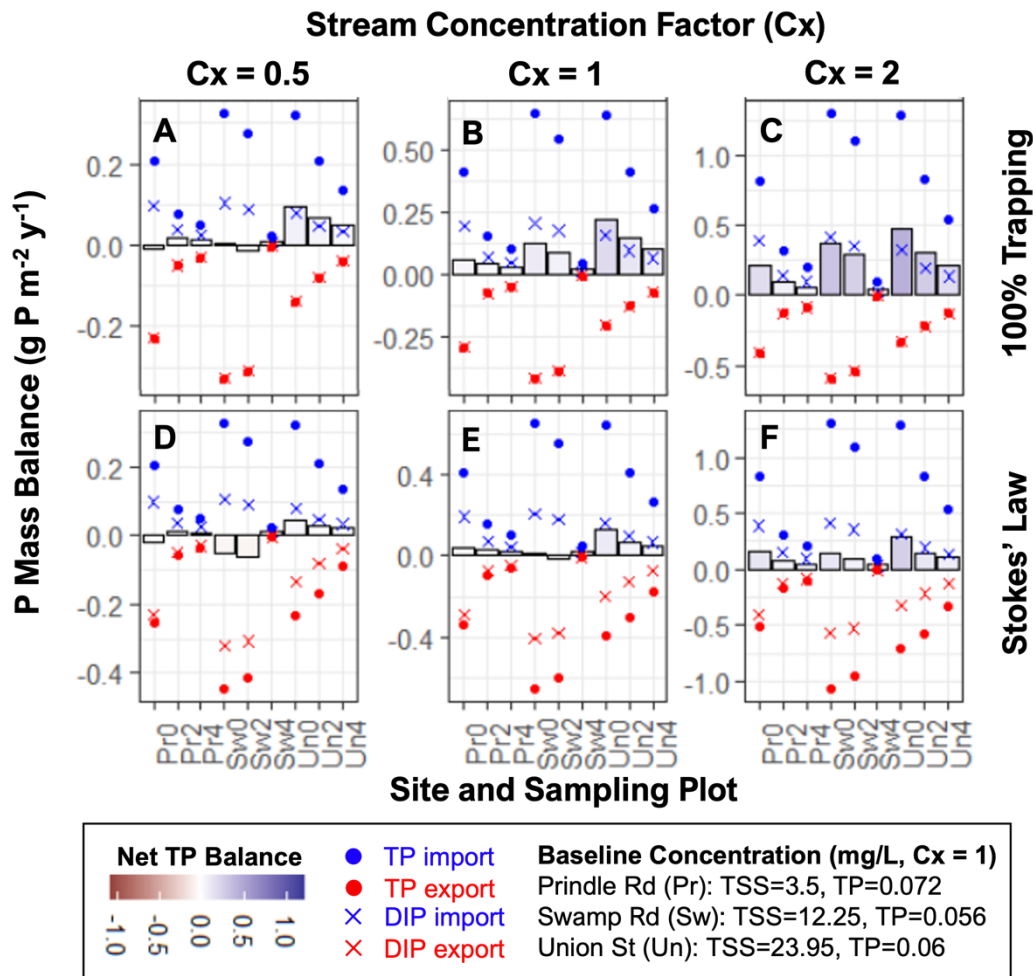
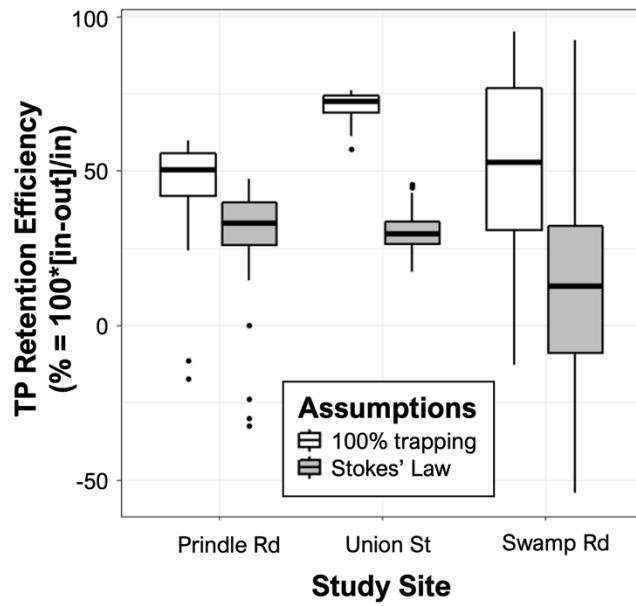
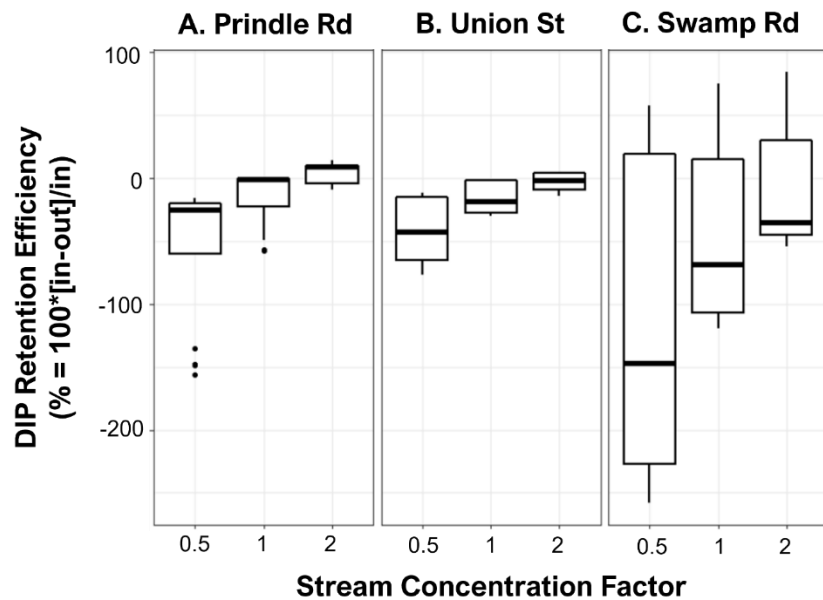


Figure 3-4 Simulated net total phosphorus (TP) balance (bars) with inflow TP and TSS concentrations set to 0.5x stream (i.e., river) median, stream median (baseline conc. 1 x), or 2x stream median for sampling plots (0, 2, 4) in Prindle Rd (Pr), Swamp Rd (Sw), and Union St (Un) sites. The baseline concentration for TP and TSS is given at the above each site. The result in the top row assumes 100% trapping, while the bottom row uses Stokes' Law to simulate settling. Gross P imports (blue) and P exports (red) on the basis of TP (circles) and SRP = DIP (X's) are also shown for various scenarios. Dynamic HRT simulated with power model.



**Figure 3-5 Box and whisker plot of TP retention efficiency (%) for all simulations of stream concentrations entering wetland plots, grey boxes indicate simulations where sedimentation is via Stokes' Law, white boxes indicate simulations where 100% particle trapping is assumed.**



**Figure 3-6 Box and whisker plots of DIP retention efficiency, grouped by site and stream concentration factor, for all simulations forced by stream concentrations**

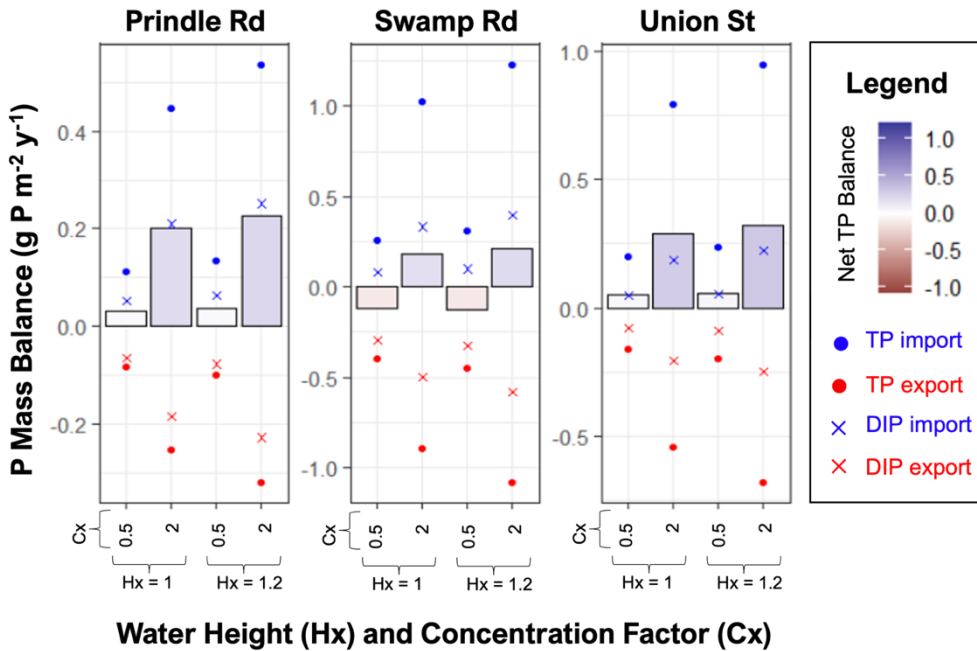


**Figure 3-7** Simulated net total phosphorus (TP) balance (bars) with inflow P and TSS concentrations set to 0.5x stream (i.e., river) median or 2x stream median at observed (x1) and larger (x1.2) flood magnitudes for median elevation plots in Prindle Rd (left), Swamp Rd (center), and Union St (right). Particle trapping is estimated based on settling velocity. Gross P imports (blue) and exports (red) on the basis of TP (circles) and SRP (X's) are also shown for various scenarios. HRT is dynamic based on site-specific power models.

### 3.4 Discussion

Before this study, the few prior estimates available in the literature for restored riparian wetlands on historically drained and farmed soils indicated that net P retention efficiency varied widely but that net P release occurred on average (Land et al., 2016b). However, many of the retention studies for this setting in the review by Land et al. (2016) were conducted within a few years post farming (Ardón, Montanari, et al., 2010a; Hoffmann et al., 2012a). The wetlands in this study had not been farmed for over 10 years prior to the 2-year monitoring period for which I generated estimates of P retention. Contrary to prior estimates, my simulations indicated that the three riparian wetlands studied in Chapter 2 function as P sinks on the landscape. Total P Retention efficiency in my simulations varied widely but averaged roughly 40% (net gain) – coincidentally this is the same value used by Singh et al. (2019) to model P load reduction from targeted wetland restoration in Lake Champlain Basin.

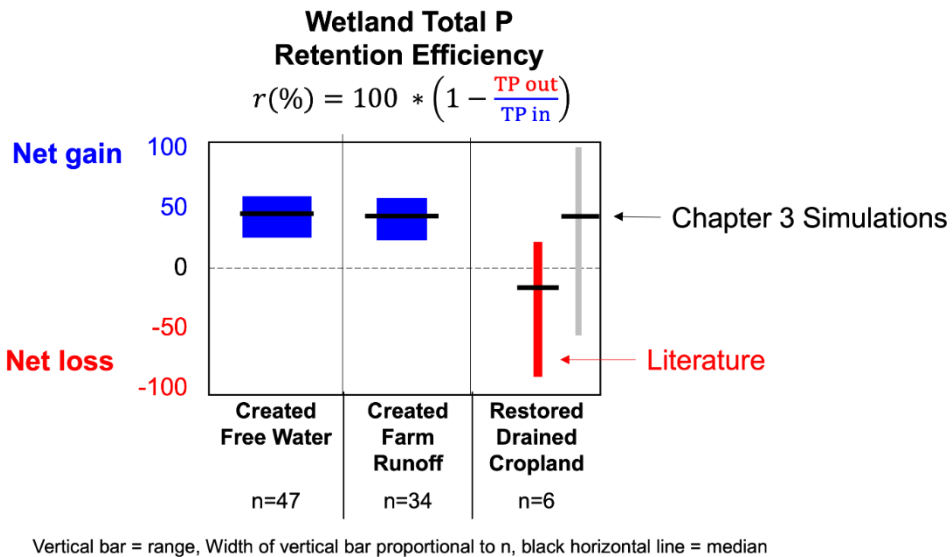


**Figure 3-8 Comparison of total P retention efficiency between estimates from studies in (Land et al. 2016) and this chapter.**

The model predicted that as more water moves through the wetland system control volume, there were minimal effects on net P retention at the scale of flow increases (1.2x on the upper extreme) that might be caused by climate change in the coming decades (Guilbert et al., 2014) (Figure 3-7). This is driven by the fact that discharge has counteracting effects on simulated TP balances in wetlands that have soils containing legacy P. More floodwater leads to more particulate P deposition, but also greater liberation and export of SRP. Combined, these dynamics lead to fairly stable net P retention estimates for a given set of influent concentration assumptions for the systems investigated in this Chapter. On the contrary modeled TP retention was highly sensitive to plausible changes in concentrations in the study wetlands. Greater particulate P concentrations can lead to increased particulate P deposition, while elevated water column SRP concentrations can decrease the SRP concentration gradient at the sediment-water interface and thereby restrict diffusion of SRP from soils to floodwater. These dynamics favor greater net P retention. The opposite would be true for reduced inflow concentrations, which leads to lower particle P deposition and greater soil SRP release, thus lowering net P retention. These results suggest that future changes in stream concentrations are more likely to impact net P retention at a given site than future changes in flow quantities.

### 3.4.1 Legacy P Impacts on Dissolved P Loads

My findings highlight the importance of considering both particulate and dissolved P in P mass balances for restored wetlands and other green infrastructure. Basing estimates of P

retention on particulate P deposition (i.e., particle trapping) alone will likely lead to overestimates of net P retention in mass per area per year. While the TP balance in my simulations tended to be positive, the balance of bioavailable SRP (i.e., DIP) tended to be negative (Figure 3-6). Furthermore, DIP retention efficiency tended to decrease with declining inflow concentrations. This relationship illustrates how legacy P and watershed P buffering capacity could frustrate efforts to reduce P loading. As upstream concentrations decrease because of adoption of best management practices, the stream/wetland/floodplain sediments and soils effectively buffer and release more SRP for the soil to come into equilibrium with influent waters.

If efforts to decrease P loading from agricultural and urban land are successful in the future and result in reduced riverine P concentrations (e.g., decreasing by a percentage similar to the 34% load reduction required by the TMDL; US EPA, 2015), floodplain soil SRP buffering could decrease the magnitude of P retention possible for riparian wetland systems. In aggregate, soil SRP buffering capacity causes watersheds to resist change in DIP concentrations while legacy P stocks slowly deplete, creating a time lag between actions (adoption of BMPs) and results (reduced SRP concentrations) (Goyette et al., 2018). Considering this, future restoration efforts that are aimed at reducing P loading from formerly farmed wetlands should examine approaches to reduce levels of potentially soluble P in the soil prior to restoration (e.g., topsoil removal, Zak et al., 2017; or biomass harvesting, Beutel et al., 2014), which in turn would lower the equilibrium DIP concentration of the soil and subsequent SRP release.

### **3.4.2 TP Loads Compared to Agriculture**

It is also important to consider the foregone agricultural P loading for parcels converted from agriculture to wetlands. P losses from fields producing corn silage or hay and having clay soils representative of the Lake Champlain Basin have been estimated to be  $\sim 1 \pm 0.2$  lb P acre $^{-1}$  yr $^{-1}$  for surface runoff and  $\sim 1 \pm 0.2$  lb P acre $^{-1}$  yr $^{-1}$  for subsurface runoff (if a field is drained) (Faulkner, personal communication). If I assume only surface runoff would have occurred at the low elevation sites that are restored back to wetlands, the overall benefit of switching from farming to wetland – including foregone P loading from agriculture and wetland P capture could be  $\sim 2$  lb P acre $^{-1}$  yr $^{-1}$  (double than if I only consider wetland function today). If a site also formerly included subsurface drainage, then the overall benefit could be  $\sim 3$  lbs P acre $^{-1}$  yr $^{-1}$ .

### 3.4.3 Assumptions

The assumptions surrounding sediment trapping were important to investigate explicitly in this Chapter because the power model for HRT and flooding depth dictates that flow rates (and particulate P loads) are highest when water levels are highest. When Stokes' Law and the power model for HRT are applied, some sediment may bypass the system before being deposited especially at the highest flooding depths. Assuming 100% trapping is reasonable for my study sites most of the time (especially during low flow periods) based on the very low TSS concentrations I observed in wetland floodwater during falling limb periods (see Chapter 2). However, assuming 100% trapping might overestimate particle retention during large events when some sediment bypasses the system due to higher velocities and preferential flow through the floodplain (Trueheart et al., 2020). Modeling particle trapping based on settling velocity results in incomplete sediment retention at high flows, due to decreasing sediment retention efficiency as HRT declines in response to increasing water level (Figure 3-3). Because the wetlands have no longitudinal spatial resolution simulating particle settling via Stokes' Law, my approach here does not account for deposition that occurs as waters move downstream through a wetland complex. Together, the two approaches that I have taken in this Chapter provide upper (100% trapping) and lower (Stokes' Law) end estimates of sediment deposition.

As mentioned above in section 3.2.2 Simplifying Assumptions, I opted to set the equilibrium DIP concentration equal to the final SRP concentration observed in intact soil cores incubations (see Chapters 1 and 2) for soils from the simulated wetland sampling plots. This decision came after I was not able to find a simple way to calibrate or model the Langmuir bond energy parameter ( $K_L = k_E$ ) across a wide range of soils. Global sensitivity analysis during preliminary model testing revealed that  $k_E$  was by far the most influential stochastic parameter on net TP retention (see Appendix of Chapter 3). The Langmuir bond energy parameter is commonly used to model adsorption in wetland P dynamics models (Hantush et al., 2013; Marois & Mitsch, 2016; Wang et al., 2003). Most studies calibrate  $k_E$  to observed water data. However, this modeling paradigm is problematic for estimating impacts of future restoration projects because it limits the modeling scope to systems with existing water data. Furthermore, calibrating the value of  $k_E$  was an extra and unnecessary step because I had estimates of equilibrium DIP from intact core incubations. For the purposes of generating “best guess” estimates of P retention in the three wetlands from Chapter 2, I opted to simply impose equilibrium DIP onto the model. By doing so, I assume that the equilibrium DIP concentration stayed constant through the relatively short 2-year simulation period. However, I also observed strong correlations between

equilibrium DIP concentration and Soil P Storage Capacity (SPSC) in intact core experiments ( $r^2=0.66$ , see Chapter 1), which indicates that in the future equilibrium DIP can be modeled from soil parameters and state variables in the model. SPSC is derived from soil P attributes that are entered as model parameters and calculated as state variables: P saturation ratio (PSR =  $k_{PSR}$ ) and P storage maximum (PSM =  $k_{Ex\_max}$ ).

I had to make several compromises to keep the model simple. Dissolved oxygen concentrations impact the solubility of redox sensitive metal-oxides and associated P in water and sediment (Forsmann & Kjaergaard, 2014). However, these dynamics are not represented by the model. To compensate for this, I imposed the final SRP from the aerobic ( $O_2$ ) intact core treatment onto equilibrium DIP concentrations in the model. The aerobic intact core treatment most closely resembled average flood conditions in the field (see Chapter 2), where dissolved oxygen in the water column fluctuated diurnally, but tended to stay aerobic. Periphyton uptake of SRP from the water column during warm periods, which I do not explicitly model, could potentially suppress SRP concentrations in floodwaters (Dodds, 2003). The model could therefore be slightly overestimating DIP concentrations and subsequent DIP export during periods of high periphyton productivity during spring and fall (although periphyton biomass can potentially become a future source of DIP following drying and rewetting cycles). On the other hand, oxygen depletion of surface waters could promote dissolution of Fe, raising equilibrium DIP concentrations (as seen in Chapters 1 and 2). Therefore, the model may underestimate DIP release during summer periods of high soil mineralization rates and high soil oxygen demand, and in winter periods of low primary productivity and ice inhibition of oxygen diffusion. It is possible that the effects of primary production, decomposition, and soil oxygen depletion on TP and DIP balances largely cancel out. However, at present it is not clear which mechanisms have a greater effect on net TP and DIP balances and more research is needed in this area.

### **3.4.4 Next Steps**

In this Chapter, I conducted a qualitative assessment of uncertainty and model sensitivity by perturbing a few local site parameters and investigating several different assumptions (e.g., 100% particle trapping vs. simulated particle settling). A quantitative assessment of model sensitivity and uncertainty should be conducted in the future, to help guide interpretation of net P retention estimates produced by the model for decision making (Hantush & Chaudhary, 2014; Chaudhary & Hantush, 2017).

In this Chapter, I demonstrated the use of the model using detailed ecosystem and hydroclimate inputs, but the model is flexible. With a few slight modifications it can simulate average hydroclimatic conditions across a range of soils with relatively few inputs: such as inundation depth, frequency, duration, and hydraulic residence time. Soil P Storage Capacity (SPSC) can be calculated within the model from P Saturation Ratio (PSR) and P Storage Maximum (PSM), which are model inputs and state variables (calculated during each iteration). Future applications of the model in Vermont wetlands can apply the regression equations between SPSC and final SRP given in Chapter 1 to simulate equilibrium DIP under a wide range of initial conditions for soils. Furthermore, using this approach allows for equilibrium DIP to be dynamically represented in the model. As P is loaded or unloaded from soils, the PSR of the soil changes, and so does equilibrium DIP. This enables simulation of soil dynamics over long time scales.

Chapter 1 data and other literature suggest that PSR and PSM could be estimated from other site data. For example, PSR could be estimated from Modified Morgan P and/or farming history, while PSM could be estimated from texture and/or farming history (Cohen et al., 2007; Kang et al., 2009; Welikhe et al., 2020). In lieu of site data, PSR and PSM could be modeled from geospatial datasets that have information on land use and soil texture (Cohen et al., 2007; Kang et al., 2009; Welikhe et al., 2020). A geospatial approach will be necessary to evaluate which management actions would be most appropriate for the many thousands of potential wetland restoration sites in Vermont (VTDEC, 2018). Once PSR and PSM can be modeled directly from geospatial data, any number of possible model applications might arise. In fact, efforts are underway to apply the model presented here to estimate the net P balance of floodplain wetlands across Vermont river corridors as part of a broader effort associated with the Vermont Functioning Floodplains Initiative (VTDEC, 2021).

### 3.5 Conclusions

In this Chapter, I leveraged the data generated in the first two Chapters to develop and test a novel process model that simulates wetland P dynamics in Vermont with a simple set of inputs. I coded the model in the programming language `R` and the model runs in RStudio, a widely used open source computing platform (R Core Team, 2020). The model I developed is the first wetland process model I am aware of to use widely measured soil metrics of PSR and PSM as input parameters and state variables. This innovation allows the model to better leverage existing data, makes the model more flexible in its application, and enables representation of soil

P dynamics through time. I simulated a two-year period at three study sites here, but the model could easily be applied to estimate net TP balances at a much larger number of sites with varying soil and hydrologic conditions.

With the model, I estimated net P retention in the three low energy floodplain wetland ecosystems from Chapter 2. To my knowledge, the net TP retention estimates I produced in this chapter are the first produced for riparian wetlands restored on lands having agricultural legacies in the northeastern United States. Wetland TP retention was much more sensitive to plausible future changes in inflow concentrations than discharge. Reductions in inflow concentrations (which may occur in the future as required TMDL reductions are met) decreased TP retention rates, due in part to a soil SRP buffering effect leading to enhanced net SRP export. Contrary to prior literature estimates, my simulations indicated that the three riparian wetlands studied in Chapter 2 – which had not been farmed for over a decade prior to the study – functioned as net P sinks on the landscape, with average net TP retention efficiency of roughly 40%. These results indicate that riparian wetland restoration reduces downstream P loads and improves water quality over the long term when compared to continued intensive farming.

### 3.6 Appendix

#### 3.6.1 Supplemental Figures and Tables

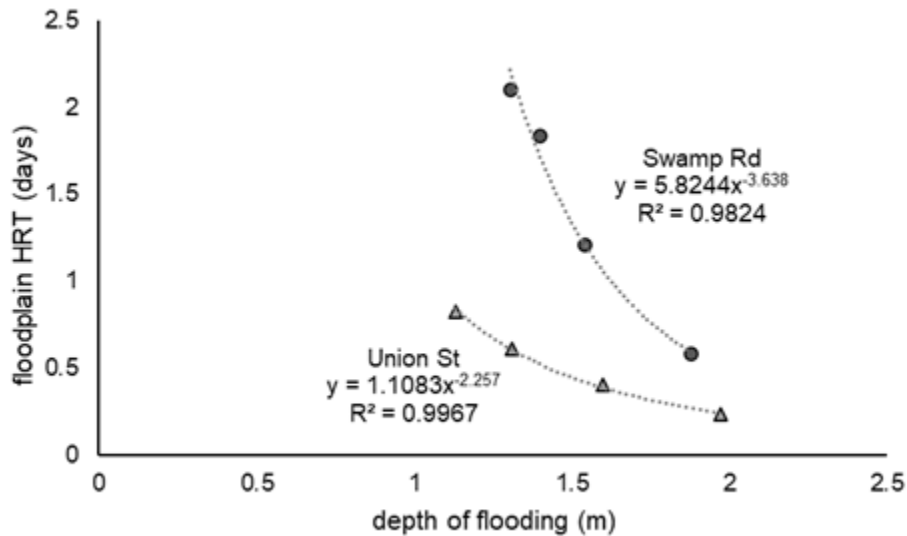


**Figure 3-9 Relationship between depth of flooding and floodplain hydraulic residence time predicted for the two Otter Creek riparian wetland sites using a 2D HEC-RAS model for Otter Creek (Trueheart, 2019).**

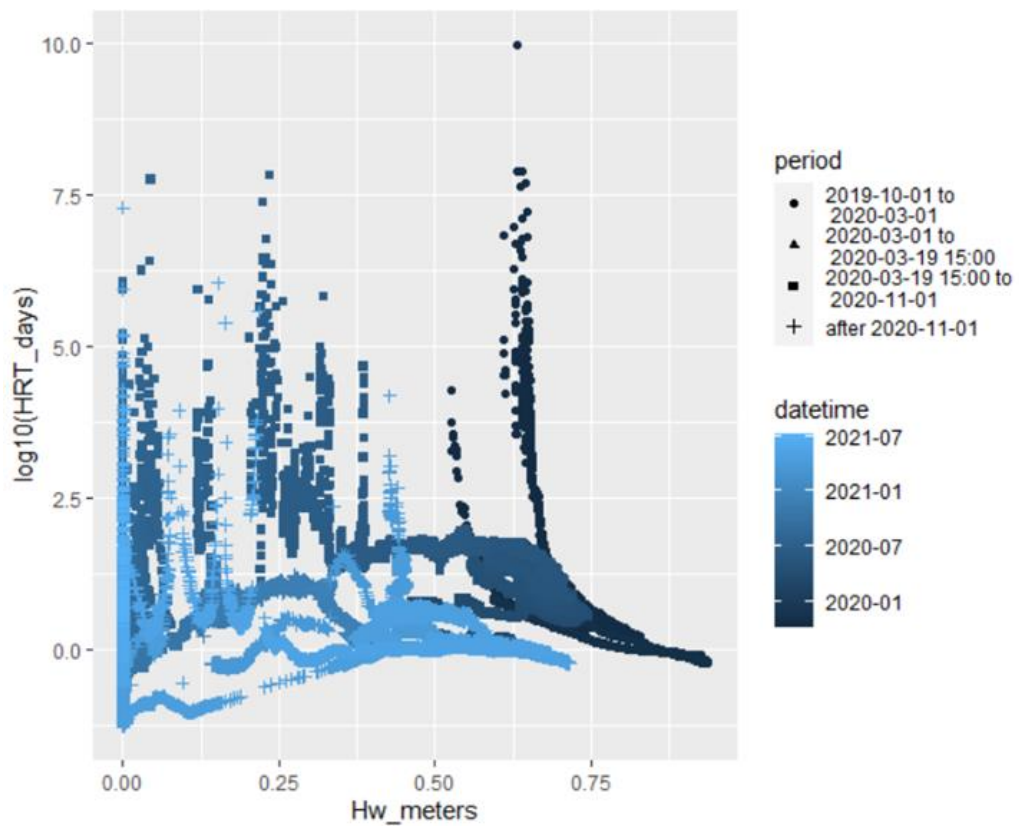


**Figure 3-10 Relationship between depth of flooding (Hw\_meters) in meters and hydraulic residence time ( $\log_{10}(\text{HRT})$ , days) based on system volume and outflow as estimated by field measurements for the Prindle Rd site. Different colors represent three distinct sections of apparent beaver dam influence during the monitoring period.**

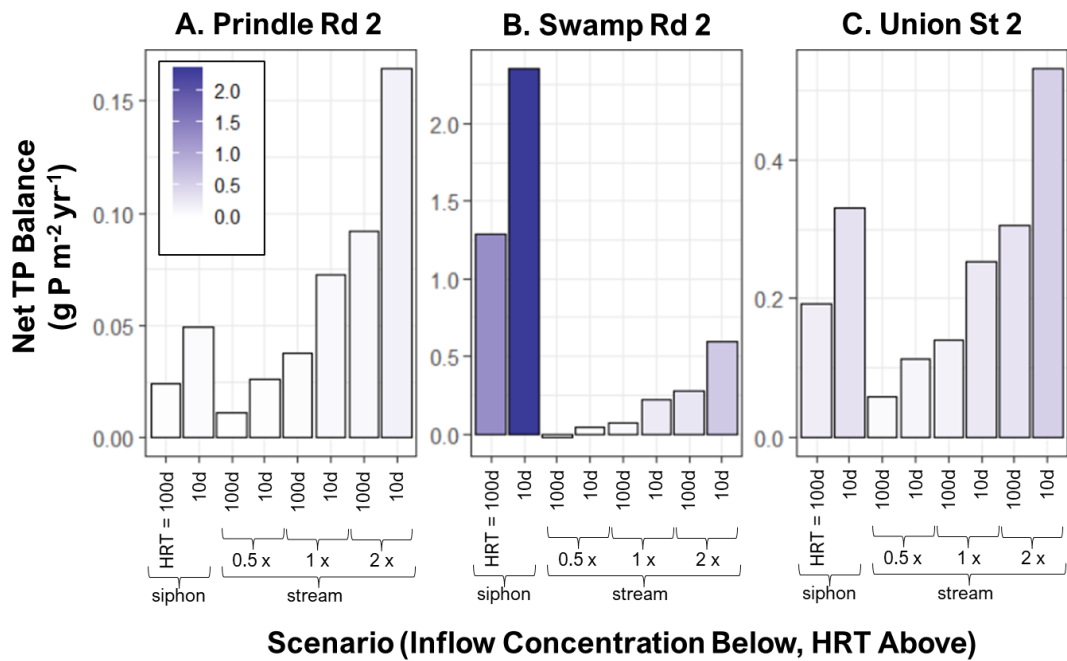


**Figure 3-11 Comparison of concentration verses HRT driven changes on net TP balance assuming 100% particle trapping for the median elevation sampling plot. Concentrations include median concentrations from passive siphons data collected at sampling plots (see Chapter 2), and stream medians multiplied by a factor of 0.5, 1 and 2, while HRT is varied between 10 and 100 days.**

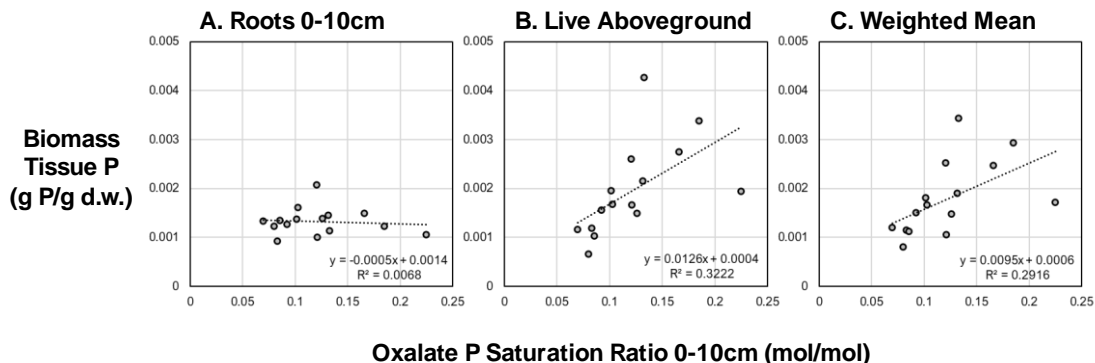


**Figure 3-12 Biomass tissue P concentrations verses oxalate P saturation ratio for various above and belowground biomass.**

### **3.6.2 Calibration**

#### **3.6.2.1 Calibration to Intact Cores**

Stochastic parameters that affect adsorption and diffusion were calibrated by simulating a 2 week incubation of cylindrical (7.6 cm diameter) intact soil cores that were maintained at a water depth ( $H_w$ ) of 0.2 (m). Surface area ( $A$ ) was set to 0.0181 ( $m^2$ , calculated from diameter,  $\pi \cdot (\text{diameter}/2)^2$ ), and volume of the water column aboveground ( $V_w$ ) was set to 0.00362 ( $m^3$ , calculated as  $A \cdot H_w$ ). The hydroclimatic forcing variables were the same for each intact core except for temperature (which was set to the mean of the incubation). Precipitation ( $Q_{\text{precip}}$ ) and net infiltration of groundwater ( $Q_{\text{ground}}$ ) were set to zero, surface outflow ( $Q_{\text{out}}$ ) was set equal to 5e-6 ( $m^3$ , 5ml daily water samples collected from each core), surface inflow ( $Q_{\text{in}}$ ) was set to the 7e-6 ( $m^3$ , set equal to the average daily volume added across all cores of 7ml), and  $Q_{\text{ET}}$  was set to the difference between  $Q_{\text{in}}$  and  $Q_{\text{out}}$ . All model processes were simulated during this experiment accept assimilation of inorganic P by biomass. Biomass and litter stocks were set equal to zero. Input concentrations of TSS were set equal to zero, and the soluble-reactive fraction of TP was set to 1.

The local (measured) parameters that were varied by site were organic matter content of the soil ( $k_{\text{LOI}}$ , g/g, soil loss-on-ignition), the maximum P storage capacity of a soil ( $k_{\text{Ex\_max}}$ , g P/kg,  $31 \cdot [\text{Ox-Al}/27 + \text{Ox-Fe}/56]$ ), the initial ratio of particulate inorganic P (PIP) to the maximum P storage capacity ( $k_{\text{PSR}}$ , mol/mol, oxalate P saturation ratio =  $[\text{Ox-P}/31]/[\text{Ox-Al}/27 + \text{Ox-Fe}/56]$ ), and the initial inflow concentration of TP ( $k_{\text{TP}}$ , equal to the initial SRP concentration of filtered site water). The stochastic parameters that affect adsorption and diffusion are the adsorption bond strength coefficient ( $k_E$ ), adsorption rate coefficient ( $k_{\text{ad}}$ ), and effective diffusion rate coefficient ( $k_{\text{diff}}$ ). I first estimated the value of  $k_E$ , by a minimizing the sum of squared residuals to the calculated equilibrium DIP concentration ( $DIP_E = k_{\text{Ex\_max}} \cdot k_{\text{PSR}} / (1 - k_{\text{PSR}} \cdot k_{\text{Ex\_max}}) \cdot k_E$ ) and final SRP value observed in intact cores. Next, I adjusted the values of the  $k_{\text{ad}}$  and  $k_{\text{diff}}$  so that the shape of the DIP vs time curve in model simulations lined up reasonably well with observed data and recorded a range of plausible values.

#### **3.6.2.2 Calibration to Field Data**

To calibrate/verify the model against data measured in the field, I simulated monitoring plots (15 total) of three wetland ecosystems sites for one wet season from October 1, 2019 to July 15, 2020. Like in the simulation of intact cores  $k_{\text{LOI}}$ ,  $k_{\text{Ex\_max}}$ , and  $k_{\text{PSR}}$ , were used as

local parameters to initialize the belowground compartment. In addition, TSS ( $k_{TSS}$ ,  $\text{g/m}^3 = \text{mg/L}$ ) and TP ( $k_{TP}$ ,  $\text{g/m}^3$ ), the organic fraction of TSS ( $k_f_{OSS}$ ,  $\text{g/g}$ ), and the soluble-reactive fraction of TP ( $k_f_{SRP}$ ,  $\text{g/g}$ ) were used as local parameters and for conversions to the various stocks represented in the model (IM, OM, PIP, LOP, ROP, and DIP) using three stochastic parameters ( $k_{SRP2LOP}$ ,  $k_{ISS2PIP}$ ,  $k_{OSS2ROP}$ ) that were fit to data collected from all three sites. The values for  $k_{TP}$ ,  $k_{TSS}$ ,  $k_f_{OSS}$  and  $k_f_{SRP}$  were set equal to the median value observed at inflow monitoring locations of each site. At Prindle Road, I used data from the northern and eastern culverts. At Swamp Road, I used data from the bridge and the southern ditch (DS). At Union Street, I used data from the bridge, the ditch plug (DP), and the second culvert east of the bridge (C2).

Inorganic accretion is affected by in large part by hydroclimatic forcing variables and the following local parameters: hydraulic residence time ( $HRT = k_{HRT}$ ), the influent concentration of TSS ( $k_{TSS}$ ,  $\text{mg dw/L}$ ) and TP ( $k_{TP}$ ,  $\text{mg P/L}$ ), the organic fraction of TSS ( $k_f_{OSS}$ ,  $\text{g OSS/g TSS}$ ), and soluble-reactive fraction of TP ( $k_f_{SRP}$ ,  $\text{mg SRP/mg TP}$ ). Once inorganic accretion rates were adequately reproduced by the model, I calibrated assimilation and decomposition parameters to the stocks of litter P observed in the wetlands during litter bag decomposition experiments. Organic matter accumulations accretion rates are sensitive to assimilation, mortality, hydrologic inflows, and inflow concentrations. Stochastic parameters that affect organic accretion are the annual rate of net primary productivity ( $k_{NPP}$ ,  $\text{g/m}^2/\text{yr}$ ), the mortality rate of live biomass ( $k_M$ ,  $\text{g/g}$ ), the P content of biomass and all forms of organic matter ( $k_{BM2P}$ ,  $\text{g P/g dw}$ ), the labile fraction of OM/P ( $k_f_{labile}$ ,  $\text{g/g}$ ), and the decomposition rates of litterM/P ( $k_{decay\_litter}$ ,  $\text{g/g}$ ), LOM/P ( $k_{decay\_LOP}$ ,  $\text{g/g}$ ), and ROM/P ( $k_{decay\_ROP}$ ,  $\text{g/g}$ ). The plausible range for parameter values were first informed by the literature. Then I manually estimated values of  $k_M$  and  $k_{NPP}$  that yielded stable stocks of below ground biomass between 1000 and 2000  $\text{g dw m}^{-2}$  while also yielding peak aboveground biomass values of 400-800  $\text{g dw m}^{-2}$ , approximate averages observed at our three field sites. Then I adjusted litter decompositions rates until litter P fell within the range of field observations of stocks. Once biomass and litter were in line, I checked that soil organic matter content was not increasing by more than 2% per year, and repeated the process as needed until all calibration criteria were met. Figures 3-13 through 3-16 below show results from this process.

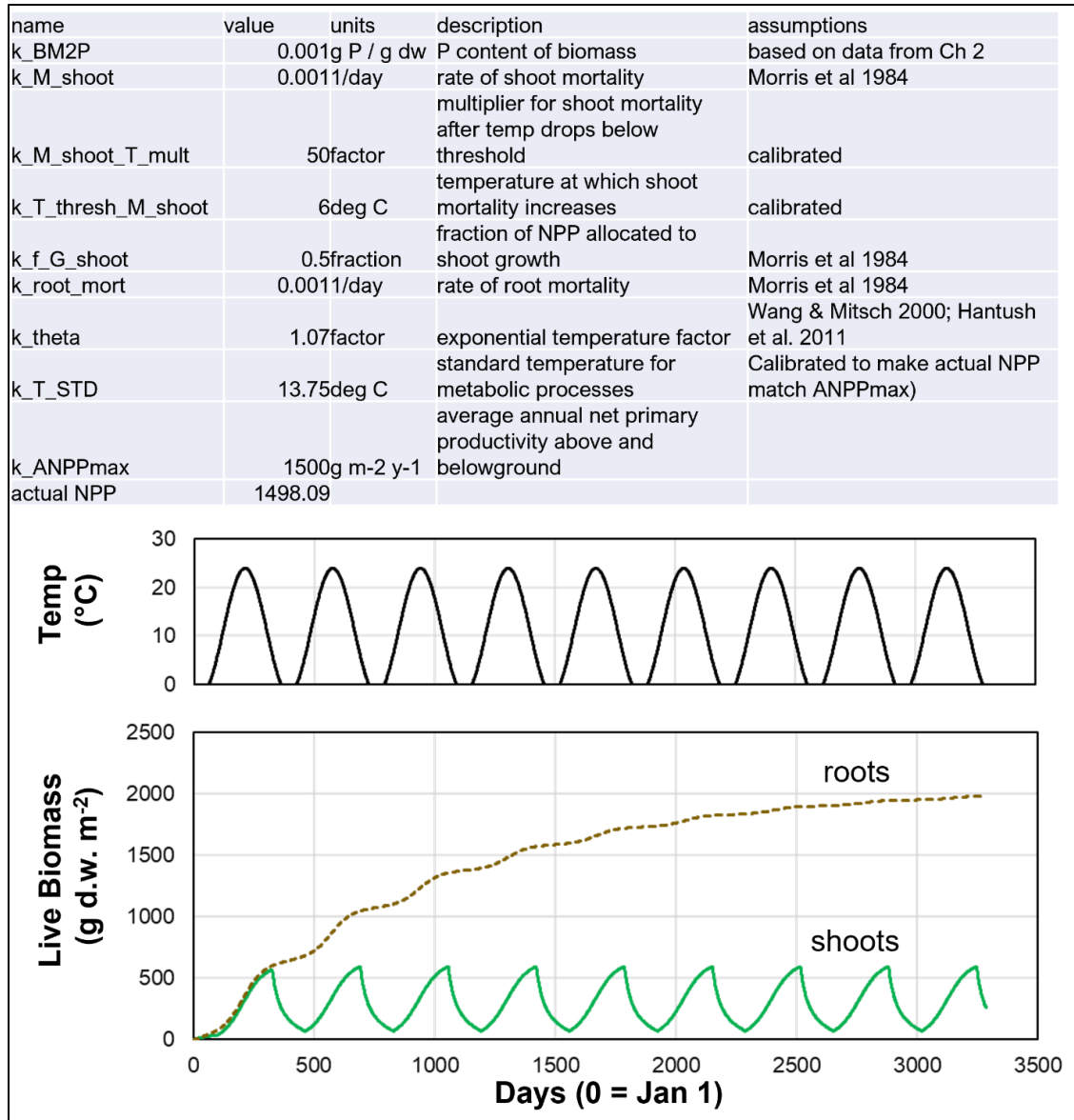


**Figure 3-13 Biomass calibration results showing parameter table (top), plots of temperature (middle), and biomass (bottom) over time in days starting on January 1.**

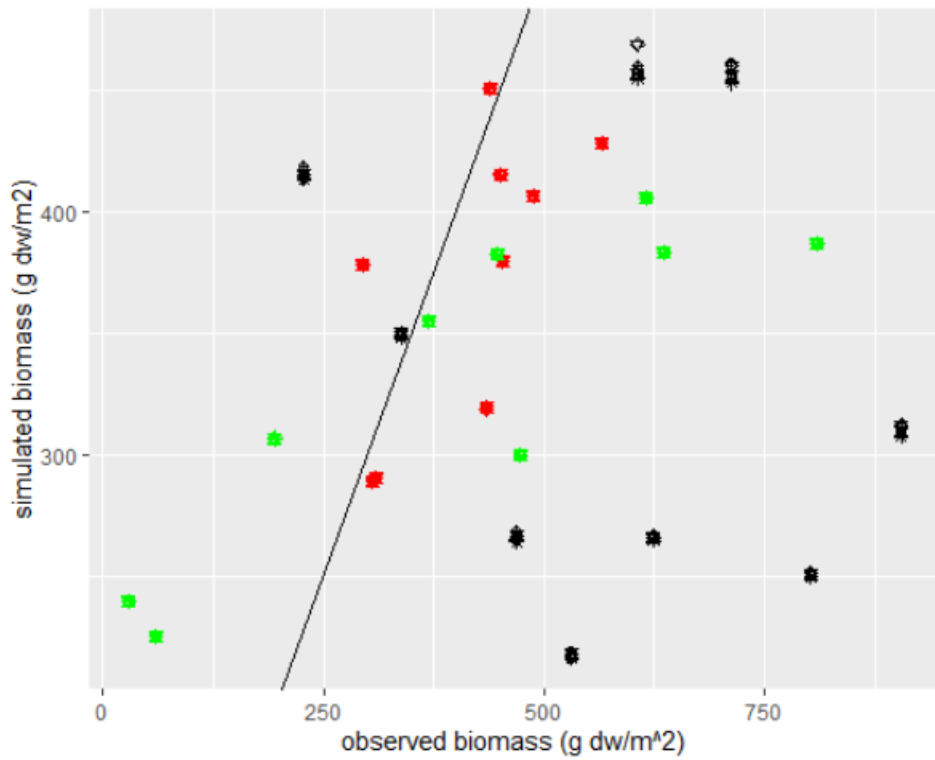


**Figure 3-14 Simulated vs observed biomass for plots 0, 2, and 4 at all sites. Red points are biomass stocks observed on 9/02/19, green points are biomass + fresh litter collected on 10/15/19, and black points are biomass and fresh litter observed on 10/15/20. The black line is the 1:1 line.**

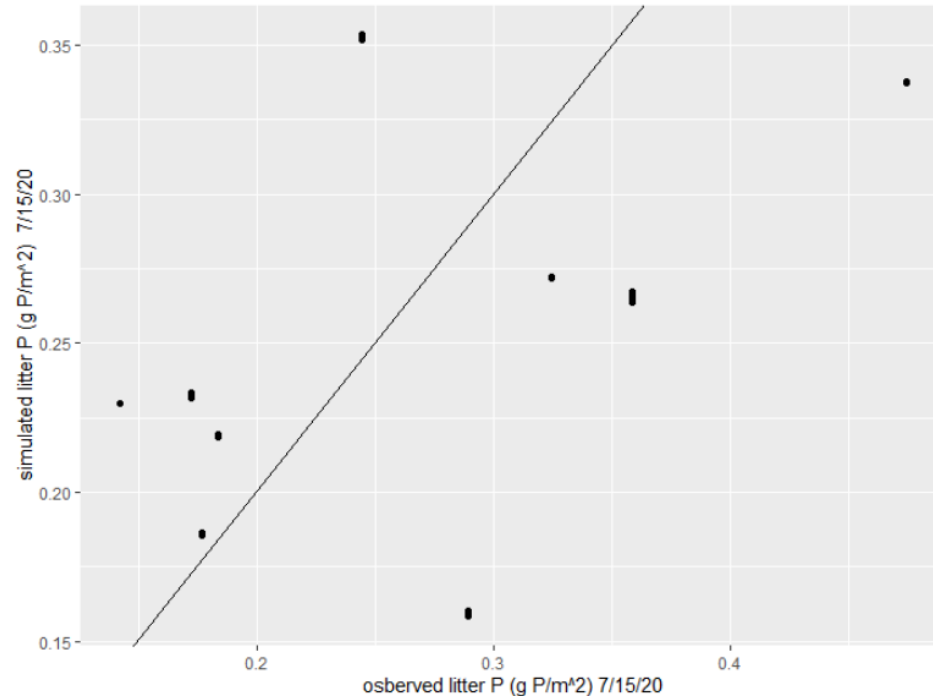


**Figure 3-15 Observed verses modeled stock of litter P 7/15/20 for plots 0, 2, and 4 at all sites.  
The black line is the 1:1 line.**

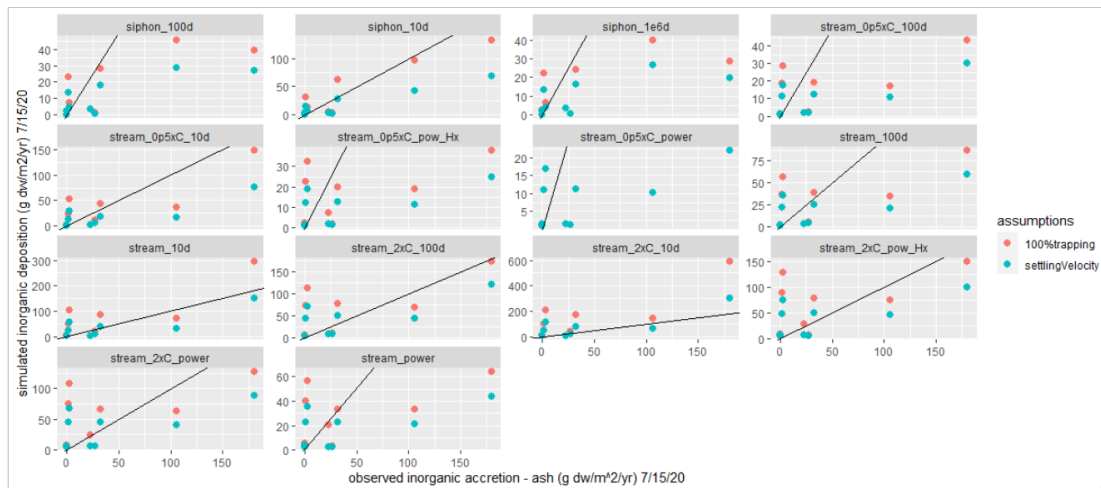


**Figure 3-16 Observed versus simulated change in inorganic matter for plots 0, 2, and 4 for a range of concentration, HRT assumptions, and particle trapping assumptions. Siphon = median siphon concentrations at each plot, stream = median stream concentrations, 0p5xC = 0.5 x stream median concentration, 2xC = 2 x stream concentration, power = power model of HRT, 10d = 10 day HRT, 100d = 100 day HRT. Red/pink points = 100% particle trapping, blue points = modeled particle trapping.**

### 3.6.3 Inflow Concentrations

Inflow concentrations affect many processes that influence P balance, including sedimentation, adsorption, and diffusion. I used TSS, the organic fraction of TSS ( $k_f_{OSS}$ ), TP, and the soluble reactive fraction of TP ( $k_f_{SRP}$ ) as input parameters to the model, then converted these into various mass stocks represented in the model: IM, OM, PIP, LOP, ROP, DIP. I assumed that IM was equal to  $ISS = TSS * (1 - k_f_{ISS})$ , and that DIP was equal to  $SRP = TP * k_f_{SRP}$ . I calculated observed non-SRP as the difference between TP and SRP and assumed that non-SRP was the sum of PIP, LOP and ROP. I assumed that ROP and LOP scaled proportionately to OSS, PIP scales proportionately in part with ISS and in part with SRP. I calculated LOM and ROM based on estimated LOP and ROP concentrations, and  $k_{BM2P}$  (the P content of biomass) and  $k_f_{labile}$  (the labile fraction of live biomass), and OM as the sum of LOM and ROM. Each of LOP, ROP, and PIP, were calculated using a scaling coefficient to convert SRP to PIP ( $k_{SRP2PIP}$ ), ISS to PIP ( $k_{ISS2PIP}$ ), and OSS to ( $k_{OSS2OP}$ ). I set  $k_{OSS2OP}$  equal to 0.001 (g P/g dw) the value used for the P content of organic matter and live biomass ( $k_{BM2P}$ ). Then, I solved for the values of  $k_{ISS2PIP}$  and  $k_{SRP2LOP}$  at each site by minimizing the sum of squared errors (SSE) between the observed non-SRP (TP-SRP) and modeled non-SRP ( $k_{ISS2PIP} * ISS + k_{OSS2OP} * OSS + k_{SRP2PIP} * SRP$ ) using the GRG nonlinear optimization method from the `solver` add-in in Microsoft Excel. Figure 3-17 and Figure 3-18 show the observed versus fitted data with various approaches to estimate the parameter values. For the simulations in the scenario analysis, I used local & global fit (Figure 3-17 and Figure 3-18). For simulation of a hypothetical system, I recommend using the all global fit (Figure 3-17).

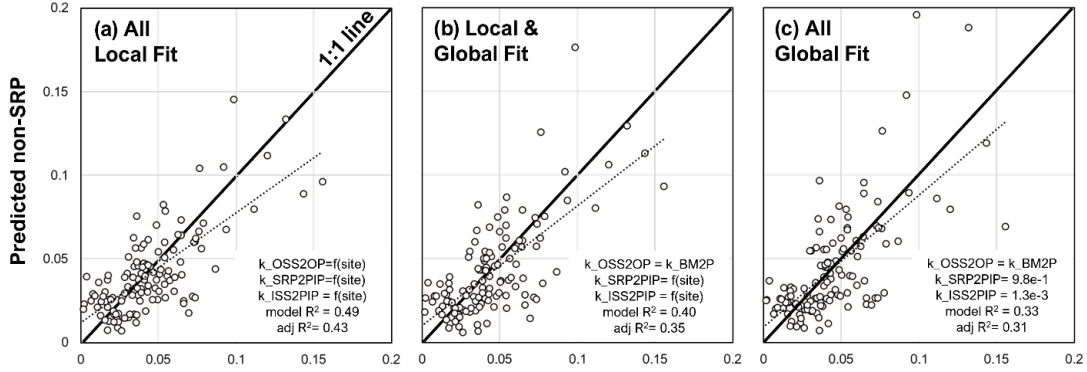


**Figure 3-17 Observed vs predicted non-SRP concentrations using local (a,  $k=9$ ), partial (b,  $k=6$ ), and global (c,  $k=3$ ) parameter estimates ( $n=131$ ).**

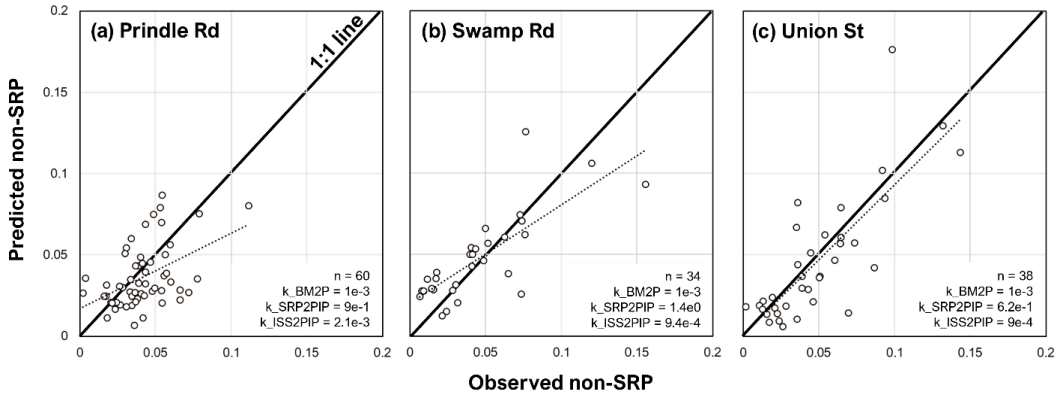


**Figure 3-18 Observed vs predicted non-SRP (TP – SRP, mg P/L) and estimates of scaling coefficients convert SRP to LOP ( $k_{SRP2LOP}$ ), ISS to PIP ( $k_{ISS2PIP}$ ), at Prindle Rd (a), Swamp Rd (b) and Union St (c). The 1:1 line is the thick black line. Dotted line shows the regression on observed (x) vs predicted (y).**

### 3.6.4 Hydroclimate Inputs

Preprocessing inputs were water elevation and temperature recorded by HOBO MX-2001 loggers at 10-minute intervals, and sub-hourly meteorological data from the Burlington airport (NOAA, n.d.), used to estimate precipitation and evapotranspiration. The HOBO data were summarized to daily values by taking the average temperature, and the maximum water height each for each calendar date in the record, then converted to estimates of water height and storage volume ( $m^3/m^2$ ) for each plot. The meteorological data was summarized to daily values by averaging temperatures and windspeed, relative humidity, and by summing precipitation. Daily evapotranspiration rates were estimated from meteorological data via the Penman-Monteith

method using the R package `evapotranspiration` (Guo et al., , 2016). Net surface flow was estimated by adjusting changes in water volume for estimated precipitation and evapotranspiration. For a given simulation, inflow and outflow were deduced from net surface flow, by adding a term for throughflow which was calculated as the water volume divided by hydraulic residence time (HRT).

### 3.6.5 Hydraulic Residence Time

Hydraulic retention time or residence time is the measure of the average amount of time a molecule of water will spend in a control volume before leaving. HRT is calculated by dividing the system volume by the volumetric outflow rate. At Prindle Road, this was achieved by creating a relationship with water height (measured continuously) and storage volume and collecting multiple outflow velocity measurements over the course of monitoring (Figure 3-19). I converted outflow velocity measurements to volumetric flow rates (discharge) by multiplying velocity by cross sectional area. To estimate cross sectional as a function of water level at the outflow, I set up a level line then measured the height of the water level sensor to the level line and measured the height of the channel bottom at every 30cm across the width of the floodplain. I fit a regression between discharge and stage to estimate discharge as a function of time, and then interpolated estimates of storage from LiDAR using the ArcGIS Storage Capacity tool.

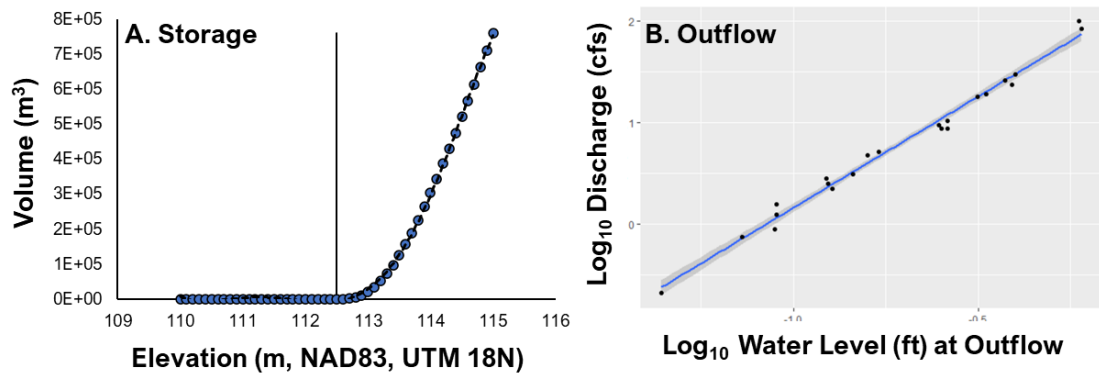


**Figure 3-19 Relationships observed between elevation/stage (continuously logged by HOBO MX2100), storage volume estimated from LiDAR (A) and outflow (B). The black vertical line on A shows the elevation of the water level logger in the wetland. Water levels were continuously logged, while discharge calculated from velocity and cross-sectional measurements at outflows.**

At Otter Creek sites, I estimated the general magnitude of HRT in the floodplains using two HEC-RAS simulated floods, May 2019 and April 2018. I did this by exporting raster grids of

the depth and velocity (magnitude) for the entire model domain at the time of peak flow at Union Street and Swamp Road bridges. This resulted in raster grids exported at four times (Table 3-1).

**Table 3-1 Date, time, location of peak discharge of Otter Creek HEC-RAS simulated flood peaks.**

Date and time	Location of Peak	Discharge at Peak
2018-05-01 09:40	Union St	96.9 m <sup>3</sup> /s (3420 cfs)
2018-05-03 18:20	Swamp Rd	89.6 m <sup>3</sup> /s (3160 cfs)
2019-04-16 16:40	Union St	254.6 m <sup>3</sup> /s (8990 cfs)
2019-04-18 06:00	Swamp Rd	168.2 m <sup>3</sup> /s (5940 cfs)

We digitized a polygon of the river and of the entire floodplain between the monitoring bridge and the next constraining feature downstream (in both cases another bridge) (Figure 3-20). I clipped each raster to the extent of the channel only, the floodplain only, and the floodplain and the channel and calculated the volume of water held in each extent. I then extracted depth and velocity values across the upstream boundary transect. For each cell along the transect, I calculated cross sectional area (depth \* width) and discharge (area \* velocity). I then summed the discharge for the channel only, floodplain only, and floodplain and channel. I calculated HRT by dividing the volume by the discharge estimated for the channel only, floodplain only, and both channel and floodplain. Floodplain HRT followed a negative power law with discharge and depth of flooding at both sites. Union Street had lower HRT than Swamp Road, with floodplain HRT ranging between 0.2-0.8 days at Union Street and 0.6-2.1 days at Swamp Road. For reference, an HRT of 0.2 days means that 5 times the control volume flows through the system each day, while an HRT of 2 means that 0.5 times the control volume flows through the system each day.

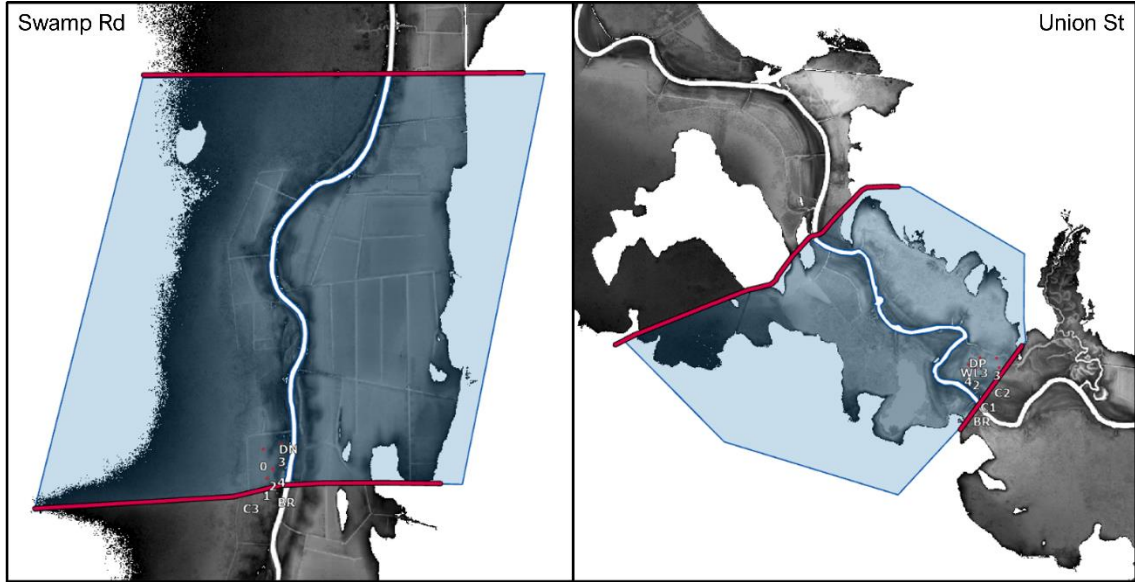


**Figure 3-20 Depth of inundation in otter creek showing location of sampling plots and the reach polygons (blue shaded areas) used to calculate system storage volume, and cross sections (red) were velocity and cross-sectional area were used to estimate discharge through the floodplain.**

### 3.6.6 Sensitivity Analysis

We used a steady state model with the calibrated default parameters to investigate model sensitivity to four tests that examined changes in the following:

- **Local water quality:** Randomly varying inflow TSS and P concentrations and initial state variables while holding hydroclimatic variables and stochastic parameters constant.
- **Local hydrology:** Randomly varying hydroclimatic variables while holding inflow TSS and P concentrations and initial state variables and stochastic parameters constant.
- **All local parameters:** Randomly varying all local parameters (concentrations, states, hydroclimatic variables) while holding stochastic parameters constant.
- **Stochastic parameters:** Randomly varying stochastic parameters while holding all local parameters constant.

We did this by employing the Global Sensitivity Analysis technique (Haan, 2002). Briefly, I conducted 10,000 Monte Carlo simulations for each sensitivity test described above, with randomly generated values for each parameter varied in the test. Random values were drawn from either a log-normal or uniform probability distribution. To ensure reproducibility, I called

the `set.seed` function with a value of 1 prior to generating the parameter values. For each simulation, I extracted the initial value of the state variables and calculated the difference and percent difference in state variables between the first and last time point. The extracted data was stored in a data table containing random values for each parameter, the name of the sensitivity test and the simulation number (1 to 10,000). To measure the relative effect that each parameter had on the model for each sensitivity test, I produced a correlation matrix between the input parameters and outputs. I computed both Pearson product moment correlation coefficient and Spearman's rank correlation coefficient (Hantush et al., 2013). The Spearman coefficient indicates the strength of a monotonic relationship (linear or nonlinear), while the Pearson coefficient indicates the strength of a linear relationship. A large difference between the Pearson and Spearman coefficients indicates nonlinearity.

Using Global Sensitivity Analysis allowed us to examine whether the model was performing as I thought it should be based on our understanding of biogeochemistry, and to assess the magnitude and direction of impacts that changes in local site conditions have on net P retention. Figure 3-21, 3-22, and 3-23 show the correlation strengths of the parameters in the suite of sensitivity tests I conducted. When local concentrations were varied and hydroclimatic parameters and stochastic variables were fixed, I found that  $k_{Ex\_max}$ ,  $k_{PSR}$ , and  $k_{LOI}$  had significant negative Spearman correlation, indicating that increases in these variables were associated with greater TP loss from the wetland. When varying all local parameters simultaneously, I found that the magnitude correlation strength for  $k_{TP}$  and  $k_{f\_SRP}$  was similar to  $k_{Ex\_max}$  and  $k_{PSR}$ , with the former having increased in correlation strength from when only concentrations were varied. When holding local parameters constant and varying all stochastic parameters, I found that  $k_E$  had by far the greatest impact on net TP balance, with a Spearman correlation  $\sim 0.7$  and a Pearson correlation near  $\sim 0.3$ , indicating nonlinearity.

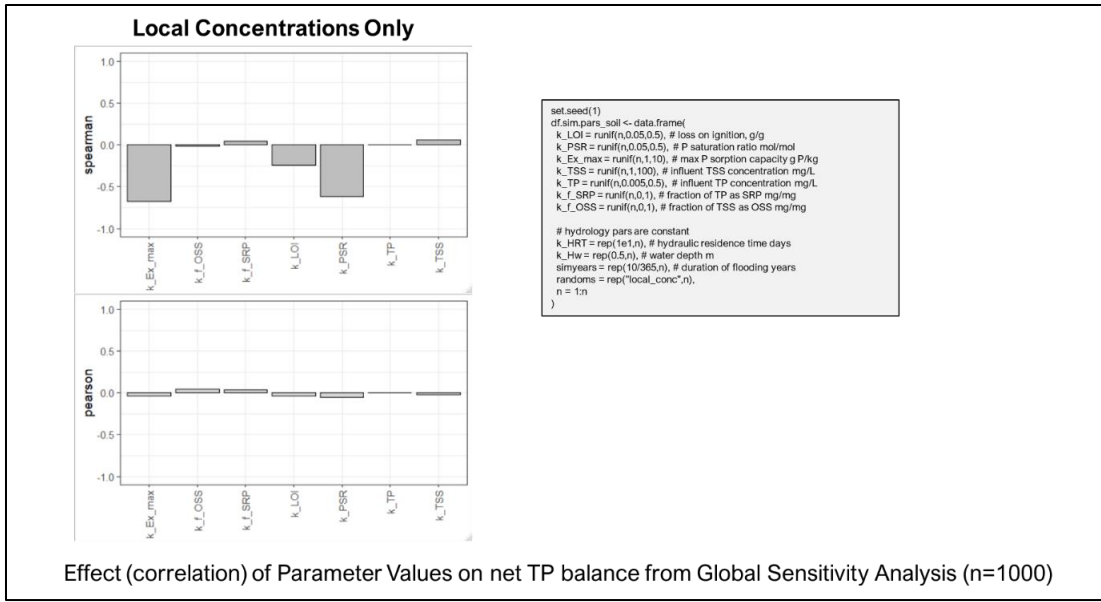


**Figure 3-21 Global sensitivity analysis showing Spearman (top) and Pearson (bottom) correlation for the varying local concentrations only. The box on the right shows the R code used to draw random values for each parameter.**

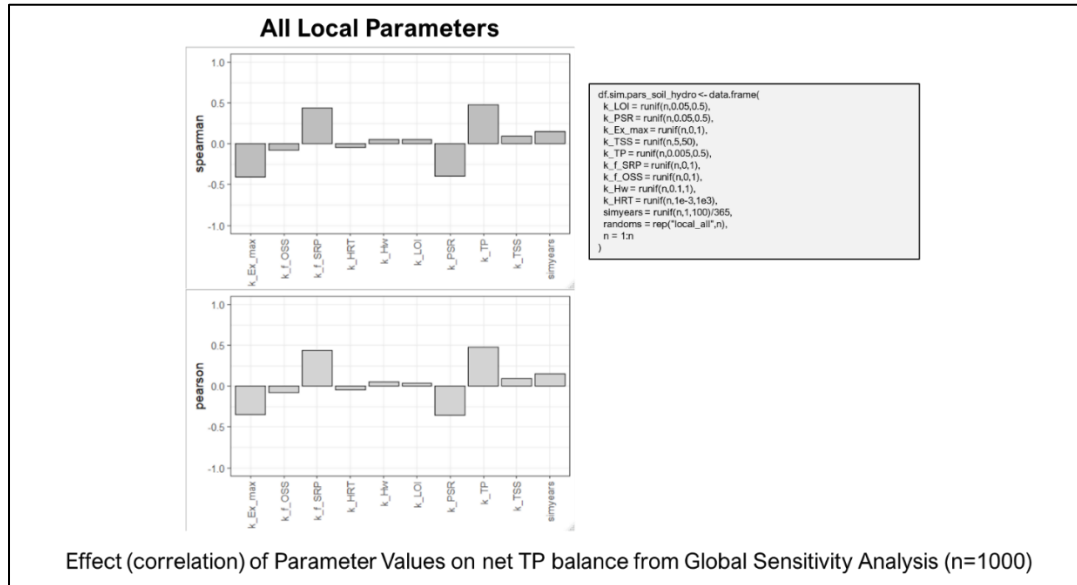


**Figure 3-22 Global sensitivity analysis showing Spearman (top) and Pearson (bottom) correlation for the varying all local parameters. The box on the right shows the R code used to draw random values for each parameter.**

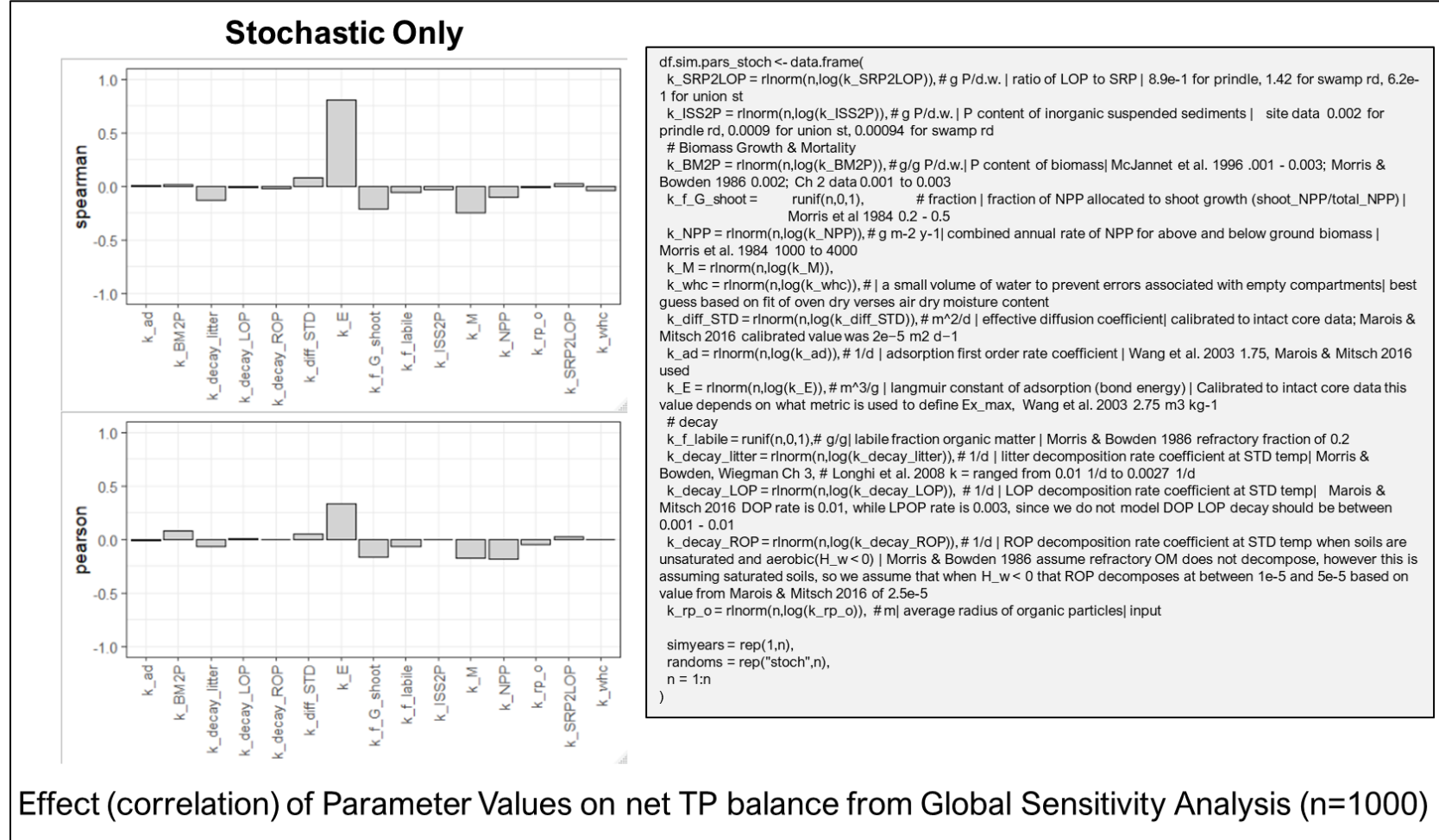


**Figure 3-23 Global sensitivity analysis showing Spearman (top) and Pearson (bottom) correlation for the varying all stochastic parameters. The box on the right shows the R code used to draw random values for each parameter.**

### 3.6.7 Modeling Langmuir Parameters

The model simulated DIP\_E in intact cores with roughly the same mean and standard deviation for the observed concentrations (Figure 3-24). However, the use of k\_E as a global stochastic rather than local parameter led to under-prediction of high SRP concentrations and/or over-prediction of low concentrations, depending on the value of k\_E. When the performance metric for calibration was the sum of squared errors (optimizing for the mean difference), the estimate for k\_E was ~ 0.55, leading to fair prediction at high concentrations but over prediction at low concentrations. When I switched the performance metric to the sum of absolute errors (optimizing for the median difference), the estimate for was k\_E ~ 1, leading to fair prediction of low concentrations but under-prediction of high concentrations.

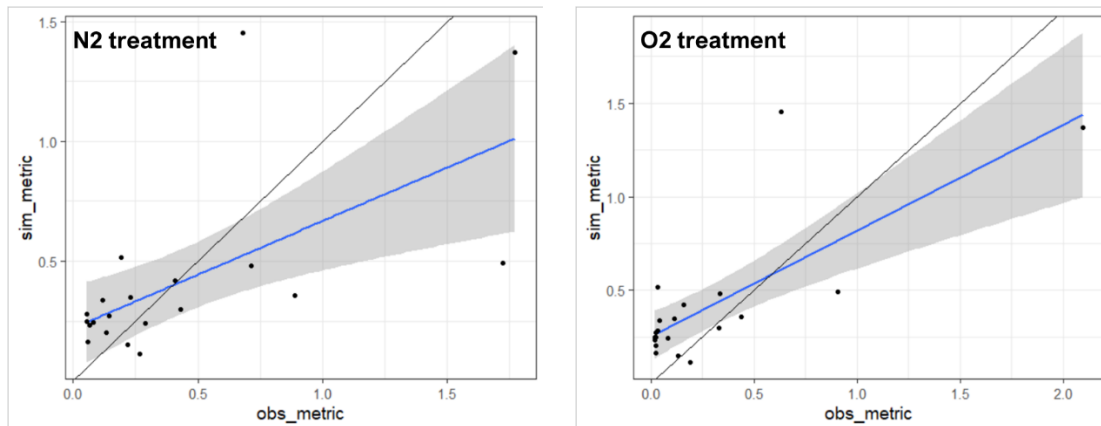


**Figure 3-24 Observed versus predicted final water column SRP (mg/L) in intact cores after ~14 day simulation.**

The inability of the model to accurately reproduce intact core concentrations across the wide range of soils was due to our treatment of k\_E as a stochastic rather than local parameter and perhaps also due to the simplicity of the adsorption model, which contains just one uniform space for adsorption. The k\_E and k\_Ex\_max terms in our model are analogous to the bond energy coefficient (aka K<sub>L</sub>) and sorption maximum (aka Smax), used in the Langmuir model of P sorption isotherm studies ( Nair & Reddy, 2013).

There is strong evidence that the Smax parameter is related to oxalate extractable Al + Fe (Reddy et al., 1998; Zhang et al., 2005). Al + Fe and Smax are also correlated to silt + clay, as well as organic matter (Kang et al., 2009). In the current version of the model, I set k\_Ex\_max as a constant value equal to the P mass equivalent of moles of oxalate extractable Al + Fe. Future

versions of the model could make k\_Ex\_max a variable function of fine sediments (silt + clay) and/or organic matter.

Dari et al. (2015) suggested that K<sub>L</sub> can be modeled using PSR or SPSC. Future iterations of the model could examine conversion of k\_E to a variable that is a function of the soil parameters of the model (k\_LOI, k\_Ex\_max, k\_PSR, k\_f\_fines). If changes are made to model's handling of k\_E and k\_Ex\_max, there is the potential for the model to reach numerical instability under certain circumstances. This might occur if both k\_E and k\_Ex\_max is variable in time and/or if one is a function of the other. Any future changes to adsorption parameters should be done with this in mind.

Other possible changes that might improve the model's ability to predict SRP concentrations might involve accounting for a diversity of adsorption surfaces and redox conditions. This could be done by adding redox dynamics to the model and splitting binding sites into redox sensitive (such as Fe, Mn) and non-redox sensitive pools (such as Al, Mg, Ca) (Hantush et al., 2013; Wang et al., 2003). This could also be done by splitting binding sites into easy-to-access (high adsorption energy, k\_E) and hard-to-access sites (low k\_E). The number of easy-to-access sites would be equal to the product of k\_Ex\_max and the threshold PSR value used in soil P storage capacity (SPSC) calculations, while hard-to-access sites would be equal to difference between k\_Ex\_max the quantity of easy-to-access sites.

## SUMMARY AND CONCLUSION

In this dissertation, I generated data and tested assumptions about factors influencing P retention and release in riparian wetlands with a history of agricultural use. My research involved a unique triangulation of field monitoring, laboratory experiments, and simulation modeling. This approach helped me to develop several important concepts relating to P dynamics in riparian wetland soils having agricultural legacies, culminating in the modeling exercise in Chapter 3 where I estimated net TP retention for three restored riparian wetland ecosystems. This is an important and timely accomplishment, especially considering the attention and resources that policymakers and resource managers are dedicating to the estimation of P load reduction benefits for wetland restoration in Vermont and elsewhere (US EPA, 2015; VTDEC, 2021).

In Chapter 1, I quantified the risk of SRP release in historically drained and farmed riparian soil across the Vermont portion of the Lake Champlain Basin. I characterized floodplain and wetland soils at sites ranging from mature wetlands to active farms and examined relationships between SRP release, soil properties, and land use metrics. An important outcome of this Chapter was that I calculated the threshold P saturation ratio for the acid ammonium oxalate extraction (PSR is the molar ratio of P to Al and Fe, see Chapter 1 Eqn. 1-1) with a rigorous survey of historically drained and farmed floodplain wetlands in Vermont. The threshold PSR is used to calculate soil P storage capacity (SPSC, see Chapter 1 Eqn. 1-2), which is a metric that has been used in a variety of settings to assess SRP loss risk from soils affected by legacy P. I also verified the use of SPSC as a predictor of SRP release at Vermont wetland sites with prolonged periods of inundation by examining the ability of SPSC to predict SRP flux rates observed during laboratory simulated floods using intact soil cores. I found that SPSC was a good ( $r^2 = \sim 0.66$ ,  $n=20$ ,  $p=1E-5$ ) predictor of SRP release (across two orders of magnitude of SRP release). Modified Morgan P (MM-P), which is the most widely used soil P test in Vermont, was a fair predictor SRP release ( $r^2 = \sim 0.46$ ,  $n=20$ ,  $p=9E-4$ ). There was a strong nonlinear relationship between MM-P and both PSR and SPSC, so MM-P data could potentially be used to estimate SPSC, PSR, and SRP release when oxalate data are unavailable.

Another key outcome of Chapter 1 was that I developed a method to classify the farming history of wetland restoration candidates using free Google software. This is important because I found that farming frequency was a suitable proxy for soil data when predicting potential soil SRP release upon flooding. Intact core SRP release was higher in the more recently and frequently farmed soils. Despite lower overall SRP release at sites with longer time since farming,

substantial SRP release occurred in soils that had not been farmed for over a decade, which indicates that legacy soil P may have lasting impacts on SRP loads to Lake Champlain. In Chapter 1, I also provided data and insights for future efforts to map legacy soil P and potential SRP release in riparian wetlands and river corridors of Vermont. For example, data from this chapter suggests that metrics of farming frequency and/or recency derived from aerial imagery or land use datasets (e.g., USDA Croplands Data Layer) (NASS, 2021) could be used in combination with soil texture layers (NRCS soil survey units) (NRCS, 2021) to estimate at a screening level the locations of hotspots of soil legacy P and potential high SRP release.

In Chapter 2, I quantified detailed P dynamics for three restored wetlands in the Otter Creek and Lewis Creek watersheds that historically had been drained and farmed prior to restoration. Through field monitoring and laboratory experiments, I quantified the P stocks in soil, vegetation, and water, and the factors affecting mass flows among them. My analysis in Chapter 2 was focused on factors related to sediment deposition (or particulate trapping) and SRP release, because they are the two key factors influencing P retention. The inorganic P deposition rates ranged from  $\sim 0.1 - \sim 1$  g P m<sup>-2</sup> yr<sup>-1</sup>, which would put these systems on the low end of the spectrum in terms of potential for particulate P retention in Vermont (Diehl et al., 2021). For context, the ecosystems studied in this chapter fall in the category of low energy (low gradient) floodplain systems which are characterized by lentic (slow moving) waters and inundation time on the order of days to weeks for a given flood pulse. Field data showed evidence that wetlands did release SRP to floodwaters at times. However, accretion data and concentrations of dissolved oxygen and SRP during floods suggest that at least some of this internally released SRP was retained by plant assimilation and or co-precipitation, though more research is needed to confirm this.

In Chapter 3, I formalized the observations and hypotheses from the previous Chapters with a numerical simulation model. I used the model to estimate net P retention over a two-year monitoring period in the wetlands studied in Chapter 2. I also examined the sensitivity of wetland net P retention to changes in factors such as upstream P concentrations and discharge through the wetland (which was modeled by changing water depth and hydraulic residence time). I found that net TP balance of the ecosystems monitored in Chapter 2 is likely positive, with average retention efficiency of ~40%, though there was substantial variability. Simulated total P balances were highly sensitive to changes in inflow concentrations. Across the three wetlands, the average total P balance for my “best guess” simulations was a net gain of  $\sim 0.1$  g P m<sup>-2</sup> yr<sup>-1</sup> or 1 lb P acre<sup>-1</sup> yr<sup>-1</sup>. For context, a recent study by University of Vermont researchers estimated that surface losses from active farm

fields is on average also roughly 1 lb P acre<sup>-1</sup> yr<sup>-1</sup> (Faulkner, personal communication), so the net benefit of the wetlands studied in Chapter 2 compared to continued farming would be roughly 2 lb P acre<sup>-1</sup> yr<sup>-1</sup>. I advise against extrapolating estimates produced in Chapter 3 to estimate P retention benefits in other settings. For context, the three wetlands I modeled were low energy floodplains (relative to all Vermont floodplains) that had not been farmed for over a decade. Peak depths were on the order of 0.1 to 1 M. Hydraulic residence times were on the order of 10 to 100 days. Inflow total P concentrations were on the order of 0.05 to 0.07 mg P L<sup>-1</sup>. Inflow SRP concentrations were on the order of 0.01 to 0.03 mg/L. In the future, the model could be used to simulate low energy floodplains with different water level dynamics, soils, and influent water quality to produce a broader range of possible net P retention outcomes.

My simulations also showed that soil SRP buffering is a key feature of historically drained and farmed wetlands that managers should be aware of. I found that reduction of inflow SRP concentrations promoted SRP release from soils through soil SRP buffering. This phenomenon may cause a time lag between adoption of upstream best management practices and reduction in downstream SRP concentrations in stream corridors that are affected by legacy P. Future modeling efforts should explore these impacts in more detail to help guide crediting systems for P load reduction.

My dissertation involved a unique combination of field monitoring, lab analysis, and computer modeling across a range of spatial scales and disciplines (e.g., geospatial analysis and biogeochemistry). It is rare that research projects in environmental sciences work across scales and disciplines. It is even rarer that such a study would also generate primary data and apply that data in a numerical model. I think that when this holistic approach is applied research efforts are more impactful compared to when field, lab, and modeling efforts are endeavored independently. For example, the parameters and input data for numerical models are often vaguely defined and cannot be directly measured or transferred from field studies. As a result, modelers often laboriously calibrate many parameters to the specific site and set of conditions under which a model is applied (DHI, 2004; M. M. Hantush et al., 2013; Jackson-Blake et al., 2017; Marois & Mitsch, 2016). This feature of many numerical models limits their scope of application to detailed study of a very limited number of locations. My aim in Chapter 3 was to develop a more generalized model that could be applied to a wide number of sites and environmental conditions. Thus, a key focus was to use a small number of parameters and metrics that are measured widely by field biogeochemists. To my knowledge, the model I developed is the first to use soil P storage capacity and related metrics as inputs.

The model resulting from my dissertation work uses three key inputs to initialize the soil compartment and parameters for several processes: (1) organic matter content, (2) the soil P saturation ratio (the molar ratio of P to Al and Fe), and (3) P storage maximum (the latter two can be used to estimate soil P storage capacity). This is an important breakthrough because the model is able to simulate both natural and agriculturally impacted soils with data from three relatively simple soil tests that are widely available in the literature and offered by most analytical labs in the United States for a total cost of less than \$50 per sample. Efforts are already underway to apply the model I developed in Chapter 3 to assess opportunities for restored riparian wetlands to serve as net phosphorus sinks across numerous sites in Vermont.

## COMPREHENSIVE BIBLIOGRAPHY

- Aldous, a R., Craft, C. B., Stevens, C. J., Barry, M. J., & Bach, L. B. (2007). Soil phosphorus release from a restoration wetland, Upper Klamath Lake, Oregon. *Wetlands*, 27(4), 1025–1035. [https://doi.org/10.1672/0277-5212\(2007\)27\[1025:SPRFAR\]2.0.CO;2](https://doi.org/10.1672/0277-5212(2007)27[1025:SPRFAR]2.0.CO;2)
- Aldous, A., McCormick, P., Ferguson, C., Graham, S., & Craft, C. (2005). Hydrologic regime controls soil phosphorus fluxes in restoration and undisturbed wetlands. *Restoration Ecology*, 13(2), 341–347. <https://doi.org/10.1111/j.1526-100X.2005.00043.x>
- Anderson, K. R., Moore, P. A., Miller, D. M., DeLaune, P. B., Edwards, D. R., Kleinman, P. J. A., & Cade-Menun, B. J. (2018). Phosphorus Leaching from Soil Cores from a Twenty-Year Study Evaluating Alum Treatment of Poultry Litter. *Journal of Environmental Quality*, 47(3), 530–537. <https://doi.org/10.2134/jeq2017.11.0447>
- Ardón, M., Montanari, S., Morse, J. L., Doyle, M. W., & Bernhardt, E. S. (2010a). Phosphorus export from a restored wetland ecosystem in response to natural and experimental hydrologic fluctuations. *Journal of Geophysical Research: Biogeosciences*, 115(4), 1–12. <https://doi.org/10.1029/2009JG001169>
- Ardón, M., Montanari, S., Morse, J. L., Doyle, M. W., & Bernhardt, E. S. (2010b). Phosphorus export from a restored wetland ecosystem in response to natural and experimental hydrologic fluctuations. *Journal of Geophysical Research: Biogeosciences*, 115(4), 1–12. <https://doi.org/10.1029/2009JG001169>
- Ardón, M., Morse, J. L., Doyle, M. W., & Bernhardt, E. S. (2010). The Water Quality Consequences of Restoring Wetland Hydrology to a Large Agricultural Watershed in the Southeastern Coastal Plain. *Ecosystems*, 13(7), 1060–1078. <https://doi.org/10.1007/s10021-010-9374-x>
- Audet, J., Zak, D., Bidstrup, J., & Hoffmann, C. C. (2019). Nitrogen and phosphorus retention in Danish restored wetlands. *Ambio*. <https://doi.org/10.1007/s13280-019-01181-2>
- Audet, J., Zak, D., Bidstrup, J., & Hoffmann, C. C. (2020). Nitrogen and phosphorus retention in Danish restored wetlands. *Ambio*, 49(1), 324–336. <https://doi.org/10.1007/s13280-019-01181-2>
- Bedford, B. L., Walbridge, M. R., & Aldous, A. (1999). Patterns in Nutrient Availability and Plant Diversity of Temperate North American. *Ecology*, 80(7), 2151–2169. <https://doi.org/10.2307/176900>
- Beutel, M. W., Morgan, M. R., Erlenmeyer, J. J., & Brouillard, E. S. (2014). Phosphorus Removal in a Surface-Flow Constructed Wetland Treating Agricultural Runoff. *Journal of Environment Quality*, 43(3), 1071. <https://doi.org/10.2134/jeq2013.11.0463>
- Bhadha, J. H., Harris, W. G., & Jawitz, J. W. (2010). Soil Phosphorus Release and Storage Capacity from an Impacted Subtropical Wetland. *Soil Science Society of America Journal*, 74(5), 1816. <https://doi.org/10.2136/sssaj2010.0063>
- Bolster, C. H., & Hornberger, G. M. (2007). On the Use of Linearized Langmuir Equations. *Soil Science Society of America Journal*, 71(6), 1796–1806.

<https://doi.org/10.2136/sssaj2006.0304>

Bouyoucos, G. J. (1962). Hydrometer method improved for making particle size analyses of soils. *Agronomy*, 54(5), 464–465.

Busse, L. B., & Gunkel, G. (2002). Riparian alder fens - Source or sink for nutrients and dissolved organic carbon? - 2. Major sources and sinks. *Limnologica*, 32(1), 44–53. [https://doi.org/10.1016/S0075-9511\(02\)80016-0](https://doi.org/10.1016/S0075-9511(02)80016-0)

Callaway, J. C., Cahoon, D. R., Lynch, J. C., DeLaune, R. D., Reddy, K. R., Richardson, C. J., & Megonigal, J. P. (2013). *The Surface Elevation Table–Marker Horizon Method for Measuring Wetland Accretion and Elevation Dynamics*. January. <https://doi.org/10.2136/sssabookser10.c46>

Carpenter, S. R. (2005). Eutrophication of aquatic ecosystems: Bistability and soil phosphorus. *Proceedings of the National Academy of Sciences*, 102(29), 10002–10005. <https://doi.org/10.1073/pnas.0503959102>

Carpenter, S. R. (2008). Phosphorus control is critical to mitigating eutrophication. *Proceedings of the National Academy of Sciences*, 105(32), 11039–11040. <https://doi.org/10.1073/pnas.0806112105>

Chapra, S. C., Boehlert, B., Fant, C., Bierman, V. J., Henderson, J., Mills, D., Mas, D. M. L., Rennels, L., Jantarasami, L., Martinich, J., Strzepek, K. M., & Paerl, H. W. (2017). Climate Change Impacts on Harmful Algal Blooms in U.S. Freshwaters: A Screening-Level Assessment. *Environmental Science and Technology*, 51(16), 8933–8943. <https://doi.org/10.1021/acs.est.7b01498>

Chaudhary, A., & Hantush, M. M. (2017). Bayesian Monte Carlo and maximum likelihood approach for uncertainty estimation and risk management: Application to lake oxygen recovery model. *Water Research*, 108, 301–311. <https://doi.org/10.1016/j.watres.2016.11.012>

Cheng, F., & Basu, N. B. (2017). Biogeochemical hotspots: Role of small water bodies in landscape nutrient processing. *Water Resources Research*, 53, 1–19. <https://doi.org/10.1002/2016WR020102.Received>

Cheng, F. Y., & Nandita, B. N. (2017). Biogeochemical hotspots: Role of small water bodies in landscape nutrient processing Frederick. *Water Resources Research*, 53, 1–19. <https://doi.org/10.1002/2016WR020102.Received>

Chimney, M. J., & Pietro, K. C. (2006). Decomposition of macrophyte litter in a subtropical constructed wetland in south Florida (USA). *Ecological Engineering*, 27(4), 301–321. <https://doi.org/10.1016/j.ecoleng.2006.05.016>

Chojnacky, D. C., Heath, L. S., & Jenkins, J. C. (2014). Updated generalized biomass equations for North American tree species. *Forestry*, 87(1), 129–151. <https://doi.org/10.1093/forestry/cpt053>

Chowdhury, R. B., Moore, G. A., Weatherley, A. J., & Arora, M. (2016). A novel substance flow analysis model for analysing multi-year phosphorus flow at the regional scale. *Science of*

*the Total Environment*, 572, 1269–1280. <https://doi.org/10.1016/j.scitotenv.2015.10.055>

Chowdhury, R. B., Moore, G. A., Weatherley, A. J., & Arora, M. (2017). Key sustainability challenges for the global phosphorus resource, their implications for global food security, and options for mitigation. *Journal of Cleaner Production*, 140, 945–963. <https://doi.org/10.1016/j.jclepro.2016.07.012>

Christensen, N., Mitsch, W. J., & Jørgensen, S. E. (1994). A first generation ecosystem model of the Des Plaines River experimental wetlands. *Ecological Engineering*, 3(4), 495–521. [https://doi.org/10.1016/0925-8574\(94\)00015-8](https://doi.org/10.1016/0925-8574(94)00015-8)

Cohen, M. J., Paris, J., & Clark, M. W. (2007). P-sorption capacity estimation in southeastern USA wetland soils using visible/near infrared (VNIR) reflectance spectroscopy. *Wetlands*, 27(4), 1098–1111. [https://doi.org/10.1672/0277-5212\(2007\)27\[1098:PCEISU\]2.0.CO;2](https://doi.org/10.1672/0277-5212(2007)27[1098:PCEISU]2.0.CO;2)

Cordell, D., & White, S. (2014). Life's Bottleneck: Sustaining the World's Phosphorus for a Food Secure Future. *Ssrn*. <https://doi.org/10.1146/annurev-environ-010213-113300>

Courchesne, F., & Turmel, M. C. (2008). Extractable Al, Fe, Mn, and Si. In M. Carter & E. Gregorich (Eds.), *Soil Sampling and Methods of Analysis* (Second Edi, pp. 307–315). CRC Press Taylor and Francis Group.

Craft, C. (2000). Co-development of wetland soils and benthic invertebrate communities following salt marsh creation. *Wetlands Ecology and Management*, 8(6), 459. <https://doi.org/10.1023/A:1026780903350>

Craft, Christopher, Broome, S., & Campbell, C. (2002). Fifteen years of vegetation and soil development after brackish-water marsh creation. *Restoration Ecology*, 10(2), 248–258. <https://doi.org/10.1046/j.1526-100X.2002.01020.x>

Cronk, J. K., & Fennessy, M. S. (2001). *WETLAND PLANTS: biology and ecology* (1st ed.). CRC Press.

Culman, S. W., Snapp, S. S., Freeman, M. A., Schipanski, M. E., Beniston, J., Lal, R., Drinkwater, L. E., Franzluebbers, A. J., Glover, J. D., Grandy, A. S., Lee, J., Six, J., Maul, J. E., Mirsky, S. B., Spargo, J. T., & Wander, M. M. (2012). Permanganate Oxidizable Carbon Reflects a Processed Soil Fraction that is Sensitive to Management. *Soil Science Society of America Journal*, 76(2), 494–504. <https://doi.org/10.2136/sssaj2011.0286>

D'Angelo, E., Crutchfield, J., & Vandiviere, M. (2001a). Rapid, Sensitive, Microscale Determination of Phosphate in Water and Soil. *Journal of Environment Quality*. <https://doi.org/10.2134/jeq2001.2206>

D'Angelo, E., Crutchfield, J., & Vandiviere, M. (2001b). Rapid, Sensitive, Microscale Determination of Phosphate in Water and Soil. *Journal of Environment Quality*, 30(6), 2206. <https://doi.org/10.2134/jeq2001.2206>

Dari, B., Nair, V. D., Colee, J., Harris, W. G., & Mylavarampu, R. (2015). Estimation of phosphorus isotherm parameters: a simple and cost-effective procedure. *Frontiers in Environmental Science*, 3(October), 1–9. <https://doi.org/10.3389/fenvs.2015.00070>

- Dari, B., Nair, V. D., Sharpley, A. N., Kleinman, P., Franklin, D., & Harris, W. G. (2018). Consistency of the Threshold Phosphorus Saturation Ratio across a Wide Geographic Range of Acid Soils. *Age*, 1(1), 0. <https://doi.org/10.2134/age2018.08.0028>
- Day, P. R. (1965). Hydrometer method of particle size analysis. Methods of soil analysis. *Agronomy*, 9, 562–566.
- DHI. (2004). *MIKE 21/3 Ecological Modelling, MIKE 21/3 ECO LAB FM - Short Description*.
- Diehl, R. M., Wemple, B. C., Underwood, K. L., & Ross, D. (2021). *Evaluating floodplain potential for sediment and phosphorus deposition: Development of a framework to assist in Lake Champlain Basin planning* (Issue 100).
- Diehl, T. H. (2007). A Modified Siphon Sampler for Shallow Water Scientific. *Transportation*, 11.
- Dinno, A. (2017). *dunn.test: Dunn's Test of Multiple Comparisons Using Rank Sums*. <https://cran.r-project.org/package=dunn.test>
- Dodd, R. J., & Sharpley, A. N. (2016). Conservation practice effectiveness and adoption: unintended consequences and implications for sustainable phosphorus management. In *Nutrient Cycling in Agroecosystems*. <https://doi.org/10.1007/s10705-015-9748-8>
- Dodds, W. K. (2003). The role of periphyton in phosphorus retention in shallow freshwater aquatic systems. *Journal of Phycology*, 39(5), 840–849. <https://doi.org/10.1046/j.1529-8817.2003.02081.x>
- Dunne, E. J., Smith, J., Perkins, D. B., Clark, M. W., Jawitz, J. W., & Reddy, K. R. (2007). Phosphorus storages in historically isolated wetland ecosystems and surrounding pasture uplands. *Ecological Engineering*, 31(1), 16–28. <https://doi.org/10.1016/j.ecoleng.2007.05.004>
- Dupas, R., Gruau, G., Gu, S., Humbert, G., Jaffrézic, A., & Gascuel-Odoux, C. (2015). Groundwater control of biogeochemical processes causing phosphorus release from riparian wetlands. *Water Research*, 84, 307–314. <https://doi.org/10.1016/j.watres.2015.07.048>
- Ecosystem modeling in theory and practice : an introduction with case histories / edited by Charles A.S. Hall, John W. Day, Jr.* (1977). Wiley.
- Faulkner, J. W. (n.d.). Personal Communication. *Email: Wednesday, September 29, 2021 3:01 PM*.
- Fisher, M. M., & Reddy, K. R. (2001). Phosphorus flux from wetland soils affected by long-term nutrient loading. *Journal of Environmental Quality*, 30(1), 261–271. <https://doi.org/10.2134/jeq2001.301261x>
- Forsmann, D. M., & Kjaergaard, C. (2014). Phosphorus release from anaerobic peat soils during convective discharge - Effect of soil Fe: P molar ratio and preferential flow. *Geoderma*, 223–225(1), 21–32. <https://doi.org/10.1016/j.geoderma.2014.01.025>
- Freeman, C., Ostle, N., & Kang, H. (2001). An enzymic “latch” on a global carbon store. *Nature*,

409(6817), 149. <https://doi.org/10.1038/35051650>

Goyette, J.-O., Bennett, E. M., & Maranger, R. (2018). Low buffering capacity and slow recovery of anthropogenic phosphorus pollution in watersheds. *Nature Geoscience*. <https://doi.org/10.1038/s41561-018-0238-x>

Graetz, D. A., & Nair, V. D. (2009). Phosphorus Sorption Isotherm Determination. In G. M. Kovar, John L. Pierzynski (Ed.), *Methods of Phosphorus Analysis for Soils, Sediments, Residuals, and Waters* (2nd ed., pp. 33–38). Southern Cooperative Series Bulletin No. 408. [http://www.sera17.ext.vt.edu/Documents/P\\_Methods2ndEdition2009.pdf](http://www.sera17.ext.vt.edu/Documents/P_Methods2ndEdition2009.pdf)

Gu, S., Gruau, G., Malique, F., Dupas, R., Petitjean, P., & Gascuel-Odoux, C. (2018). Drying/rewetting cycles stimulate release of colloidal-bound phosphorus in riparian soils. *Geoderma*. <https://doi.org/10.1016/j.geoderma.2018.01.015>

Gu, Sen, Gruau, G., Dupas, R., Petitjean, P., Li, Q., & Pinay, G. (2019a). Respective roles of Fe-oxyhydroxide dissolution, pH changes and sediment inputs in dissolved phosphorus release from wetland soils under anoxic conditions. *Geoderma*, 338(December 2018), 365–374. <https://doi.org/10.1016/j.geoderma.2018.12.034>

Gu, Sen, Gruau, G., Dupas, R., Petitjean, P., Li, Q., & Pinay, G. (2019b). Respective roles of Fe-oxyhydroxide dissolution, pH changes and sediment inputs in dissolved phosphorus release from wetland soils under anoxic conditions. *Geoderma*, 338(June 2018), 365–374. <https://doi.org/10.1016/j.geoderma.2018.12.034>

Gu, Sen, Gruau, G., Dupas, R., Rumpel, C., Crème, A., Fovet, O., Gascuel-Odoux, C., Jeanneau, L., Humbert, G., & Petitjean, P. (2017). Release of dissolved phosphorus from riparian wetlands: Evidence for complex interactions among hydroclimate variability, topography and soil properties. *Science of the Total Environment*, 598, 421–431. <https://doi.org/10.1016/j.scitotenv.2017.04.028>

Guide, A. P. (2009). A Practical Guide to Ecological Modelling. In *A Practical Guide to Ecological Modelling*. <https://doi.org/10.1007/978-1-4020-8624-3>

Guilbert, J., Beckage, B., Winter, J. M., Horton, R. M., Perkins, T., & Bomblies, A. (2014). Impacts of projected climate change over the Lake Champlain basin in Vermont. *Journal of Applied Meteorology and Climatology*, 53(8), 1861–1875. <https://doi.org/10.1175/JAMC-D-13-0338.1>

Guo, D., Westra, S., & Maier, H. R. (2016). An R package for modelling actual, potential and reference evapotranspiration. *Environmental Modelling and Software*, 78, 216–224. <https://doi.org/10.1016/j.envsoft.2015.12.019>

Güsewell, S., & Koerselman, W. (2002). Variation in nitrogen and phosphorus concentrations of wetland plants. *Perspectives in Plant Ecology, Evolution and Systematics*, 5(1), 37–61. <https://doi.org/http://dx.doi.org/10.1078/1433-8319-0000022>

Haan, C. T. (2002). *Statistical methods in hydrology* (2nd ed.). Iowa State University Press.

Hammond Wagner, C., Gourevitch, J., Horner, K., Kinnebrew, E., Maden, B., Recchia, E., White, A., Wiegman, A., Ricketts, T., Roy Citation Hammond Wagner, E., Livingston, G.,

- Markowitz, D., Audet, M., Ross, C., Kamman, N., Rupe, M., Magnan, M., Faulkner, J., Albee, R., ... Koliba, C. (2019). *Issue Paper Payment for Ecosystem Services for Vermont*. [www.uvm.edu/gund](http://www.uvm.edu/gund)
- Hantush, M. M., Kalin, L., Isik, S., & Yucekaya, A. (2013). Nutrient Dynamics in Flooded Wetlands. I: Model Development. *Journal of Hydrologic Engineering*, 18(12), 1709–1723. [https://doi.org/10.1061/\(ASCE\)HE.1943-5584.0000741](https://doi.org/10.1061/(ASCE)HE.1943-5584.0000741)
- Hantush, Mohamed M., & Chaudhary, A. (2014). Bayesian framework for water quality model uncertainty estimation and risk management. *Journal of Hydrologic Engineering*, 19(9). [https://doi.org/10.1061/\(ASCE\)HE.1943-5584.0000900](https://doi.org/10.1061/(ASCE)HE.1943-5584.0000900)
- Herndon, E., Kinsman-Costello, L., Di Domenico, N., Duroe, K., Barczok, M., Smith, C., & Wullschleger, S. D. (2020). Iron and iron-bound phosphate accumulate in surface soils of ice-wedge polygons in arctic tundra. *Environmental Science: Processes and Impacts*, 22(7), 1475–1490. <https://doi.org/10.1039/d0em00142b>
- Hoffmann, C. C., Heiberg, L., Audet, J., Schønfeldt, B., Fuglsang, A., Kronvang, B., Ovesen, N. B., Kjaergaard, C., Hansen, H. C. B., & Jensen, H. S. (2012a). Low phosphorus release but high nitrogen removal in two restored riparian wetlands inundated with agricultural drainage water. *Ecological Engineering*, 46, 75–87. <https://doi.org/10.1016/j.ecoleng.2012.04.039>
- Hoffmann, C. C., Heiberg, L., Audet, J., Schønfeldt, B., Fuglsang, A., Kronvang, B., Ovesen, N. B., Kjaergaard, C., Hansen, H. C. B., & Jensen, H. S. (2012b). Low phosphorus release but high nitrogen removal in two restored riparian wetlands inundated with agricultural drainage water. *Ecological Engineering*, 46, 75–87. <https://doi.org/10.1016/j.ecoleng.2012.04.039>
- Hoffmann, C. C., Kjaergaard, C., Uusi-Kämppä, J., Hansen, H. C. B., & Kronvang, B. (2009). Phosphorus Retention in Riparian Buffers: Review of Their Efficiency. *Journal of Environment Quality*, 38(5), 1942. <https://doi.org/10.2134/jeq2008.0087>
- Hudson, P. F., Colditz, R. R., & Aguilar-Robledo, M. (2006). Spatial relations between floodplain environments and land use - Land cover of a large lowland tropical river valley: Pánuco basin, México. *Environmental Management*, 38(3), 487–503. <https://doi.org/10.1007/s00267-003-0157-4>
- Inglett, P. W., & Inglett, K. S. (2013). Biogeochemical changes during early development of restored calcareous wetland soils. *Geoderma*, 192(1), 132–141. <https://doi.org/10.1016/j.geoderma.2012.07.009>
- Jackson-Blake, L. A., Luke, A., Vrugt, J. A., & Sanders, B. F. (2017). Are our dynamic water quality models too complex? A comparison of a new parsimonious phosphorus model, SimplyP, and INCA-P Research. *Water Resources Research*, doi:10.1002/2016WR020132, 5469–5494. <https://doi.org/10.1002/2016WR019676>. Received
- Jarvie, H. P., Sharpley, A. N., Spears, B., Buda, A. R., May, L., & Kleinman, P. J. A. (2013). Water quality remediation faces unprecedented challenges from “legacy Phosphorus.” *Environmental Science and Technology*, 47(16), 8997–8998. <https://doi.org/10.1021/es403160a>
- Johannesson, K. M., Tonderski, K. S., Ehde, P. M., & Weisner, S. E. B. (2017). Temporal

- phosphorus dynamics affecting retention estimates in agricultural constructed wetlands. *Ecological Engineering*, 103, 436–445. <https://doi.org/10.1016/j.ecoleng.2015.11.050>
- Kalin, L., & Hantush, M. M. (2017). Special issue on advances in wetland hydrology and water quality processes modeling. *Journal of Hydrologic Engineering*, 22(1), 2015–2016. [https://doi.org/10.1061/\(ASCE\)HE.1943-5584.0001483](https://doi.org/10.1061/(ASCE)HE.1943-5584.0001483)
- Kang, J., Hesterberg, D., & Osmond, D. L. (2009). Soil Organic Matter Effects on Phosphorus Sorption: A Path Analysis. *Soil Science Society of America Journal*, 73(2), 360–366. <https://doi.org/10.2136/sssaj2008.0113>
- Kassambara, A. (2020). rstatix: Pipe-friendly framework for basic statistical tests. *R Package Version 0.6. 0.*
- Ketterings, Q. (2001). *Do Modified Morgan and Mehlich-III P Have a Morgan P Equivalent?* September 2014.
- Kiedrzynska, E., Zalewski, M., & Kiedrzynska, M. (2015). *Sustainable floodplain management for flood prevention and water quality improvement*. 76, 955–977. <https://doi.org/10.1007/s11069-014-1529-1>
- Kinsman-Costello, L. E., Hamilton, S. K., O'Brien, J. M., & Lennon, J. T. (2016). Phosphorus release from the drying and reflooding of diverse shallow sediments. *Biogeochemistry*, 130(1–2), 159–176. <https://doi.org/10.1007/s10533-016-0250-4>
- Kjaergaard, C., Heiberg, L., Jensen, H. S., & Hansen, H. C. B. (2012). Phosphorus mobilization in rewetted peat and sand at variable flow rate and redox regimes. *Geoderma*, 173–174, 311–321. <https://doi.org/10.1016/j.geoderma.2011.12.029>
- Kristensen, E., Quintana, C. O., Valdemarsen, T., & Flindt, M. R. (2020). Nitrogen and Phosphorus Export After Flooding of Agricultural Land by Coastal Managed Realignment. *Estuaries and Coasts*, 2100. <https://doi.org/10.1007/s12237-020-00785-2>
- Kusmer, A. S., Goyette, J. O., MacDonald, G. K., Bennett, E. M., Maranger, R., & Withers, P. J. A. (2018). Watershed Buffering of Legacy Phosphorus Pressure at a Regional Scale: A Comparison Across Space and Time. *Ecosystems*, 1–19. <https://doi.org/10.1007/s10021-018-0255-z>
- Land, M., Granéli, W., Grimvall, A., Hoffmann, C. C., Mitsch, W. J., Tonderski, K. S., & Verhoeven, J. T. A. (2016a). How effective are created or restored freshwater wetlands for nitrogen and phosphorus removal? A systematic review. *Environmental Evidence*, 5(1), 1–26. <https://doi.org/10.1186/s13750-016-0060-0>
- Land, M., Granéli, W., Grimvall, A., Hoffmann, C. C., Mitsch, W. J., Tonderski, K. S., & Verhoeven, J. T. A. (2016b). How effective are created or restored freshwater wetlands for nitrogen and phosphorus removal? A systematic review. *Environmental Evidence*, 5(1), 1–8. <https://doi.org/10.1186/s13750-016-0060-0>
- Levy, E. T., & Schlesinger, W. H. (1999). A comparison of fractionation methods for forms of phosphorus in soils. *Biogeochemistry*, 47(1), 25–38. <https://doi.org/10.1007/bf00993095>

- Maberly, S. C., King, L., Dent, M. M., Jones, R. I., & Gibson, C. E. (2002). Nutrient limitation of phytoplankton and periphyton growth in upland lakes. *Freshwater Biology*, 47(11), 2136–2152. <https://doi.org/10.1046/j.1365-2427.2002.00962.x>
- Maranguit, D., Guillaume, T., & Kuzyakov, Y. (2017). Effects of flooding on phosphorus and iron mobilization in highly weathered soils under different land-use types: Short-term effects and mechanisms. *Catena*, 158(March), 161–170. <https://doi.org/10.1016/j.catena.2017.06.023>
- Marois, D. E., & Mitsch, W. J. (2016). Modeling phosphorus retention at low concentrations in Florida Everglades mesocosms. *Ecological Modelling*, 319, 42–62. <https://doi.org/10.1016/j.ecolmodel.2015.09.024>
- McLeod, A. I., Xu, C., & Lai, Y. (2020). *bestglm: Best Subset GLM and Regression Utilities*. <https://cran.r-project.org/package=bestglm>
- McMillan, S. K., & Noe, G. B. (2017). Increasing floodplain connectivity through urban stream restoration increases nutrient and sediment retention. *Ecological Engineering*, 108(March), 284–295. <https://doi.org/10.1016/j.ecoleng.2017.08.006>
- Meli, P., Benayas, J. M. R., Balvanera, P., & Ramos, M. M. (2014). Restoration enhances wetland biodiversity and ecosystem service supply, but results are context-dependent: A meta-analysis. *PLoS ONE*, 9(4). <https://doi.org/10.1371/journal.pone.0093507>
- Mendes, L. R. D., Tonderski, K., & Kjaergaard, C. (2018). Phosphorus accumulation and stability in sediments of surface-flow constructed wetlands. *Geoderma*, 331(March), 109–120. <https://doi.org/10.1016/j.geoderma.2018.06.015>
- Mitsch, W. J., & Gosselink, J. G. (2013). *Wetlands* (5th ed.). Wiley.
- Morris, J. T., Barber, D. C., Callaway, J. C., Chambers, R., Hagen, S. C., Hopkinson, C. S., Johnson, B. J., Megonigal, P., Neubauer, S. C., Troxler, T., & Wigand, C. (2016). Contributions of organic and inorganic matter to sediment volume and accretion in tidal wetlands at steady state. *Earth's Future*, 4(4), 110–121. <https://doi.org/10.1002/2015EF000307>
- Morris, J. T., & Bowden, W. B. (1986). A Mechanistic, Numerical Model of Sedimentation, Mineralization, and Decomposition for Marsh Sediments1. *Soil Science Society of America Journal*, 50(1), 96. <https://doi.org/10.2136/sssaj1986.03615995005000010019x>
- Moser, K. F., Ahn, C., & Noe, G. B. (2009). The influence of microtopography on soil nutrients in created mitigation wetlands. *Restoration Ecology*, 17(5), 641–651. <https://doi.org/10.1111/j.1526-100X.2008.00393.x>
- Motew, M., Chen, X., Booth, E. G., Carpenter, S. R., Pinkas, P., Zipper, S. C., Loheide, S. P., Donner, S. D., Tsuruta, K., Vadas, P. A., & Kucharik, C. J. (2017). The Influence of Legacy P on Lake Water Quality in a Midwestern Agricultural Watershed. *Ecosystems*, 1–15. <https://doi.org/10.1007/s10021-017-0125-0>
- Muggeo, V. M. R. (2008). segmented: An R package to Fit Regression Models with Broken-Line Relationships. *R News*, 8(May), 20–25. <https://doi.org/10.1111/j.1467-9644.2008.00328.x>

- Mukherjee, A., Nair, V. D., Clark, M. W., & Reddy, K. R. (2009). Development of Indices to Predict Phosphorus Release from Wetland Soils. *Journal of Environment Quality*, 38(3), 878. <https://doi.org/10.2134/jeq2008.0230>
- Murphy, J., & Riley, J. P. (1962). A modified single solution method for the determination of phosphate in natural waters. *Analytica Chimica Acta*, 27(C), 31–36. [https://doi.org/10.1016/S0003-2670\(00\)88444-5](https://doi.org/10.1016/S0003-2670(00)88444-5)
- Nair, V. D., Clark, M. W., & Reddy, K. R. (2015). Evaluation of Legacy Phosphorus Storage and Release from Wetland Soils. *Journal of Environment Quality*, 44(6), 1956. <https://doi.org/10.2134/jeq2015.03.0154>
- Nair, V. D., & Harris, W. G. (2004). A capacity factor as an alternative to soil test phosphorus in phosphorus risk assessment. *New Zealand Journal of Agricultural Research*, 47(4), 491–497. <https://doi.org/10.1080/00288233.2004.9513616>
- Nair, Vimala D, & Reddy, K. R. (2013). Phosphorus Sorption and Desorption in Wetland Soils. In *Methods in Biogeochemistry of Wetlands* (pp. 667–681). Soil Science Society of America. <https://doi.org/10.2136/sssabookser10.c34>
- NASS. (2021). *CropScape and Cropland Data Layer*. United States Department of Agriculture: National Agricultural Stastics Service. [https://www.nass.usda.gov/Research\\_and\\_Science/Cropland/SARS1a.php](https://www.nass.usda.gov/Research_and_Science/Cropland/SARS1a.php)
- Neitsch, S. L., Arnold, J. G., Kiniry, J. R., Srinivasan, R., & Williams, J. R. (2002). Soil and Water Assessment Tool User's Manual. *TWRI Report TR-192*, 412. <http://swat.tamu.edu/media/1294/swatuserman.pdf>
- Nixon, S. W. (2009). *Eutrophication and the macroscope*. 5–19. <https://doi.org/10.1007/s10750-009-9759-z>
- NOAA. (n.d.). *National Climate Data Center: Ciimate Data Online Search*. <https://www.ncdc.noaa.gov/cdo-web/search>
- NOAA. (2021). *North American Drought Monitor*. <https://www.ncdc.noaa.gov/temp-and-precip/drought/nadm/>
- Noe, G. B., & Hupp, C. R. (2009). Retention of riverine sediment and nutrient loads by coastal plain floodplains. *Ecosystems*, 12(5), 728–746. <https://doi.org/10.1007/s10021-009-9253-5>
- Noe, G. B., Hupp, C. R., & Rybicki, N. B. (2013). Hydrogeomorphology Influences Soil Nitrogen and Phosphorus Mineralization in Floodplain Wetlands. *Ecosystems*, 16(1), 75–94. <https://doi.org/10.1007/s10021-012-9597-0>
- NRCS. (2021). *SSURGO*. United States Department of Agriculture: Natural Resources Conservation Service. [https://www.nrcs.usda.gov/wps/portal/nrcs/detail/soils/survey/office/ssr12/tr/?cid=nrcs142p2\\_010596](https://www.nrcs.usda.gov/wps/portal/nrcs/detail/soils/survey/office/ssr12/tr/?cid=nrcs142p2_010596)
- O'Dell, J. W. (1993). Method 365.1,Determination of Phosphorus By Semi-Automated Colorimetry. *Epa, August*, 1–15.

- Pant, H. K., & Reddy, K. R. (2003). Potential internal loading of phosphorus in a wetland constructed in agricultural land. *Water Research*, 37(5), 965–972. [https://doi.org/10.1016/S0043-1354\(02\)00474-8](https://doi.org/10.1016/S0043-1354(02)00474-8)
- Patton, C. J., & Kryskalla, J. R. (2003). Methods of Analysis by the U.S. Geological Survey National Water Quality Laboratory—Evaluation of Alkaline Persulfate Digestion as an Alternative to Kjeldahl Digestion for Determination of Total and Dissolved Nitrogen and Phosphorus in Water. In *Water-Resources Investigations Report* (Vols. 03-4174).
- Paudel, R., & Jawitz, J. W. (2017). Spatially distributed hydrodynamic modeling of phosphorus transport and transformation in a cell-network treatment wetland. *Journal of Hydrologic Engineering*, 22(1), 1–15. [https://doi.org/10.1061/\(ASCE\)HE.1943-5584.0001403](https://doi.org/10.1061/(ASCE)HE.1943-5584.0001403)
- Pentrák, M., Pentráková, L., & Stucki, J. W. (2013). Iron and Manganese Reduction–Oxidation. In *Methods in Biogeochemistry of Wetlands* (pp. 701–721). Soil Science Society of America. <https://doi.org/10.2136/sssabookser10.c36>
- Perillo, V. L., Ross, D. S., Wemple, B. C., Balling, C., & Lemieux, L. E. (2019). Stream Corridor Soil Phosphorus Availability in a Forested–Agricultural Mixed Land Use Watershed. *Journal of Environment Quality*, 48(3), 783. <https://doi.org/10.2134/jeq2018.05.0186er>
- Petzoldt, T. (2018). Package ‘deSolve’.
- Poole, G. C. (2010). Stream hydrogeomorphology as a physical science basis for advances in stream ecology. *Journal of the North American Benthological Society*, 29(1), 12–25. <https://doi.org/10.1899/08-070.1>
- Preiner, S., Bondar-Kunze, E., Pitzl, B., Weigelhofer, G., & Hein, T. (2020). Effect of Hydrological Connectivity on the Phosphorus Buffering Capacity of an Urban Floodplain. *Frontiers in Environmental Science*, 8(August), 1–13. <https://doi.org/10.3389/fenvs.2020.00147>
- R Core Team. (2020). *R: A Language and Environment for Statistical Computing*. <https://www.r-project.org/>
- Rahutomo, S., Kovar, J. L., & Thompson, M. L. (2019). Malachite Green Method for Determining Phosphorus Concentration in Diverse Matrices. *Communications in Soil Science and Plant Analysis*. <https://doi.org/10.1080/00103624.2019.1635140>
- Ready, K. R., Kadlec, R. H., Flaig, E., & Gale, P. M. (1999). Phosphorus retention in streams and wetlands: A review. *Critical Reviews in Environmental Science and Technology*, 29(1), 83–146. <https://doi.org/10.1080/10643389991259182>
- Reddy, K. R., Clark, M. W., DeLaune, R. D., & Kongchum, M. (2013). Physicochemical Characterization of Wetland Soils. In *Methods in Biogeochemistry of Wetlands* (pp. 41–53). Soil Science Society of America. <https://doi.org/10.2136/sssabookser10.c3>
- Reddy, K. R., & Delaune, R. D. (2008). *Biochemistry of wetland science and application*.
- Reddy, K. R., O Connor, G. a., & Gale, P. M. (1998). Phosphorus Sorption Capacities of Wetland Soils and Stream Sediments Impacted by Dairy Effluent. *Journal of Environment Quality*,

- 27(2), 438. <https://doi.org/10.2134/jeq1998.00472425002700020027x>
- Reddy, K. R., Wang, Y., DeBusk, W. F., Fisher, M. M., & Newman, S. (1998). Forms of Soil Phosphorus in Selected Hydrologic Units of the Florida Everglades. *Soil Science Society of America Journal*, 62(4), 1134–1147.  
<https://doi.org/10.2136/sssaj1998.03615995006200040039x>
- Redhead, J. W., May, L., Oliver, T. H., Hamel, P., Sharp, R., & Bullock, J. M. (2018). National scale evaluation of the InVEST nutrient retention model in the United Kingdom. *Science of the Total Environment*, 610–611, 666–677. <https://doi.org/10.1016/j.scitotenv.2017.08.092>
- Rejmáneková, E., & Houdková, K. (2006). Wetland plant decomposition under different nutrient conditions: what is more important, litter quality or site quality? *Biogeochemistry*, 80, 245–262. <https://doi.org/10.1007/s10533-006-9021-y>
- Richardson, C. J., & Reddy, K. R. (2013). Methods for Soil Phosphorus Characterization and Analysis of Wetland Soils. In *Methods in Biogeochemistry of Wetlands* (pp. 603–638). Soil Science Society of America. <https://doi.org/10.2136/sssabookser10.c32>
- Ringuet, S., Sassano, L., & Johnson, Z. I. (2011). A suite of microplate reader-based colorimetric methods to quantify ammonium, nitrate, orthophosphate and silicate concentrations for aquatic nutrient monitoring. *J. Environ. Monit.*, 13(2), 370–376.  
<https://doi.org/10.1039/C0EM00290A>
- Rode, M., Wade, A. J., Cohen, M. J., Hensley, R. T., Bowes, M. J., Kirchner, J. W., Arhonditsis, G. B., Jordan, P., Kronvang, B., Halliday, S. J., Skeffington, R. A., Rozemeijer, J. C., Aubert, A. H., Rinke, K., & Jomaa, S. (2016). Sensors in the Stream: The High-Frequency Wave of the Present. *Environmental Science and Technology*, 50(19), 10297–10307.  
<https://doi.org/10.1021/acs.est.6b02155>
- Rowe, H., Withers, P. J. A., Baas, P., Chan, N. I., Doody, D., Holiman, J., Jacobs, B., Li, H., MacDonald, G. K., McDowell, R., Sharpley, A. N., Shen, J., Taheri, W., Wallenstein, M., & Weintraub, M. N. (2016). Integrating legacy soil phosphorus into sustainable nutrient management strategies for future food, bioenergy and water security. *Nutrient Cycling in Agroecosystems*, 104(3), 393–412. <https://doi.org/10.1007/s10705-015-9726-1>
- Roy, E. D., Nguyen, N. T., Bargu, S., & White, J. R. (2012). Internal loading of phosphorus from sediments of Lake Pontchartrain (Louisiana, USA) with implications for eutrophication. *Hydrobiologia*, 684(1), 69–82. <https://doi.org/10.1007/s10750-011-0969-9>
- Roy, E. D., Nguyen, N. T., & White, J. R. (2017). Changes in estuarine sediment phosphorus fractions during a large-scale Mississippi River diversion. *Science of the Total Environment*, 609, 1248–1257. <https://doi.org/10.1016/j.scitotenv.2017.07.224>
- Roy, E. D., Smith, E. A., Bargu, S., & White, J. R. (2016). Will Mississippi River diversions designed for coastal restoration cause harmful algal blooms? *Ecological Engineering*, 91, 350–364. <https://doi.org/10.1016/j.ecoleng.2016.02.030>
- Roy, E. D., Willig, E., Richards, P. D., Martinelli, L. A., Vazquez, F. F., Pegorini, L., Spera, S. A., & Porder, S. (2017). Soil phosphorus sorption capacity after three decades of intensive fertilization in Mato Grosso, Brazil. *Agriculture, Ecosystems and Environment*, 249(July),

206–214. <https://doi.org/10.1016/j.agee.2017.08.004>

Schlesinger, W. H., & Bernhardt, E. S. (2020). *Biogeochemistry and Analysis of Global Change* (Fourth Edi). Academic Press.

Scholz, R. W., Ulrich, A. E., Eilittä, M., & Roy, A. (2013). Sustainable use of phosphorus: A finite resource. *Science of the Total Environment*, *468*, 432–437. <https://doi.org/10.1016/j.scitotenv.2013.05.043>

Schönbrunner, I. M., Preiner, S., & Hein, T. (2012). Impact of drying and re-flooding of sediment on phosphorus dynamics of river-floodplain systems. *Science of the Total Environment*, *432*, 329–337. <https://doi.org/10.1016/j.scitotenv.2012.06.025>

Sharifi, A., Kalin, L., Hantush, M. M., Dahlgren, R. A., O'Geen, A. T., & Maynard, J. J. (2017). Capturing spatial variability of biogeochemical mass exchanges and reaction rates in wetland water and soil through model compartmentalization. *Journal of Hydrologic Engineering*, *22*(1). [https://doi.org/10.1061/\(ASCE\)HE.1943-5584.0001196](https://doi.org/10.1061/(ASCE)HE.1943-5584.0001196)

Sharpley, A., Jarvie, H. P., Buda, A., May, L., Spears, B., & Kleinman, P. (2013). Phosphorus Legacy: Overcoming the Effects of Past Management Practices to Mitigate Future Water Quality Impairment. *Journal of Environment Quality*, *42*(5), 1308. <https://doi.org/10.2134/jeq2013.03.0098>

Singh, N., Gourevitch, J. D., Wemple, B. C., Watson, K. B., Rizzo, D. M., Polasky, S., & Ricketts, T. (2019). Optimizing wetland restoration to improve water quality at a regional scale. *Environmental Research Letters*. <https://doi.org/10.1088/1748-9326/ab1827>

Singh, N. K., Gourevitch, J. D., Wemple, B. C., Watson, K. B., Rizzo, D. M., Polasky, S., & Ricketts, T. H. (2019). Optimizing wetland restoration to improve water quality at a regional scale. *Environmental Research Letters*, *14*(6). <https://doi.org/10.1088/1748-9326/ab1827>

Smagin, A. V. (2018). *Biological Oxygen Demand in Soils and Litters*. March. <https://doi.org/10.1134/S1064229318010143>

Smil, V. (2000). *P HOSPHORUS IN THE ENVIRONMENT: Natural Flows and Human Interferences*. 53–88.

Smyth, A. R., Loecke, T. D., Franz, T. E., & Burgin, A. J. (2018). Using high-frequency soil oxygen sensors to predict greenhouse gas emissions from wetlands. *Soil Biology and Biochemistry*, *128*(October 2018), 182–192. <https://doi.org/10.1016/j.soilbio.2018.10.020>

Soetaert, K., Petzoldt, T., & Setzer, R. W. (2010). Solving differential equations in R: Package deSolve. *Journal of Statistical Software*, *33*(9), 1–25. <https://doi.org/10.18637/jss.v033.i09>

Soil Science Division Staff. (2017). *Soil Survey Manual, USDA Handbook 18*. *18*, 639.

Surridge, B. W. J., Heathwaite, A. L., & Baird, A. J. (2012). Phosphorus mobilisation and transport within a long-restored floodplain wetland. *Ecological Engineering*, *44*, 348–359. <https://doi.org/10.1016/j.ecoleng.2012.02.009>

Syvitski, J., Waters, C. N., Day, J., Milliman, J. D., Summerhayes, C., Steffen, W., Zalasiewicz,

- J., Cearreta, A., Gałuszka, A., Hajdas, I., Head, M. J., Leinfelder, R., McNeill, J. R., Poirier, C., Rose, N. L., Shotyk, W., Wagreich, M., & Williams, M. (2020). Extraordinary human energy consumption and resultant geological impacts beginning around 1950 CE initiated the proposed Anthropocene Epoch. *Communications Earth & Environment*, 1(1), 1–13. <https://doi.org/10.1038/s43247-020-00029-y>
- Tessier, J. T., & Raynal, D. J. (2003). Use of nitrogen to phosphorus ratios in plant tissue as an indicator of nutrient limitation and nitrogen saturation. *Journal of Applied Ecology*, 40(3), 523–534. <https://doi.org/10.1046/j.1365-2664.2003.00820.x>
- Thorslund, J., Jarsjo, J., Jaramillo, F., Jawitz, J. W., Manzoni, S., Basu, N. B., Chalov, S. R., Cohen, M. J., Creed, I. F., Goldenberg, R., Hylin, A., Kalantari, Z., Koussis, A. D., Lyon, S. W., Mazi, K., Mard, J., Persson, K., Pietro, J., Prieto, C., ... Destouni, G. (2017). Wetlands as large-scale nature-based solutions: Status and challenges for research, engineering and management. *Ecological Engineering*, 108, 489–497. <https://doi.org/10.1016/j.ecoleng.2017.07.012>
- Trentman, M. T., Tank, J. L., Jones, S. E., McMillan, S. K., & Royer, T. V. (2020). Seasonal evaluation of biotic and abiotic factors suggests phosphorus retention in constructed floodplains in three agricultural streams. *Science of the Total Environment*, 729, 138744. <https://doi.org/10.1016/j.scitotenv.2020.138744>
- Trueheart, M. E., Dewoolkar, M. M., Rizzo, D. M., Huston, D., & Bomblies, A. (2020). Simulating hydraulic interdependence between bridges along a river corridor under transient flood conditions. *Science of the Total Environment*, 699, 134046. <https://doi.org/10.1016/j.scitotenv.2019.134046>
- Upreti, K., Maiti, K., & Rivera-Monroy, V. H. (2019). Microbial mediated sedimentary phosphorus mobilization in emerging and eroding wetlands of coastal Louisiana. *Science of the Total Environment*, 651, 122–133. <https://doi.org/10.1016/j.scitotenv.2018.09.031>
- US EPA. (2015). *Phosphorus TMDLs for Vermont segments of Lake Champlain*.
- van Groenendael, J. M. (1997). An introduction to ecological modelling. In *Trends in Ecology & Evolution* (Vol. 12, Issue 12). [https://doi.org/10.1016/S0169-5347\(97\)84411-4](https://doi.org/10.1016/S0169-5347(97)84411-4)
- VanZomeren, C. M., Berkowitz, J. F., Lemke, A. M., & Kirkham, K. G. (2019). Soil P Storage Capacity in Agricultural Treatment Wetlands: Can a System Designed for N Reduction Also Retain P? *Wetlands*. <https://doi.org/10.1007/s13157-019-01205-3>
- Vitousek, P. M., Porder, S., Houlton, B. Z., Oliver, A., Vitousek, P. M., Porder, S., Houlton, B. Z., & Chadwick, O. A. (2010). Terrestrial phosphorus limitation : mechanisms , implications , and nitrogen — phosphorus interactions Published by : Wiley on behalf of the Ecological Society of America Stable URL : <http://www.jstor.org/stable/27797785> REFERENCES Linked references are a. *Ecological Applications*, 20(1), 5–15. <https://doi.org/10.1007/s11060-010-0360-0>
- VTADS. (2021). *Vermont Center for Geographic Information*. Vermont Agency of Digital Services. <https://vcgi.vermont.gov/>
- VTDEC. (2018). *RCPP WETLAND RESTORATION SITE PRIORITIZATION PROJECT MAP*

*INTRODUCTION* (Issue August). VERMONT DEPARTMENT OF ENVIRONMENTAL CONSERVATION WATERSHED MANAGEMENT DIVISION.

- VTDEC. (2021). *FUNCTIONING FLOODPLAIN INITIATIVE*. Vermont Department of Environmental Conservation 1 National Life Drive; Montpelier, VT. [dec.vermont.gov/ffi](http://dec.vermont.gov/ffi)
- Walker, T. W., & Syers, J. K. (1976). The fate of phosphorus during pedogenesis. *Geoderma*, 15(1), 1–19. [https://doi.org/10.1016/0016-7061\(76\)90066-5](https://doi.org/10.1016/0016-7061(76)90066-5)
- Walton, C. R., Zak, D., Audet, J., Petersen, R. J., Lange, J., Oehmke, C., Wichtmann, W., Kreyling, J., Grygoruk, M., Jabłońska, E., Kotowski, W., Wiśniewska, M. M., Ziegler, R., & Hoffmann, C. C. (2020). Wetland buffer zones for nitrogen and phosphorus retention: Impacts of soil type, hydrology and vegetation. *Science of the Total Environment*, 727. <https://doi.org/10.1016/j.scitotenv.2020.138709>
- Wang, H., Appan, A., & Gulliver, J. S. (2003). Modeling of phosphorus dynamics in aquatic sediments: I - Model development. *Water Research*. [https://doi.org/10.1016/S0043-1354\(03\)00304-X](https://doi.org/10.1016/S0043-1354(03)00304-X)
- Weigelhofer, G., Preiner, S., Funk, A., Bondar-Kunze, E., & Hein, T. (2015). The hydrochemical response of small and shallow floodplain water bodies to temporary surface water connections with the main river. *Freshwater Biology*, 60(4), 781–793. <https://doi.org/10.1111/fwb.12532>
- Weil, R. R., Islam, K. R., Stine, M. A., Gruver, J. B., & Samson-Liebig, S. E. (2003). Estimating active carbon for soil quality assessment: A simplified method for laboratory and field use. *American Journal of Alternative Agriculture*, 18(1), 3–17. <https://doi.org/10.1079/AJAA2003003>
- Welikhe, P., Brouder, S. M., Volenec, J. J., Gitau, M., & Turco, R. F. (2020). Development of phosphorus sorption capacity-based environmental indices for tile-drained systems. *Journal of Environmental Quality*, 49(2), 378–391. <https://doi.org/10.1002/jeq2.20044>
- Wickham, H., Averick, M., Bryan, J., Chang, W., McGowan, L. D., François, R., Grolemund, G., Hayes, A., Henry, L., Hester, J., Kuhn, M., Pedersen, T. L., Miller, E., Bache, S. M., Müller, K., Ooms, J., Robinson, D., Seidel, D. P., Spinu, V., ... Yutani, H. (2019). Welcome to the {tidyverse}. *Journal of Open Source Software*, 4(43), 1686. <https://doi.org/10.21105/joss.01686>
- Young, E. O., & Ross, D. S. (2001). Phosphate Release from Seasonally Flooded Soils. *Journal of Environment Quality*, 30(1), 91. <https://doi.org/10.2134/jeq2001.30191x>
- Young, E. O., & Ross, D. S. (2016). Total and Labile Phosphorus Concentrations as Influenced by Riparian Buffer Soil Properties. *Journal of Environment Quality*, 45(1), 294. <https://doi.org/10.2134/jeq2015.07.0345>
- Young, E. O., & Ross, D. S. (2018). *Phosphorus Mobilization in Flooded Riparian Soils From the Lake*. 6(October), 1–12. <https://doi.org/10.3389/fenvs.2018.00120>
- Young, E. O., Ross, D. S., & Hoskins, B. R. (2017). Communications in Soil Science and Plant Analysis Phosphorus in Morgan Soil Test Extracts Measured By Molybdate Colorimetric

and Inductively Coupled Plasma Spectroscopy Methods Phosphorus in Morgan Soil Test Extracts Measured By Molybdate. *Communications in Soil Science and Plant Analysis*, 48(20), 2434–2446. <https://doi.org/10.1080/00103624.2017.1411936>

Zak, D., Meyer, N., Cabezas, A., Gelbrecht, J., Mauersberger, R., Tiemeyer, B., Wagner, C., & McInnes, R. (2017). Topsoil removal to minimize internal eutrophication in rewetted peatlands and to protect downstream systems against phosphorus pollution: A case study from NE Germany. *Ecological Engineering*, 103, 488–496.  
<https://doi.org/10.1016/j.ecoleng.2015.12.030>

Zhang, H., Schroder, J. L., Fuhrman, J. K., Basta, N. T., Storm, D. E., & Payton, M. E. (2005). Path and Multiple Regression Analyses of Phosphorus Sorption Capacity. *Soil Science Society of America Journal*, 69(1), 96. <https://doi.org/10.2136/sssaj2005.0096dup>